ANALYSIS OF MONODISPERSE MICROFLUIDIC DROPLET GENERATION AND ITS BIOCHEMICAL APPLICATIONS

A DISSERTATION SUBMITTED TO
THE GRADUATE SCHOOL OF ENGINEERING AND SCIENCE
OF BILKENT UNIVERSITY
IN PARTIAL FULFILLMENT OF THE REQUIREMENTS FOR
THE DEGREE OF
DOCTOR OF PHILOSOPHY
IN
MATERIALS SCIENCE AND NANOTECHNOLOGY

By
Ali Kalantarifard
November 2020

ANALYSIS OF MONODISPERSE MICROFLUIDIC DROPLET GENERATION AND ITS BIOCHEMICAL APPLICATIONS

By Ali Kalantarifard

November 2020

We certify that we have read this dissertation and that in our opinion it is fully adequate, in scope and in quality, as a dissertation for the degree of Doctor of Philosophy.

Çağlar Elbüken(Advisor)

Emine Yegan Erdem Ercan

Ender Yıldırım

Fatih İnci

Mustafa Serdar Önses

Approved for the Graduate School of Engineering and Science:

Ezhan Karaşan
Director of the Graduate School

ABSTRACT

ANALYSIS OF MONODISPERSE MICROFLUIDIC DROPLET GENERATION AND ITS BIOCHEMICAL APPLICATIONS

Ali Kalantarifard
Ph.D. in Materials Science and Nanotechnology
Advisor: Çağlar Elbüken
November 2020

Droplet fluidic systems have dramatically improved precision in many applications, such as polymerase chain reaction, biochemical analysis, and particle synthesis in which accurate control of sample volume plays a significant role. Despite the well-understood physics of squeezing regime droplet formation in two-phase flow systems, the long-sought-after goal of generating identical, equal size droplets is challenging. Although the individual parameters that affect the droplet size were identified as channel dimension, wettability, viscosity, and flow rate or pressure ratio of the two immiscible fluids, the governing mechanism of droplet size variation is not completely analyzed. More importantly, the limit of monodispersity for droplet generation systems is still unknown. This is due to the difficulty in analytical modeling of droplet formation that is usually compensated by experimental approaches, which fall short in leading to universal conclusions.

In this thesis, depending on the flow source used for driving fluids we present an analytical approach that takes into account all the system dynamics and internal and external factors that disturb monodispersity. We use the analogy between fluidic and electrical circuits to analyze the factors that influence droplet monodispersity. Interestingly, we enable to model the dynamics of a segmented two-phase flow system using a single-phase flow analogy, electron flow, in electrical circuits. Doing so, we reveal the sources of disturbances that lead to variation in droplet volume. We offered a unique solution and designed guidelines to ensure ultra-monodisperse droplet generation. Our analytical conclusions are experimentally verified using a T-junction and flow-focusing droplet generator design driven by a pressure supply. Equally importantly, we show the limiting experimental factors for reaching the theoretical maximum of monodispersity. For the displacement pump case, we propose a more effective and widely applicable solution to improve flow stability, by controlling off-chip compliances to minimize fluctuations due to the flow source. Eventually, we compare the performance of the two common drive

units (pressure-driven and displacement pump) in terms of droplet monodispersity, while using our proposed methods and guidelines. Finally, we did study in reaction kinetics of poly dopamine and hydrogen peroxide and synthesize silica and polyethylene glycol (PEG) particles and supramolecular polymer capsules with high monodispersity using ultra-monodisperse droplets.

Keywords: Microfluidics, Microdroplet, Droplet monodispersity, Particle synthesis.

ÖZET

EŞDAĞILIMLI MİKROAKIŞKAN DAMLACIK OLUŞUMUNUN ANALİZİ VE BİYOKİMYASAL UYGULAMALARI

Ali Kalantarifard
Malzeme Bilimi ve Nanoteknoloji, Doktora
Tez Danışmanı: Çağlar Elbüken
Kasim 2020

Damlacık akışkan sistemler, örnek hacminin kontrolünün önemli rol oynadığı polimeraz zincir reaksiyonu, biyokimyasal analiz ve parçacık sentezi gibi bir çok uygulamada, kesinliği önemli ölçüde geliştirmiştir. İki fazlı akış sistemlerinde, sıkışma rejimi ile damlacık oluşumu fiziğinin çok iyi anlaşılmasına rağmen, özdeş boyutta damlacık oluşturabilme, hala ulaşılması zor bir hedeftir. Damlacık büyüklüğünü etkileyen parametreler, kanal boyutu, ıslanırlık, vizkozite, akış miktarı ve basınç oranı olarak tanımlansa da, damlacık büyüklük varyasyonlarını belirleyen mekanizma tam anlamıyla analiz edilmemiştir. Daha önemlisi, damlacık oluşum sistemleri için eşdağılımlılık limiti hala bilinmemektedir. Bunun nedeni, damlacık oluşumunun analitik modellemesindeki zorluktur. Zira, modelleme genellikle deneysel yaklaşımlarla kompanse edilmektedir ki bu evrensel sonuçlara yönlendirmede yetersiz kalmaktadır.

Bu tezde, akışkanları sürmek için kullanılan akış kaynağına bağlı olarak, eşdağılımlılığı bozan bütün sistem dinamiklerini, iç ve dış faktörleri hesaba katarak, analitik bir yaklaşım sunulmaktadır. Akışkan ve elektrik devrelerdeki analojiyi kullanarak, damlacık eşdağılımlılığını etkileyen faktörleri analiz ettik. İlginç şekilde, tek faz akış analojisi ve devrelerdeki elektron akışı kullanılarak, parçalı iki faz akış sisteminin dinamiklerini modellemeyi başardık. Bunu yaparak, damlacık hacminde varyasyonlara neden olan bozulmaların kaynağını ortaya çıkardık. Özgün bir çözüm önerdik ve yüksek eşdağılımlı damlacık oluşumu için bir kılavuz hazırladık. Analitik sonuçlarımız deneysel olarak, basınç kaynağı marifetiyle T-kesişim ve akış-odaklama damlacık oluşturucularıyla doğrulandı. Eşit önemde, eşdağılımlılığın teorik maksimumuna ulaşmadaki limitleyici deneysel faktörleri gösterdik. Yerdeğişim pompası durumunda, akış stabilitesini geliştirmek için, daha etkili ve geniş çerçevede uygulanabilir bir çözüm önerdik. Bunu, akış kaynağı nedenli değişimleri azaltmak için, çip dışı uyunç

yeteneğini kontrol ederek yaptık. Sonunda, iki yaygın sürüş biriminin (basınç ve yerdeğişim pompaları) performaslarını, önerdiğimiz metotlar da kullanılarak, damlacık eşdağılımlılığı açısından karşılaştırdık. En nihayetinde, poli dopamin ve hidrojen peroksidin reaksiyon kinetiği üzerine çalıştık ve silika ve polietilen glikol (PEG) parçacıklar ile supramoleküler polimer kapsüller, yüksek eşdağılımlı damlacıklar yoluyla yüksek eşdağılımlılıkla sentezlenmiştir.

Anahtar sözcükler: Mikroakışkanlar, Mikrodamlacık, Damlacık eş dağılımı, Parçacık sentezi.

Acknowledgement

I would first like to thank my supervisor, Professor Caglar Elbuken, whose expertise was invaluable in the research. His knowledge, experience and insightful advice and ideas pushed me to sharpen my thinking and brought my work to a higher level. Not only has he helped me improve myself academically, but also he has become an excellent mentor, role-model, and life-long friend for me. I am deeply indebted to you for being more than a supervisor.

I owe a gratitude to my committee members Prof. Yegan Erdem, Prof. Ender Yildirim, Prof. Fatih Inci and Prof. Serdar Onses for improving my thesis with their invaluable guidance and feed-backs. I am grateful to Prof. Aykutlu Dana, Prof. Engin Durgun and Prof. Parviz Elahi for devoting their valuable time to share their life experiences, and friendly advice. They are truly enlightened my way during this journey. I am grateful to Prof. Donus Tuncel and Prof. Bulend Ortac for opening their lab to me and allowing to use their instruments or collaborate in their study. I would like to thank my group members and collaborators, Abtin Saateh, Dr. Elnaz Alizadeh Haghighi, Dr. Ziya Isiksacan, Dr. Mustafa Tahsin Guler, Dr. Murat Serhatlioglu, Mohammad Asghari, Tolga O. Celik, Seyed Ehsan Hadi, Melis Ozkan, Sepehr Elahi, Dr. Fatemeh Kalantarifard, Dr. Pinar Beyazkilic, Dr. Nuray Gunduz, Dr. Athina Gkouti, Resul Saritas, Dr. Merve Marcali and Pelin Kubra Isgor. Many thanks to your help and wise discussions. I would like to thank Prof. Mehmet Bayindir and Prof. H. Volkan Demir and all their support team for their tremendous contributions to the Bilkent community and UNAM.

My heart goes out to my beloved grandfather and two grandmothers, whom I lost during my PhD study. It is hard to accept the absence and I will miss you forever. In addition, I would like to thank my friends for their wise counsel and sympathetic ear. You are always there for me. I could not have completed this dissertation without the support of my friends, Nima Taghipour, Amin Dadvar, Mohammad reza Jokar, Amir Shenasa, Dr. Alireza Dastan, Soheil Firouz, Dr. Muammer Kanli, Dr. Ali Haider, Dr. Talha Masood Khan, Dr. Naveed Mehmood, Jamoliddin Khanifaev, Dr. Petro Deminskyi, Begimai Adilbekova, Yakup Midilli, Arsalan Nikdoost, alireza javanmardi, daniyal namdar, Hamid

Reza Rasouli, Mohammad Fathi Tovini, Dr. Mahdi Shakiba Herfeh and Mirali Jahangirzadeh Varjovi who provided stimulating discussions as well as happy distractions to rest my mind outside of my research.

I wish to acknowledge the support and great love of my parents and siblings, specially my sister Fatemeh and her husband Parviz. They kept me going on and this work would not have been possible without their input.

For the last but the most, I extend my deepest heartfelt thanks to my wife, Bahareh Atashbarghi. It is whole-heartedly appreciated that your great sacrifice for my study proved monumental towards the success of this study. Our sons Nikan and Rayan are smiles of God. They made our life precious and unique. Thank both of you for shaping my life with your existence and heartfelt love. There are more names, professors, colleagues, and friends that I may have forgotten to list here; however, I am very indebted and grateful to each one of them for their support and love.

Contents

1 Introduction **1**

1.1 Droplet-based Microfluidics 2

1.2 Segmented microfluidic system 4

1.3 Droplet length correlations and predictive models 7

1.4 Flow instability 8

1.5 Thesis Outline 9

2 Monodisperse droplet generation using damping effect **12**

2.1 introduction 13

2.2 Hydrodynamic damping using flexible tubing 15

2.3 Damping effect for syringe pump and pressure driven system . . . 19

2.4 Monodisperse droplet generation using hydrodynamic damping . . 24

2.4.1 Experimental setup 25

2.4.2 Numerical modeling 27

2.4.3 Results and discussion 31

2.5 Conclusion 36

3 Ultra monodisperse droplet generation and theoretical limit of droplet monodispersity **37**

3.1 introduction 38

3.2 Theory 39

3.3 Analogy and numerical results 42

3.4 Experimental results 45

4 High throughput ultra-monodisperse droplet generation **62**

4.1 introduction 63

4.1.1 Monodisperse droplet generation using pressure pump . . . 64
4.1.2 Monodisperse droplet generation using syringe pump . . . 72

5 Particle synthesis and reaction kinetics using monodisperse droplets 79
5.1 Silica particle synthesis . . . 80
5.2 PEG particle synthesis . . . 82
5.3 Supramolecular polymer capsule synthesis . . . 85
5.4 Reaction kinetics . . . 86

6 Summary and Future Directions 90
6.1 Summary . . . 90
6.2 Future Directions . . . 91

A Publication List 104

List of Figures

1.1 Various microfluidic droplet platforms: (a) dispensed droplets; (b) slip-chip; (c) digital droplets; (d) segmented flow droplets. 3
1.2 Schematic representation of water droplet generation inside oil (W/O) at different droplet generation regimes in a T-junction microfluidic device: (a) squeezing regime; (b) dripping regime; (c) jet flow. 5

2.1 Schematic of the microfluidic system used to test the effect of the tubing as a hydrodynamic fluctuation damping element. 15
2.2 Pressure recording of syringe pump-driven flow in time (a) and frequency (b) domain for varying lengths of flexible silicone tubing (0, 5, 10, 20, 50 and 100 cm) connecting the pump and the microchannel. 17
2.3 Pressure recording of syringe pump-driven flow in time (a) and frequency (b) domain for varying lengths of rigid PTFE tubing (0, 5, 10, 20, 50 and 100 cm) connecting the pump and the microchannel. 18
2.4 Schematic and circuit representation of microfluidic systems driven by syringe pump or pressure pump. (a) Syringe pump case in which subscripts t and c stand for tubing and channel, respectively. (b) Pressure pump case in which C_a shows the compressibility of the air inside tubing and reservoir. Air tubing is denoted by subscript at. The dotted section shows the analogous electrical model of the fluid tubing in the equivalent circuit model which precedes the inlet of the microfluidic device, which is denoted by node A. . . . 20

2.5 Pressure recording of pressure pump driven flow in time (a) and frequency (b) domain for varying lengths of flexible silicone tubing (0, 5, 10, 20, 50 and 100 cm) connecting the pump and the microchannel. 23
2.6 Schematic of the experimental setup. (a) Syringe pump (SP) actuated system, (b) pressure pump (PP) actuated system, (c) droplet morphometry and velocimetry (DMV) software for calculating droplet area [1]. 26
2.7 COMSOL simulation illustrating formation of the droplet. 29
2.8 Histogram of the droplet area obtained experimentally for 100 droplets, using two different tubing lengths for syringe pump (SP) and pressure pump (PP) driven systems. 32
2.9 Histogram of the droplet area obtained numerically for 36 droplets in three conditions of numerical simulation for SP and PP cases. . 33
2.10 Comparison of droplet lengths obtained experimentally using 20 cm-long tubing and 100 cm-long tubing in two cases: (a) Syringe pump driven system. (b) Pressure driven system. The insets show the normalized droplet lengths, L_d. 35

3.1 Schematic representation of fluidic and electric circuit and numerical results for the effect of fluctuating terms on droplet generation using the conventional (with two separate sources) and the proposed method (with a single source). a, Schematic illustration of the conventional, two source-driven, experimental setup. b, Schematic illustration of the proposed, single source-driven, experimental setup. c, Equivalent circuit of a T-junction droplet generator design driven by pressure supplies. Both two source- and single source (grey background)-driven architectures are shown. d, Fluctuation of $\frac{\alpha'}{\Delta V_c}$ for the conventional and proposed methods. Note that this fraction approaches unity in the proposed method. e, Fluctuation of $\frac{\Delta V_L}{\Delta V_c}$ for the conventional and proposed methods. f, Resultant fluctuations calculated by the difference of the previous two terms, representing the flow rate ratio fluctuations for the conventional and proposed methods. 41

3.2 Electrical circuit equivalent of a T-junction droplet generator used for LTSpice simulation. Two voltage sources analogous to pressure pump are used to supply the desired voltage. The imperfection of the flow source (external fluctuations) is integrated into the voltage source as white noise. Varistors (voltage-dependent resistors) A_1, A_2 and A_3 are used to have periodic fluctuations in $R_m^{'}$, $R_{LP}^{'}$. Note that $A_1 = A_2$ and $R_1^{'} = R_2^{'} = 2R_m^{'}$ for all simulations. s, i, j, c, d and L denote source, inlet, junction, continuous phase, dispersed phase and Laplace Pressure, respectively. 43

3.3 Experimental (a) and numerical (b) results of droplet monodispersity values, %coefficient of variation (CV), obtained for single-source and two-source configurations. a, For the experimental results, an image processing software, Droplet Morphometry and Velocimetry (DMV), was used to measure the size variation of droplets. 150 droplets were measured for each experiment and the mean droplet length was noted. Each experiment was carried out in four repetitions, error bars denote standard deviation. The insets show the normalized size of individual droplets for 700 mbar/7.0V inlet pressure/voltage value. 47

3.4 Electrical circuit equivalent of a T-junction droplet generator. KCL was written for the two nodes A and B which are identified in blue and orange, respectively. 48

3.5 Experimental and numerical results of droplet monodispersity, CV% as a function of Laplace pressure (R_{LP}), main channel length (R_m) and (R_c/R_d) ratio. a, Interfacial tension was reduced by adding SDS to the dispersed phase. b, The main channel length was varied using five different devices, n denotes the number of droplets accommodated in the main channel for each design. Each experiment was carried out in four repetitions, error bars denote standard deviation. c The hydrodynamic resistance ratio was varied using a screw valve located over the dispersed phase inlet. . . 50

3.6 Photograph of the device and experimental results of using two different techniques to make monodisperse droplets in different sizes. a, Photograph of the microfluidic T-junction device with three parallel dispersed phase channels equipped with micro plug valves. b, Droplet lengths for different pressures and hydrodynamic resistance ratios for various micro plug valve configurations. c, Photograph of the microfluidic T-junction device equipped with screw valve. d, Droplet lengths for different pressures and rotation angles of the screw valve. The results are the average length of 100 droplets for each case. 52

3.7 The schematic drawing (a) and the photo (b) of the monodispersity evaluation chip, (c) Pareto chart of effects. The inlets were connected to a single pressure supply (P_{in}) using a bifurcated tubing. A screw valve was used to change the inlet channel resistance ratio (R_c/R_d). The effective main channel length (R_m) was varied using plug valves. Coplanar microelectrodes were used to obtain impedimetric signals. These were analysed in real time using impedimetric droplet measurement (iDM) software to obtain real-time droplet monodispersity, CV%, for any given configuration. 54

3.8 Experimental results of varying inlet pressure (P_{in}), main channel length (R_m) and inlet resistance ratio (R_c/R_d) on droplet monodispersity, CV%. The effect of changing R_c/R_d (for each L_m) on CV% is presented by blue dash lines. The green dash line shows the effect of changing L_m on CV%. 56

3.9 Droplet monodispersity comparison. If multiple CV values are reported in the article, the best-reported value is chosen. Some articles only reported the maximum CV% obtained. 60

4.1 Schematic representation of (a) the conventional and (b) proposed method for supplying fluids. 66

4.2 (a) Experimental results of droplet monodispersity values in different applied pressures. (b) Distribution of normalized size of individual droplets for a single and two pressure sources configuration. 68

4.3 Experimental results of droplet monodispersity, CV% (left y-axix) as a function of main channel length (R_m). Distribution of normalized size of 400 individual droplets is shown in blue dots (right y-axis). The chip is equipped with micro plug valves that allows to have a main channel in five different lengths. The experiments were performed for four iterations. The red circles and boxes show CV% value at each iteration and distribution of CV% values, respectively. 70
4.4 Experimental results of droplet monodispersity, CV% as a function of hydrodynamic resistance ratio (R_c/R_d) for the microfluidic device equipped with the screw valve to adjust the R_c/R_d. 71
4.5 Schematic representation of (a) the conventional and (b) proposed method for supplying fluids. 73
4.6 (a) Experimental results of droplet monodispersity values in different applied flow rates. (b) Distribution of normalized size of individual droplets for single and two flow sources configuration. . 75
4.7 CV% and normalized droplet length results of different elastomeric off-chip tubing lengths for the applied 1 µl/min. 77

5.1 Schematic representation of droplet generation inside T-junction microfluidic device. 81
5.2 Silica Microparticles were synthesized by Interfacial Polymerization. (a) Polydisperse silica particle (CV=4%). (b) Monodisperse silica particle (CV=2.2%). 82
5.3 (a) histogram of droplet length results measured by DMV for single pressure source and conventional method with two pressure sources for the applied pressure of 30mbar. (b) histogram of polyethylene glycol (PEG) particle diameters synthesized using microfluidic system with single pressure source and two pressure sources for the applied pressure of 30 mbar measured by optical image processing. (c) optical image of monodisperse droplets produced applying single pressure source. (d) optical microscopy image of polydisperse droplets produced applying two pressure sources. e) Electron microscopy images of PEG particles. 84

5.4 The schematic representation (a) and the photograph (b) of the microfluidic flow-focusing device used for supramolecular capsule generation. (c) The ultra-monodisperse microdroplets stored in a petri dish. (d) Optical microscopy image of wrinkled shape supramolecular capsules. 85
5.5 Schematic of ultra-monodisperse droplet system used for reaction kinetics investigation. Merging of H_2O_2 and polydopamine droplets were studied. 87
5.6 Fabricated microfluidic device containing two T-junction droplet generation module, a passive droplet merging unit and long channel segments for temporal study of the reaction. 88
5.7 (a) Bulk spectrometer fluorescence intensity at 490 nm in the presence of 1 mM, 5 mM and 10 mM H_2O_2 . (b) Time-dependent fluorescence spectra of PDA inside droplets for 50 mM H_2O_2. . . . 88

A.1 Lab on a Chip cover [2]. 105

List of Tables

2.1 Microfluidic device dimension. 29
2.2 Equivalent circuit parameters. 30

3.1 Microfluidic device dimension. 47
3.2 Experimental results of fluidic evaluation chip. 55
3.3 Overview over different microfluidic droplet generators. 59

Chapter 1

Introduction

This thesis introduces the basis of monodisperse microfluidic droplet generation and its applications. First, a general background and overview of microfluidic systems, specifically the droplet-based microfluidics are provided with a classification of droplet-based lab on a chip platforms and droplet generation regimes. Then, droplet length correlations and the parameters which contribute to droplet size are mentioned. Also, the source and effect of undesired parameters like flow instability that disturb droplet monodispersity are explained. In the following chapters, based on a flow source that is used in the droplet-based microfluidic system, a novel and practical method to decrease the effect of flow instability and therefore making ultra-monodisperse droplets is proposed. We have shown that the presented guidelines is applicable to all common droplet microfluidic systems including a flow source and microfluidic platform. More importantly, we have improved level of droplet monodispersity one order of magnitude, using our universal method. Finally, the application of the monodisperse droplets in reaction kinetics studies and particle synthesis is shown experimentally.

A portion of the content of this chapter was published in [3, 4, 5, 6].

1.1 Droplet-based Microfluidics

The interest in the ability to manipulate fluids at small scale grew steadily leading to a variety of platform technologies. The initial methods in studying microfluidics were mostly inherited from microelectromechanical systems. The microfabricated channels, valves, and pumps were brought together for ingenious applications such as internal combustion [7] and ink-jet printers [8]. As expected, there were apparent advantages of these systems such as having low sample volume, utilization of different performances, higher sensitivity and good control of heat and mass transport. Among all these advantages, having precise control over droplet generation was critical from the beginning. Despite of massive efforts that have been devoted to develop droplet-based techniques, having precise control over droplet size as a key benefit of droplet microfluidic systems, is not boosted enough. While, the other benefits of droplet microfluidic systems such as throughput or making droplet as small as possible have been studied and improved from the very first conventional method of droplet generation.

In general, as a conventional method of droplet generation, droplets could be formed by putting together two immiscible liquids (dispersed phase inside carrier phase) in a batch, so-called emulsion [9]. Although the throughput of such systems has been improved by applying different forms of energy such as finely controlled oscillation [10], shaking [11] or stirring [12] to the mixture of the immiscible liquids, generated droplet size distribution have never meet various demands arising from applications. Since the ability of monodisperse droplet generation at high throughput has been a demanding feature of droplet systems, researchers prefer to use droplet-based microfluidic systems as an alternative to the conventional methods.

Droplet-based microfluidic systems as an alternative to conventional method of droplet generation systems are classified into four categories: dispensed (or printed) droplet systems, segmented droplet systems, digital droplet systems, and slip-chip devices [4]. Schematic representation of these systems is given in Figure

1.1. As seen from this figure dispensed droplet (Figure 1.1a) and slip-chip (Figure 1.1b) devices provide stationary droplets, whereas digital (Figure 1.1c) and segmented (Figure 1.1d) microfluidic systems study moving droplets. Another distinction can be drawn regarding the throughput. Dispensed and digital microfluidic droplet systems are suitable for low-throughput applications, whereas slip-chip and segmented droplet systems can be preferred for high-throughput uses.

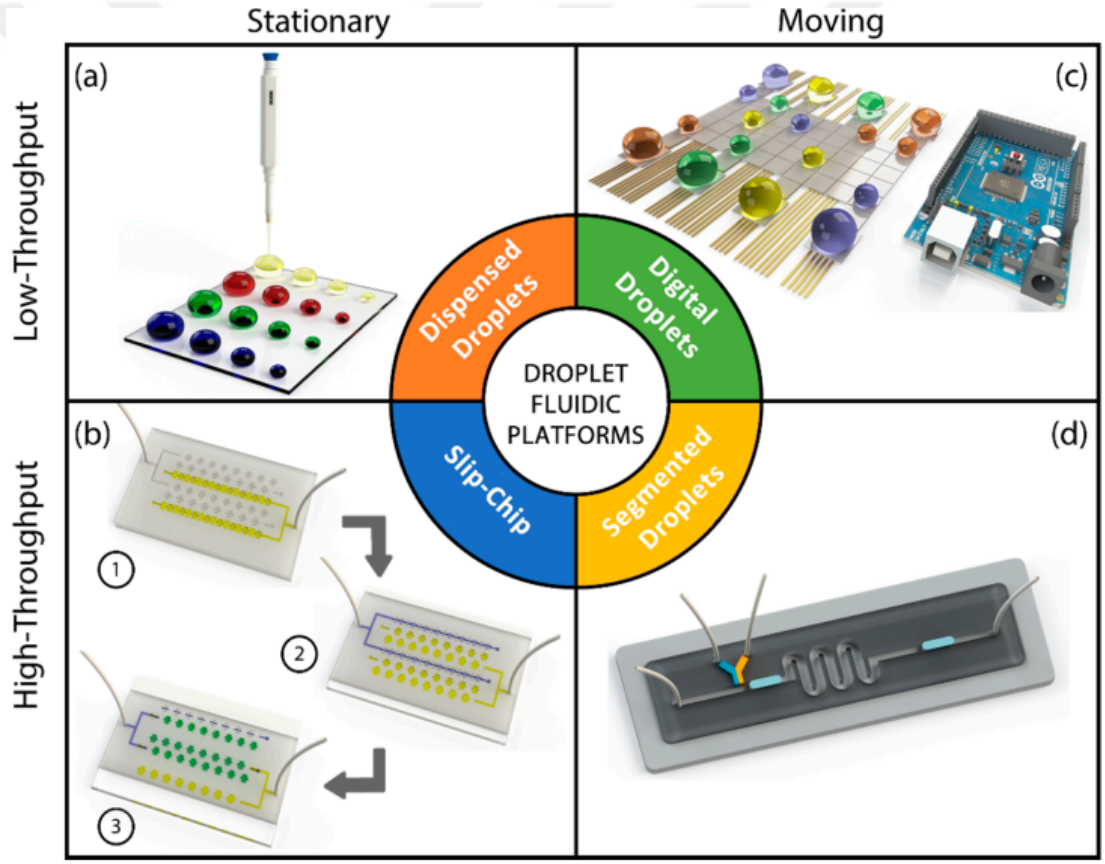

Figure 1.1: Various microfluidic droplet platforms: (a) dispensed droplets; (b) slip-chip; (c) digital droplets; (d) segmented flow droplets.

In this thesis, we have used segmented microfluidic systems since they are the most preferred droplet-based systems which are based on compartmentalization of one fluid (dispersed phase) within another fluid (continuous phase) inside microchannels (Figure 1d) [13].

1.2 Segmented microfluidic system

A typical segmented microfluidic system includes a flow source and a microfluidc platform where two immiscible fluids mostly water and oil are introduced. Using a flow source, which is mostly a pressure or a syringe pump, the two fluids are supplied to different channel of a microfluidic platform that end at an intersection point. Based on the competition between surface tension and viscous drag force across an interface between the two immiscible fluids, the droplets form in different rates at the intersection point [14]. Also, depending on having hydrophobic or hydrophilic surface of the channel after intersection point, water droplet inside oil (W/O) or oil droplet inside water (W/O) can be made, respectively [15]. The two most preferred geometries used at these systems are T-junction [14] and flow-focusing [16] geometries that can both operate in different flow regimes such as squeezing, dripping, and jetting [17] (Fig. 1.2).

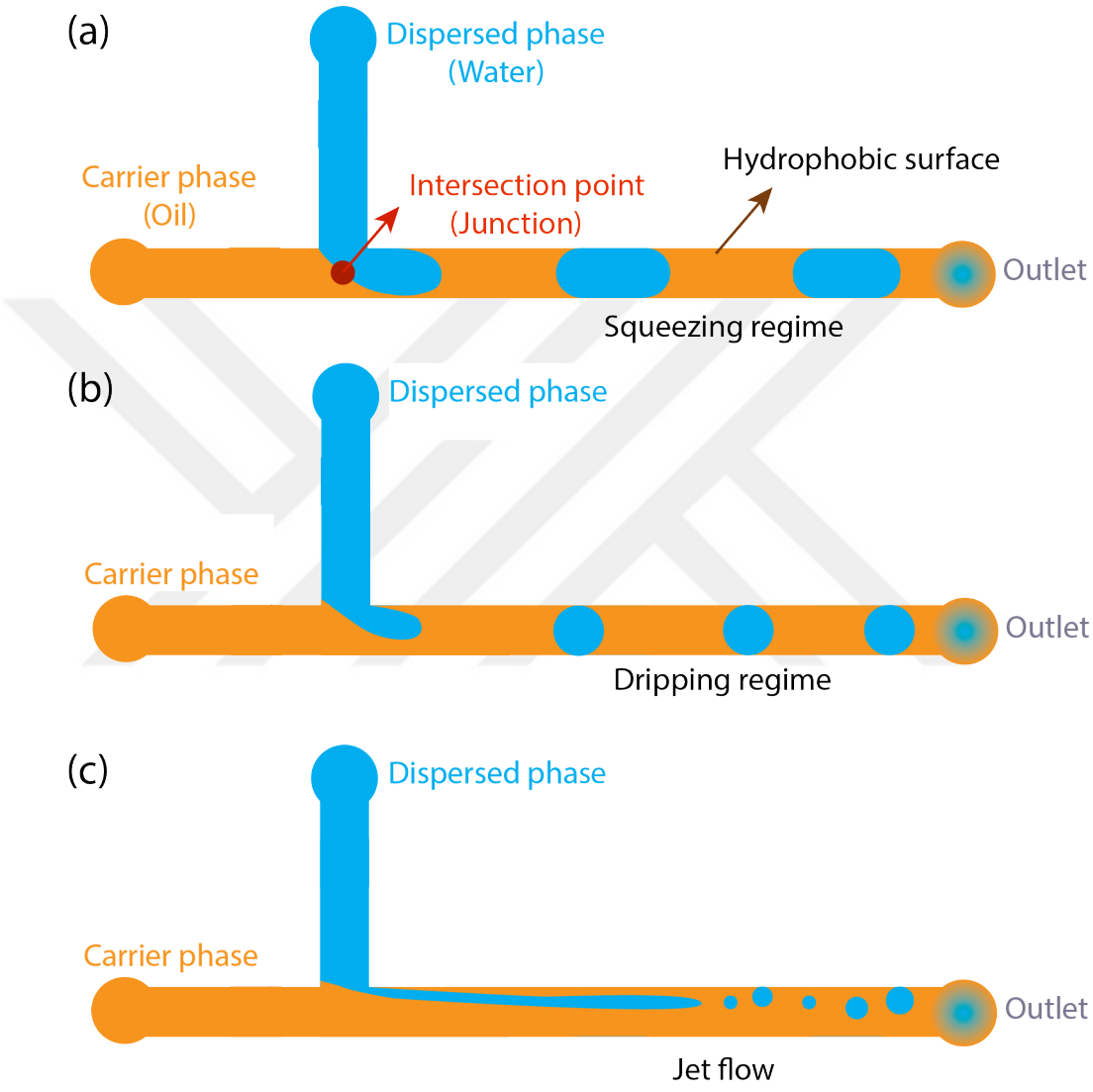

Figure 1.2: Schematic representation of water droplet generation inside oil (W/O) at different droplet generation regimes in a T-junction microfluidic device: (a) squeezing regime; (b) dripping regime; (c) jet flow.

Based on the capillary number ($Ca = \frac{\eta u}{\sigma}$, where η, u are viscosity and velocity of the continuous phase, respectively, and σ is the interfacial tension between the two immiscible fluids), these different regimes of droplet generation are identified. In other words, the capillary number reflects the competition between

surface tension and viscous drag force. For capillary number less than 0.01, the generated droplet shows plug-like shape constrained by the channel wall, named as squeezing regime (Fig. 1.2(a)). As Ca increases, the droplet shape turns to isolated sphere, and its size does not change for a relatively large range of Ca, named as dripping regime (Fig. 1.2(b)). At Ca larger than 0.1, the droplet detachment point gets far away from the junction (where the two immiscible fluids meet), which leads to small polydisperse spherical droplet formation, say jet flow [18] (Fig. 1.2(c)). The size of droplets and frequency of droplet generation can be modulated by channel geometry and applied pressure or flow rate. The presence of a microchannel provides these systems an exquisite control on droplet positioning that is used for multiple droplet operations such as droplet transporting, merging, splitting and mixing [19]. Thanks to these features, such microfluidic droplet generators enabled encapsulation of biological materials such as nucleic acids, proteins, virus, single cells, into desired size of individual droplets. Also, the ability to manipulate droplets by merging, splitting, sorting, restoring, incubating these droplets provided the researchers a plethora of tools and interesting features that they can combine for their application of interest.

An awareness of the achievable high level of droplet monodispersity can open new avenues for desired applications of droplets. To this end, a thorough understanding of droplet generator technologies is required when aiming for ultra-monodispersity of droplets. In this thesis, we aim to analyze and improve droplet monodispersity as a key benefit of droplet-based microfluidic systems. As also can be seen from the exemplary systems covered in this thesis, analyzing droplet monodispersity in a segmented microfluidic system, including a flow source and microfluidic platform, requires understanding every single parameter that affect droplet size. Therefore, in this thesis, instead of classifying the droplet-based microfluidic systems in terms of microfluidic platforms or different droplet generation regimes, we prefer to focus on the analysis of parameters like flow instability which has a significant effect on droplet monodispersity. This way, we can lay out the universal monodisperse droplet generation methods that can be used for any given flow source or microfluidic device.

Note that, in this thesis, we analyze droplet monodispersity in the two common

segmented microfluidic system, T-junction and flow-focusing, at squeezing and dripping regimes.

1.3 Droplet length correlations and predictive models

As discussed before, in order to improve level of droplet monodispersity we need to know fundamental parameters which contribute to droplet formation. For that, we did a review on a droplet length correlations in common microfluidic devices; T-junction and flow-focusing device. As explained in the previous section, competition between surface tension and viscous drag forces influences the droplet formation and dictates the droplet size [14]. Several groups have discussed and analyzed parameters that contribute to droplet size to have a better understanding of the reason behind droplet size variation. They have shown that for the most commonly used microfluidic devices such as T-junction, flow-focusing, and co-flow there is a correlation between the length of a droplet, geometrical parameters, volumetric flow rate ratio of dispersed and continuous phases, and capillary number ($Ca = \frac{\eta u}{\sigma}$, where η, u are viscosity and velocity of the continuous phase, respectively, and σ is the interfacial tension between the two immiscible fluids) [20, 21, 22]. In 2005 Ward et al. experimentally studied the microdroplet production in a flow-focusing geometry using either the flow-rate ratio or the inlet pressure ratio as the flow-control parameter. They gave empirical correlation obtained by a best fit of the data which indicates a power-law relationship between droplet length and flow rate/pressure ratio:

$$\frac{l}{a} = 2.35(\frac{Q_w}{Q_o})^{0.25} \tag{1.1}$$

$$\frac{l}{a} = 8.45(\frac{P_w}{P_o})^2 \tag{1.2}$$

where $l, a, Q_w/P_w$ and Q_o/P_o are droplet length, junction contraction width, water and oil flow rate/pressure, respectively. In 2006, for a T-junction microfluidic device, Garstecki et al. suggested a quantitative model for the plug-like droplet

length which was valid in squeezing regime. The model had a good agreement with experimental results in squeezing regime.

$$\frac{L}{w} = 1 + \alpha \frac{Q_d}{Q_c} \tag{1.3}$$

where L, w, Q_d and Q_c are droplet length, channel width, dispersed phase and continuous phase flow rate, respectively. Also, α is a constant depending on geometrical parameters in the T-junction microfluidic device. Two years later, Xu et al. improved the correlation between droplet length and flow rate ratio by taking capillary number into account. They presented correlations which is valid for the dripping, squeezing and transient regimes.

$$\frac{l}{w} = 0.75(\frac{Q_d}{Q_c})^{1/3}(\frac{1}{Ca_c})^{1/5} \tag{1.4}$$

$$\frac{l}{w} = 1.59(\frac{Q_d}{Q_c})^{1/5}(\frac{1}{Ca_c})^{1/5} \tag{1.5}$$

where equation 1.4 and 1.5 are for a T-junction and flow-focusing device, respectively. In the all mentioned correlations, the droplet size is strongly affected by the channel dimension and flow rate/pressure ratio. Since the channel dimension does not change during experiment, flow rate/pressure ratio is the critical parameter that plays a significant role in droplet formation. Thus, ideally, keeping the flow rate ratio constant would result in the generation of identical droplets. In other words, any kind of alteration in the flow rate/pressure of the fluids results in fluctuations in the size of the droplets.

1.4 Flow instability

Experimental and numerical analysis have shown that droplet uniformity suffers from two sources of the fluctuations that are classified into an external and internal one [23]. External fluctuation is due to the mechanism of the flow sources that are used to introduce fluids to the chip, whereas inherent fluctuation, so-called internal fluctuation, is due to the pressure fluctuation at the point of droplet formation, which is owing to the variation of the hydrodynamic resistance of the main channel when droplets enter or leave the main channel. Based on how we

drive the fluids, either internal or external fluctuation will be dominant. Although some simple and applicable ways have been used to decrease external fluctuations due to the flow source, eliminating those oscillations is arduous. Also, it is not possible to omit internal fluctuation since it is inherent and in the nature of formation and motion of droplets inside the microfluidic device [5]. However, it has been shown that working at high capillary number leads to having less pressure oscillation at the junction of microfluidic droplet generator [24, 25]. Although diminishing internal or external fluctuations will lead to more uniformity and stability of droplet generation, experimental efforts to obtain monodisperse droplets have been hampered by the microfluidic device cumbersomeness or the lack of high-quality flow sources.

1.5 Thesis Outline

At this thesis, we show that achieving ultra monodisperse droplets requires a good analysis of the droplet generation rather than a precise pump or complicated feedback systems. This thesis has primarily focused on generating extremely monodisperse droplets and its biochemical applications such as reaction kinetics study and particle synthesis using a simple universal method.

The ultimate aim of this study is to analyze and do ultra-monodisperse droplet generation using a simple universal method. The significance of this study is that such a holistic analysis and proposed method explains the whole story behind droplet monodispersity and applies to all common microfluidic devices. Also, it brings benefits in terms of cost, availability, portability, simplicity and number of flow source required for droplet generation. Our central goal is introducing a new approach to analyse droplet size variation that eventually leads to a thorough understanding of the root causes of droplet polydispersity. We model the dynamics of a segmented two-phase flow system using a single-phase flow analogy, electron flow, in electrical circuits. Finally we present flow source and design recommendations that enables achieving absolute droplet monodispersity, i.e. 0% CV. In addition, we compare the performance of common flow sources such as pressure

driven and displacement pump that are used in a droplet microfluidic systems in terms of droplet monodispersity. Also, using a T-junction or flow-focusing microfluidic device and a pressure pump, we synthesize mesoporous silica particle, polyethylene glycol (PEG) and supra-molecular capsules in a well-ordered packed pattern. Also, using monodisperse droplets, the reaction kinetics of poly dopamine and hydrogen peroxide has been investigated.

The rest of the thesis is organized as follows:

In Chapter 2, we describe a simple and practical method that enables damping external fluctuations due to the flow source. We demonstrate that compliance of elastomeric off-chip tubings can be used to damp fluctuations and lead to steady flow rates. We analyze the whole microfluidic system using electrical circuit analogies, and demonstrate that off-chip compliances are significant, especially for displacement pump driven systems. Additionally, we demonstrated that pressure pumps inherently use this effect, and have so far led the high performances reported in the literature in terms of droplet monodispersity.

In Chapter 3, we present an analytical approach that takes into account all the system dynamics and internal/external factors that disturb monodispersity. Interestingly, we are able to model the dynamics of a segmented microfluidic system using a single-phase flow analogy, electron flow, in electrical circuits. We offer a unique solution and design guidelines to ensure ultra-monodisperse droplet generation. Our analytical conclusions are experimentally verified using a T-junction droplet generator. Equally importantly, we show the limiting experimental factors for reaching the theoretical maximum of monodispersity.

In Chapter 4, we compare the performance of the syringe pump and pressure pump as a flow source for supplying fluids with the conventional and proposed method (presented in chapter 3) in terms of droplet monodispersity. We show that supplying an identical flow rate/pressure from a single source makes the microfluidic droplet system immune to the external fluctuations that come from the imperfection of a flow source. Also, we show that the proposed design guidelines are applicable for common microfluidic devices, with either T-junction or

flow-focusing.

In Chapter 5, we study the reaction kinetics of poly dopamine and hydrogen peroxide and synthesize silica and polyethylene glycol (PEG) particles and supramolecular capsules in very low polydispersity using all of the guidelines presented in the previous chapters (3 and 4).

In Chapter 6, we give our concluding remarks and propose several future directions towards which this study could go on.

Chapter 2

Monodisperse droplet generation using damping effect

Monodispersity of microdroplets formed by microfluidic droplet generation systems is influenced by the internal pressure fluctuations due to droplet formation and external fluctuations caused by flow sources. It is critical to minimize these fluctuations which requires a thorough analysis of the source of unsteadiness. At this chapter, we present a method that can be used to analyze the whole droplet generation system including the off-chip components and the microchannel for both displacement driven and pressure driven systems. A T-junction microfluidic droplet generator is used as a model system and droplets are produced by using either a syringe pump or a pressure pump. Also, we demonstrate a way to model a microfluidic droplet generation system using numerical simulations and electrical circuit analogy of fluidic systems considering hydrodynamic resistance and compliance of system components. We provide a method to dampen the fluctuations caused by external flow sources, thus achieving a much higher droplet monodispersity. Applying this method, droplet monodispersity obtained using a syringe pump driven system was increased from 4.5% CV to 0.4% CV.

The content of this chapter was published in [5] as; Kalantarifard. Ali and

Alizadeh-Haghighi. Elnaz and Elbuken. Caglar, Damping hydrodynamic fluctuations in microfluidic systems, Chemical Engineering Science, vol. 178, pp. 238-247, 2018.

2.1 introduction

Flow instability, reflected in the microfluidic system as pressure or flow rate fluctuations, is the source of droplet polydispersity. First step to improve droplet monodispersity is diminishing those fluctuations which mostly come from flow sources. There are two kinds of fluctuations, which affect droplet monodispersity: inherent fluctuations related to the generation and motion of droplets inside the main channel (the channel that occupies droplets) [26, 23, 27] and external fluctuations due to the flow sources [28, 29, 30, 31]. It has been shown that for commonly used syringe pump driven droplet systems, the external fluctuation due to the stepper motor in the syringe pump dominates the inherent fluctuations inside the microchannel [32]. Efforts have been devoted to analyze and minimize these external fluctuations to generate highly monodisperse droplets [29].

Several studies have focused on differences between displacement driven and pressure driven microfluidic droplet systems in terms of the monodispersity of droplet generation. It has repeatedly been shown that pressure pumps perform better than syringe pumps to achieve higher droplet monodispersity [28, 31]. As a more in-depth analysis the fluctuations caused by flow sources has been characterized by a non-dimensional analysis using Strouhal number [32]. It has been shown that using softer polydimethylsiloxane (PDMS) channels, by increasing the base polymer / curing agent ratio, fluctuations can be dampened. Similarly, in another study it has been shown that making a PDMS microchannel in which one surface is composed of a thin layer acting as a membrane, fluctuations can be damped and droplet monodispersity can be improved [33]. Although these studies demonstrate improvements in droplet monodispersity, they have several limitations. These approaches are bound to elastomeric microchannels and need modification of the microchannel design, to incorporate membrane-like surfaces,

or modification of channel elasticity which can only be varied within a tight window. Additionally, softening the PDMS channels makes them susceptible to pronounced leeching and adsorption issues. Here, we propose a more effective and widely applicable solution to improve droplet monodispersity by controlling off-chip compliance to minimize fluctuations due to flow sources. Our approach is applicable to both elastomeric (PDMS) and rigid (acrylic, polycarbonate, glass) microfluidic devices.

We demonstrate a holistic approach in designing microdroplet generation systems which considers resistive and compliance effects of off-chip components and microchannels. We model a T-junction droplet generation system using an equivalent electrical circuit model and demonstrate the fundamental difference between pressure driven and displacement driven microdroplet generators. This approach laid out that pressure pump systems inherently make use of compliance effect which decrease the uncertainty and the pressure fluctuation caused by the pressure regulator, thus achieve the higher monodispersity results demonstrated in the literature. However, since syringe pump driven systems are set by bubble-free connections and lack such a dampening mechanism, so far they remained inferior. We demonstrate that adding off-chip compliances to syringe pump driven systems has a significant effect on improvement of fluctuation dampening which results in remarkable enhancement in microdroplet monodispersity. Resultantly, we show that syringe pump driven systems are not destined to perform low on droplet monodispersity.

We present a very effective way to considerably reduce the fluctuations caused by flow sources by adding compliances upstream the microchannel inlets. Tuning compliance of the system by altering the inlet tubing length, the droplet monodispersity was investigated for syringe pump (SP) and pressure pump (PP) driven systems. Additionally, we have quantified the effect of internal and external fluctuations on droplet monodispersity using numerical modelling. Comparing droplet monodispersity obtained in the simulations with and without inlet fluctuations, we were able to analyze the impact of external fluctuations on droplet monodispersity. In the literature the best coefficient of variation (CV) of droplets that have been achieved using T-junction devices is in the range of

1-3% [34, 35, 36, 33, 37]. However, in this thesis it was demonstrated that using a syringe pump with long-enough flexible tubing is a practical and effective way of generating highly monodisperse droplets with CV of less than 0.4%.

2.2 Hydrodynamic damping using flexible tubing

The proposed damping mechanism uses a flexible tubing that connects a pump to the microfluidic device, as shown in Fig. 2.1.

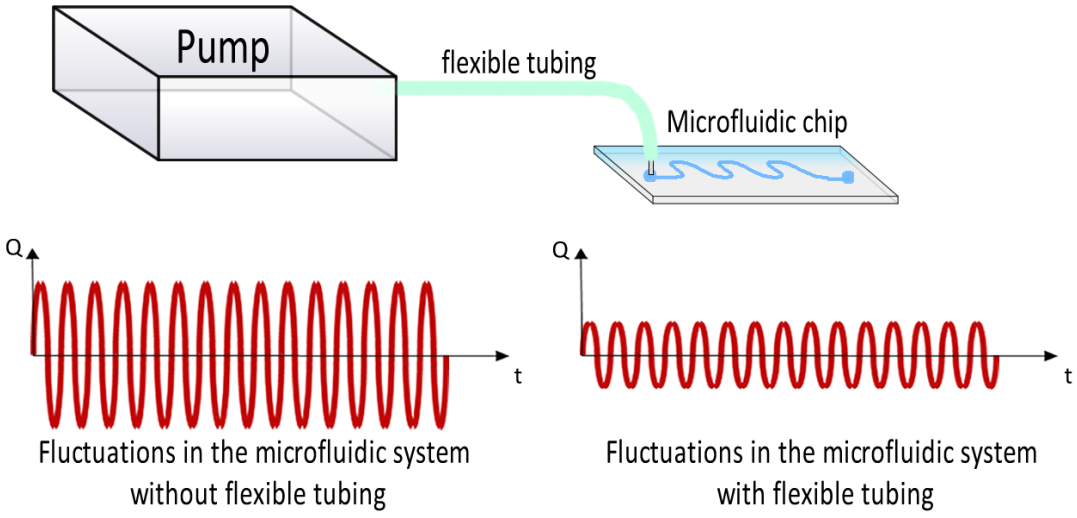

Figure 2.1: Schematic of the microfluidic system used to test the effect of the tubing as a hydrodynamic fluctuation damping element.

Experiments have been conducted to show the performance of the flexible tubing, which functions similarly to a low-pass filter in electrical circuits. The initial experiments were performed using a syringe pump-driven flow along a PDMS microfluidic device. The 5-cm long microchannel has one inlet and one outlet; the width and height of the channel is 300 µm and 80 µm, respectively. The mold was prepared using a silicon substrate with SU-8 photoresist patterning. Sylgard 184 silicone elastomer, mixed at a weight ratio of 10:1 base polymer to

curing agent (Dow Corning Corp), was used to fabricate the microchannels. After the bubbles were removed, the mixture was poured onto the mold and heated on a hotplate at 90 °C for 8 hr. Then, inlet/outlet holes were punched, and PDMS channel was bonded to a glass slide using O_2 plasma activation. Silicone oil (SF 50) with a density and dynamic viscosity of 1000 kg/m^3 and 50 mPa s was driven through the microchannel. The sample was introduced to the microchannel at a constant flow rate of 3 µl/min using a syringe pump (KDScientific 270).

The fluidic connection from the pump to the microchip was made using five different lengths of tubing (5, 10, 20, 50 and 100 cm). First, flexible silicone tubing (Cole-Parmer) with 0.8 mm inner diameter (I.D.) and 2.4 mm outer diameter (O.D.) was used. The Young's modulus and Poisson's ratio of the flexible tubing are 1.9 MPa and 0.48, respectively. Then, rigid PTFE tubing was used for comparison. The rigid tubing (Cole-Parmer) has an I.D. of 0.8 mm and O.D. of 1.41 mm. Young's modulus and Poisson's ratio of the rigid tubing are 334.7 MPa and 0.48, respectively.

A pressure sensor (Honeywell 40PC015G1A 0-15 psi) was used for continuous monitoring of pressure fluctuations caused by the flow source. The pressure sensor has a linear response with an accuracy of 0.2% and sensitivity of 266.6 mV/psi. The pressure values were recorded using a data acquisition unit (NI DAQ Pad-6015). The data were processed using Matlab, and the time domain and frequency domain signals for different lengths of flexible and rigid tubings are shown in Figs. 2.2 and 2.3, respectively.

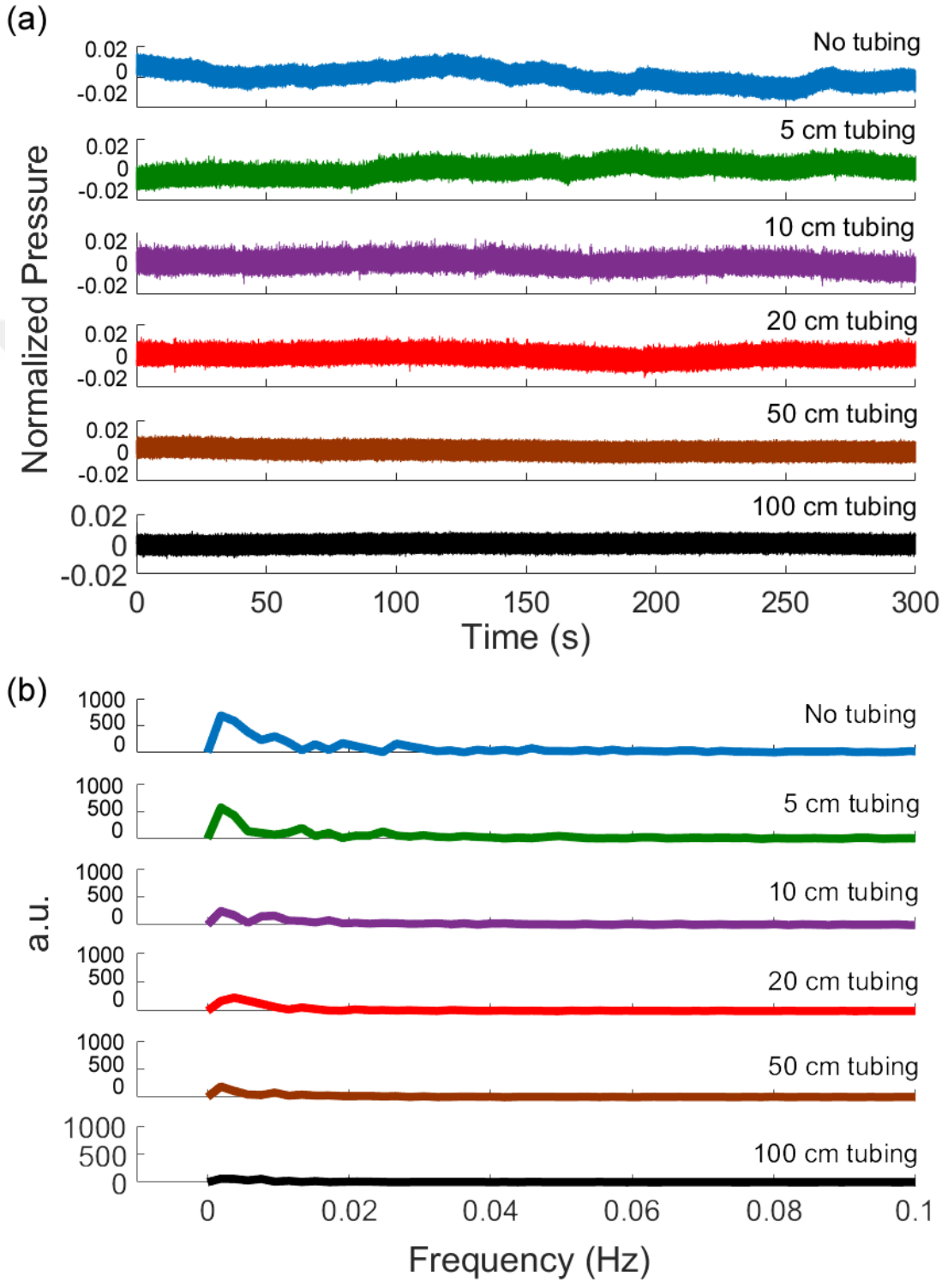

Figure 2.2: Pressure recording of syringe pump-driven flow in time (a) and frequency (b) domain for varying lengths of flexible silicone tubing (0, 5, 10, 20, 50 and 100 cm) connecting the pump and the microchannel.

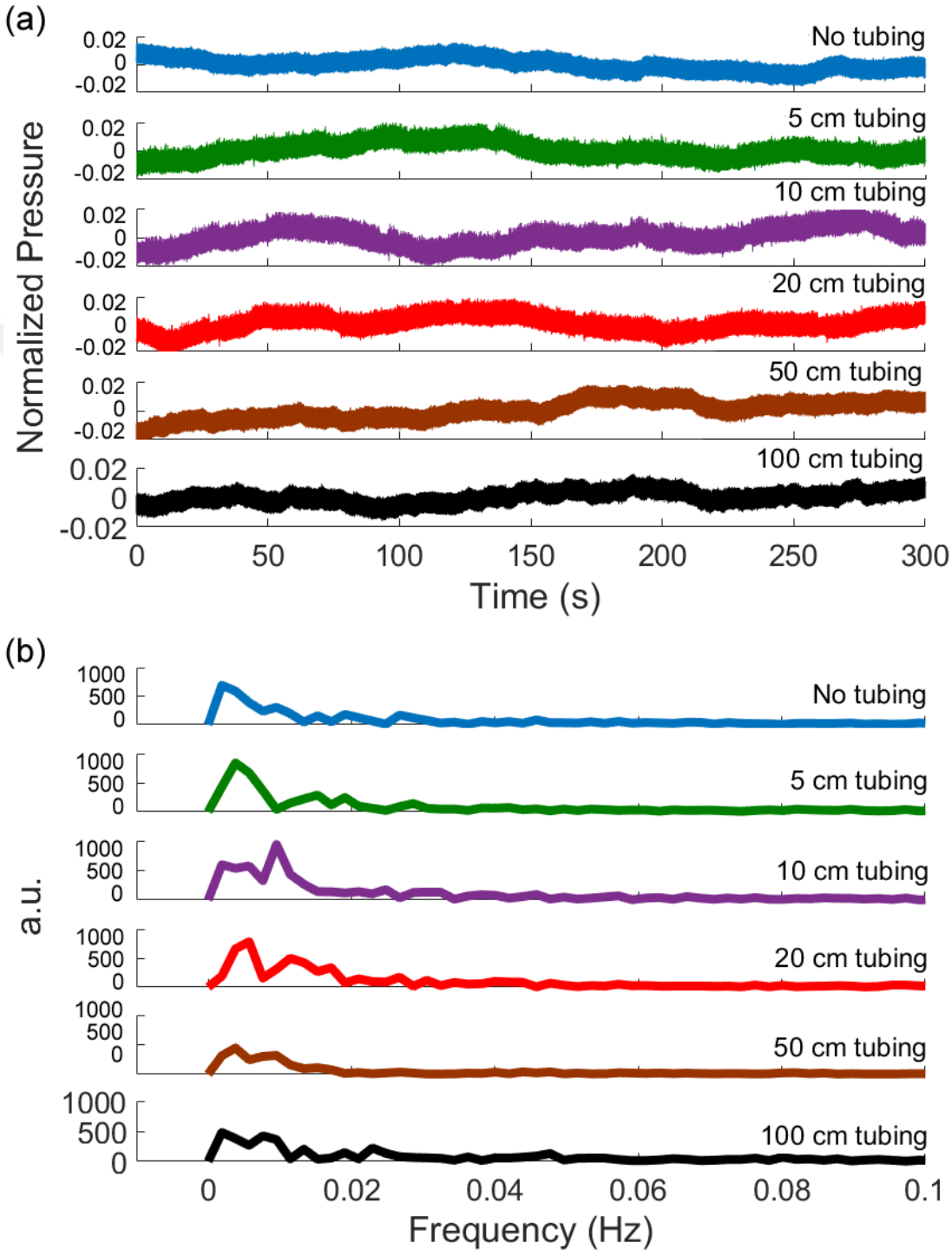

Figure 2.3: Pressure recording of syringe pump-driven flow in time (a) and frequency (b) domain for varying lengths of rigid PTFE tubing (0, 5, 10, 20, 50 and 100 cm) connecting the pump and the microchannel.

As demonstrated in Fig. 2.2, increasing the tubing length from 5 to 100 cm has a remarkable effect on fluctuation damping. Fig. 2.2a shows the normalized pressure values read by the pressure sensor placed at the outlet of the syringe pump. Fig. 2.2b shows the frequency components of the time domain signals, shown in Fig. 2.2a, after Fourier transform. The comparison of the time domain and frequency domain signals shows that increasing the length of flexible tubing decreases hydrodynamic pressure fluctuations.

As a control experiment, a similar measurement was performed using rigid PTFE tubings of the same length, as shown in Fig. 2.2. The results given in Fig. 2.3 show that almost no difference was observed in terms of pressure fluctuations when the tubing length was increased. During these measurements, rigid connectors (ColeParmer) were used to prevent additional compliance, so that only the effect of the tubing were analyzed.

2.3 Damping effect for syringe pump and pressure driven system

The development of rapid fabrication methods has enabled researchers to prototype microfluidic systems fairly easily. This sometimes leads to an oversimplification of the design process, which requires modeling of the systems parameters for demanding applications. Hydrodynamic damping and obtaining stable flow conditions is one of the cases that require modeling of the whole microfluidic system. Analysis of the system characteristics and optimization of each component is routinely performed for electrical circuit design. Thankfully, fluidic circuits can also be modeled using electrical circuit analogy and using the tools available for electrical engineers [38]. We apply this approach to model the hydrodynamic damping effect and demonstrate the differences between syringe pump- and pressure pump-driven systems as illustrated in Fig. 2.4a and b, respectively. The equivalent circuit component for any flexible structure in the system, such as tubing (t) or channel (c), includes a resistor (R_t, R_c) and a capacitor (C_t, C_c)

[39]. The resistor is placed as two half-value resistances in series, so that the compliance of the tubing is applied at mid-length. Moreover, there is capacitance for the pressure pump-driven system, due to the compressibility of the air (a) inside the reservoir (C_a), and through the tubing in the pressure regulator chamber (C_{at}). The equivalent circuit model makes it possible to analyze the effect of different parameters such as tubing length, diameter, Young's modulus and reservoir air volume on the fluctuations due to the flow source.

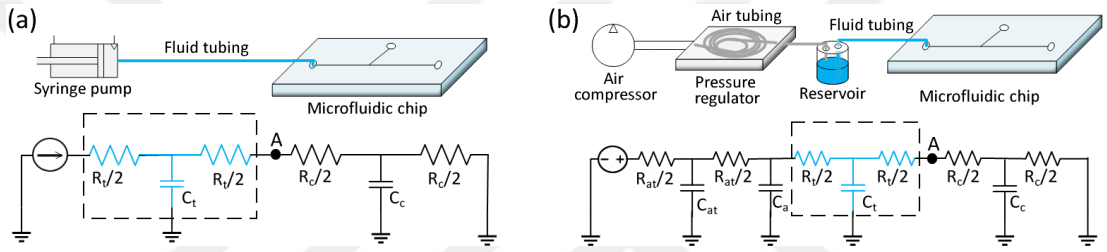

Figure 2.4: Schematic and circuit representation of microfluidic systems driven by syringe pump or pressure pump. (a) Syringe pump case in which subscripts t and c stand for tubing and channel, respectively. (b) Pressure pump case in which C_a shows the compressibility of the air inside tubing and reservoir. Air tubing is denoted by subscript at. The dotted section shows the analogous electrical model of the fluid tubing in the equivalent circuit model which precedes the inlet of the microfluidic device, which is denoted by node A.

The components in the electrical circuit model can be calculated analytically. The Hagen–Poiseuille Law for the laminar steady state flow of incompressible fluid at constant flow rate through a finite geometry is stated as:

$$\Delta P = R_H Q \tag{2.1}$$

where ΔP is the pressure drop, R_H is hydrodynamic resistance and Q is the flow rate along the conduit. For a cylindrical tubing, R_H is defined as:

$$R_h = 8\eta L/\pi r_i^4 \tag{2.2}$$

where η is the fluid dynamic viscosity, L is the tubing length, and r_i is the tubing inner radius. For a rectangular microchannel (width w and height h), with a high

aspect ratio ($w < h$), the hydrodynamic resistance can be calculated as in [38]:

$$R_h = \frac{12\eta L}{wh^3(1 - \frac{0.63h}{w})} \tag{2.3}$$

The pressure change caused by the conduit flexibility or fluid compressibility results in change in the volume of the fluid along the conduit. This behavior is similar to the capacitance in the electric circuit. Therefore, the hydrodynamic capacitance is defined by the following equation:

$$Q = \frac{dV}{dt} = \frac{dV}{dP}\frac{dP}{dt} = C_h\frac{dP}{dt} \tag{2.4}$$

where C_h is the hydrodynamic capacitance. Due to the internal pressure induced by the fluid, the shape of the flexible tubing changes in the radial direction. For the elastic thick wall tube, which is subjected only to internal pressure, the elastic stresses on the internal surface of the tubing are given by the Lame equations [40].

$$\sigma_r = -P \qquad \sigma_\theta = \frac{(r_i^2 + r_o^2)P}{(r_o^2 - r_i^2)} \qquad \sigma_a = \frac{r_i^2 P}{(r_o^2 - r_i^2)} \tag{2.5}$$

where σ_r, σ_θ and σ_a, are radial stress, circumferential stress and axial stress, respectively, while r_i and r_o stand for inner and outer radiuses, respectively, and P indicates internal pressure. Using $V = \pi r_i^2 L$ and $dV = 2\pi r_i L.dr$, the radial strain (ϵ_r) is determined as:

$$\epsilon_r = \frac{dr}{r_i} = \frac{dV}{2\pi r_i^2 L} \tag{2.6}$$

where L and V are the length and volume of the tubing, respectively. According to Hook's law, for an isotropic material, the radial strain is proportional to the stress as follows:

$$\epsilon_r = \frac{1}{E}[\sigma_r - \nu(\sigma_\theta + \sigma_a)] \tag{2.7}$$

where E and ν are Young's modulus and Poisson's ratio, respectively. Using Eqs. 2.4-2.7, the hydrodynamic capacitance of the tubing (C_t) is defined as:

$$C_t = \frac{2\pi r_i^2 L[(1+\nu)r_o^2 - (1-2\nu)r_i^2]}{E(r_o^2 - r_i^2)} \tag{2.8}$$

which is proportional to the tubing length. In addition, the capacitance of the rectangular microchannel (C_c) is defined as [41]:

$$C_c = \frac{\alpha h w L(1+\nu)}{E} \tag{2.9}$$

where h, w and L are the height, width and length of the channel, respectively. Poisson's ratio and Young's modulus of PDMS was taken as 0.5 and 2 MPa, respectively. In addition, a is approximately constant for a given microchannel and on the order of 1 [41]. In addition, there is another capacitance due to the compressed air inside the tubing and reservoir for the pressure pump-driven system. The compressibility of the air (β) is defined as:

$$\beta = -\frac{1}{V}\frac{\partial V}{\partial P} \tag{2.10}$$

From Eq. 2.10, and due to air compression, we have:

$$Q = -\frac{dV}{dt} = V(-\frac{1}{V}\frac{\partial V}{\partial P})\frac{dp}{dt} = V\beta\frac{dp}{dt} \tag{2.11}$$

Using the ideal gas law and Eqs. 2.10 and 2.11, the air capacitance (C_a) is defined as:

$$C_a = \frac{V}{P} \tag{2.12}$$

This analysis allows one to derive the equivalent model of a microfluidic system. Additionally, it should be noted that the flow sources in Fig. 2.4 were modeled as current and voltage sources for the syringe pump and pressure pump, respectively. In the previous section, we demonstrated that by using a flexible tubing to connect a syringe pump to a microfluidic channel, hydrodynamic fluctuations can be damped to varying extents, depending on the tubing length. We repeated the same experiment for a pressure pumpgenerated flow. A pressure pump (Elveflow OB1) was connected to the PDMS microchannel using flexible silicone tubing of varying lengths. Pressure was set to a constant 150 mbar, so that the mean flow rate at the microchannel was the same as in the syringe pump-driven system, explained in Fig. 2.2. The pressure values recorded for a time duration of 300 s were given in Fig. 2.5, in both time domain and frequency domain. As seen, there is only marginal increase in the hydrodynamic fluctuation damping with increasing tubing length. The comparison between Figs. 2.2 and 2.5 demonstrates that the damping effect of the flexible tubing is much more significant in the case of a syringe pump-driven system, compared to a pressure pump-driven system.

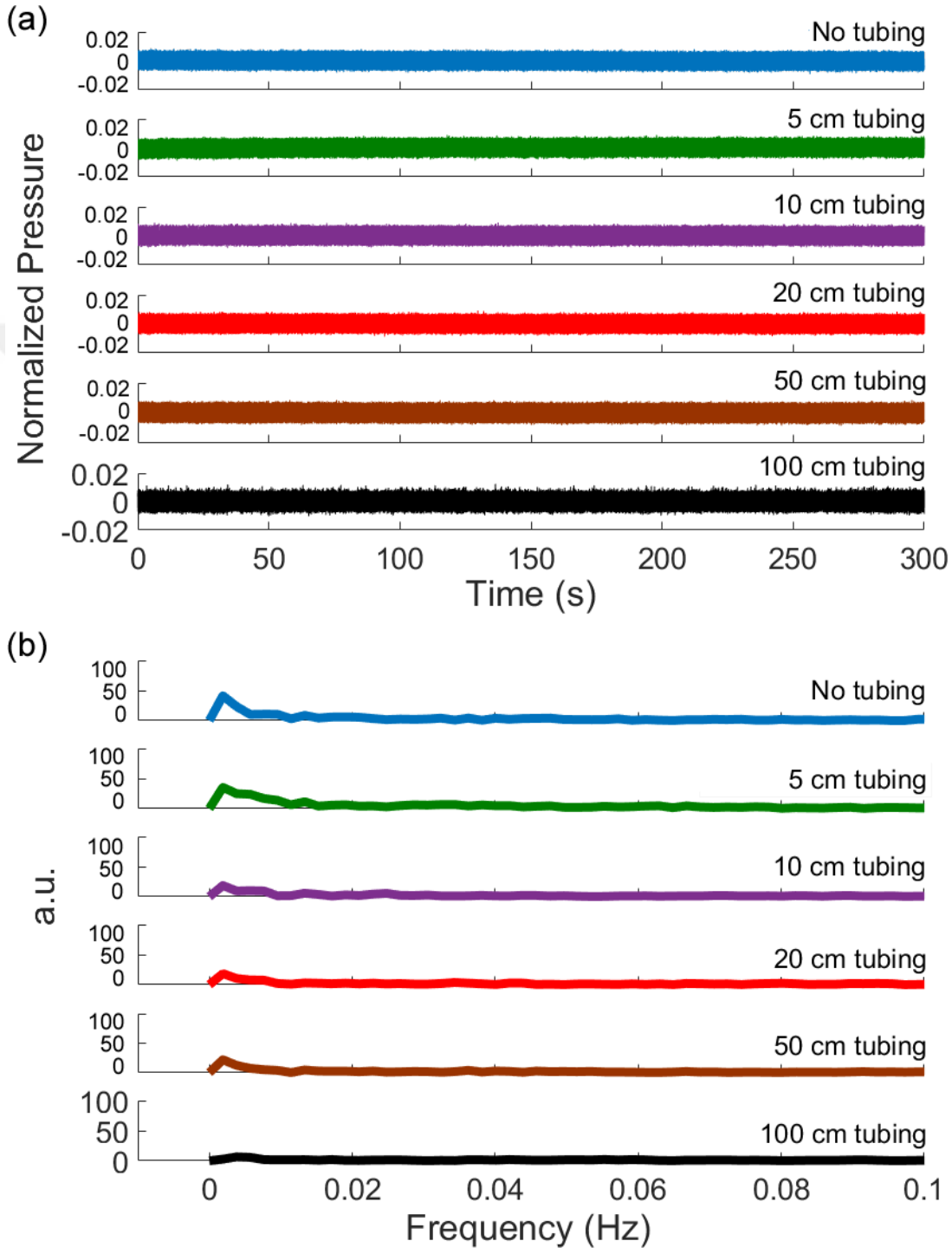

Figure 2.5: Pressure recording of pressure pump driven flow in time (a) and frequency (b) domain for varying lengths of flexible silicone tubing (0, 5, 10, 20, 50 and 100 cm) connecting the pump and the microchannel.

This observation can be explained by calculating the compliance values for the pressure-driven flow shown in Fig. 4b. When 100-cm long silicone tubing was used, C_t is 5.84×10^{-13} m^3/Pa, whereas C_{at} and C_a values are 5.1×10^{-9} and 1.53×10^{-9} m^3/Pa, respectively. Thus, the compliance effect of the tubing is negligible compared to the compliance of the air inside the fluidic system. These results clearly demonstrate that pressure pumps operate with an inherent hydrodynamic damping mechanism. Therefore, the contribution of the additional damping, due to the flexible tubing used upstream the microchannel inlet, is relatively low, depending on the pump's internal tubing parameters (length, Young's modulus, and inner diameter), the air volume left in the sample reservoir, and the supplied pressure.

2.4 Monodisperse droplet generation using hydrodynamic damping

Droplet-based microfluidics is an important class of microfluidic platforms, utilized in many biochemical analyses. Using droplet-based systems, one can carry out experiments rapidly and perform reactions in a large number of isolated droplets. Access to a large number of identical droplets enables researchers to obtain a uniform and reliable pack of data for analysis. One of the most common rationales for using droplet-based systems is the ability to form monodisperse droplets. To understand the governing physics, earlier studies on droplet monodispersity focused on controlling the parameters that contribute to droplet size such as surfactant, wettability, flow rate ratio, interfacial tension, viscosity ratio, microchannel geometry and capillary number [21, 42, 43, 44, 45, 46, 47, 22, 48, 49]. More recently, the contribution of flow sources to droplet formation dynamics has also been studied [32].

Monodispersity of microdroplets formed by microfluidic droplet generation systems is influenced by internal pressure fluctuations due to droplet formation, and

external fluctuations caused by flow sources. It is critical to minimize these fluctuations, which requires a thorough analysis of the source of unsteadiness. In this section, the effect of hydrodynamic damping on droplet monodispersity in a droplet-generating system is analyzed for both displacement-driven and pressure-driven systems.

2.4.1 Experimental setup

2.4.1.1 Microfluidic chip

Experimental droplet generation was performed using a PDMS T-junction microfluidic device. Fig. 2.6 shows the schematic of the experimental setups used for syringe pump- and pressure pumpdriven systems. There are two inlets and one outlet in the microchannel. Two immiscible fluids were driven through the microchannels to generate droplets. Silicone oil (SF 50) with density and dynamic viscosity of 1000 kg/m^3 and 50 mPa s was used as the continuous fluid. Distilled water was driven into the second inlet as the dispersed phase with density and dynamic viscosity of 1000 kg/m^3 and 1 mPa s, respectively. The width and height of all channels were 300 µm and 80 µm, respectively. The experiments were performed using the same microfluidic device, in order to make a fair comparison between the performance of the syringe pump and the pressure pump.

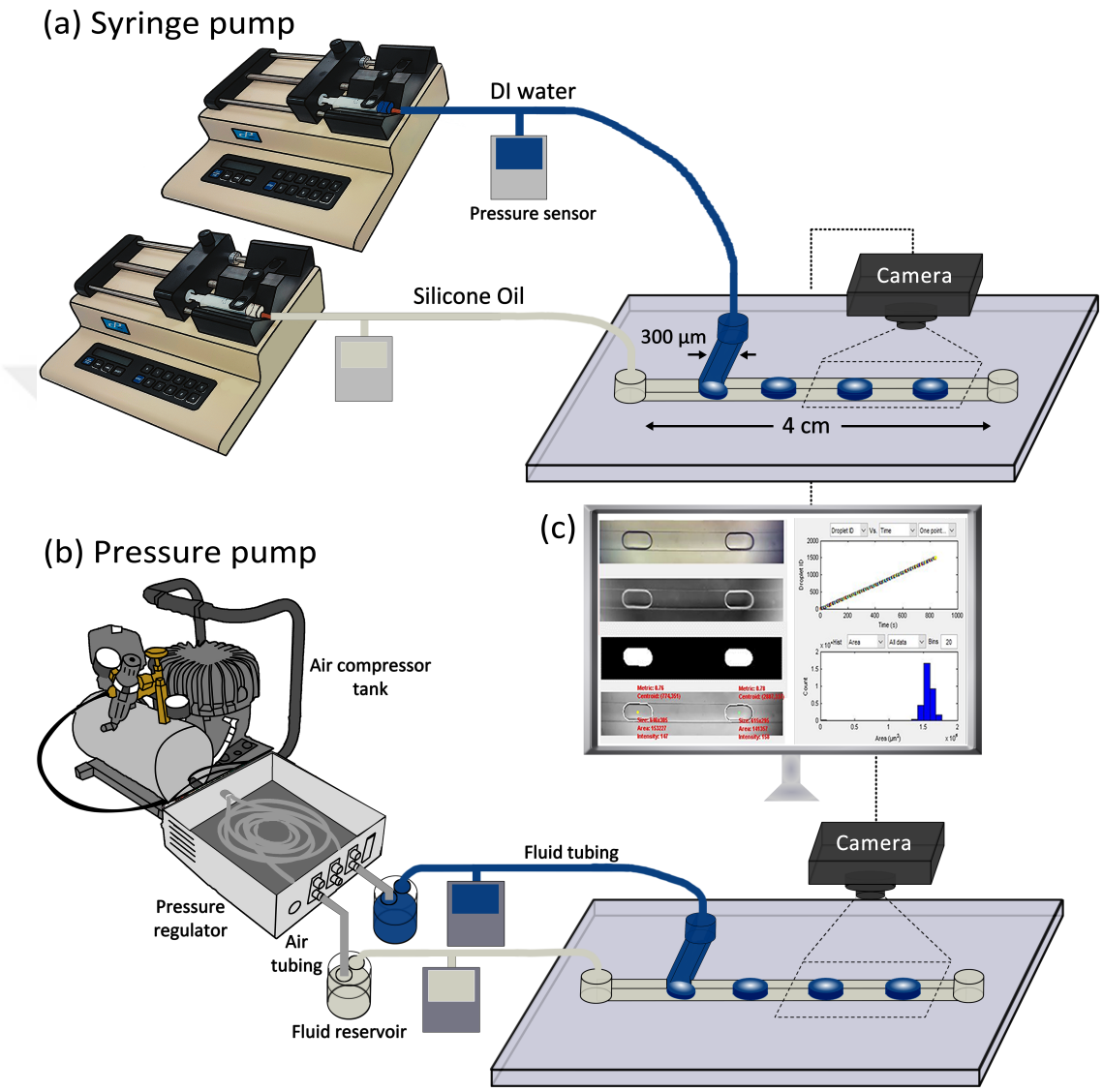

Figure 2.6: Schematic of the experimental setup. (a) Syringe pump (SP) actuated system, (b) pressure pump (PP) actuated system, (c) droplet morphometry and velocimetry (DMV) software for calculating droplet area [1].

2.4.1.2 Flow sources and peripheral components

As illustrated in Fig. 2.6, our goal is to compare the two most commonly utilized flow sources used in microfluidic systems. For the first setting, the two immiscible fluids were introduced to the microchannel at constant flow rates using syringe

pumps (KDScientific 270). Two syringe pumps were used to drive oil and water at 3 µl/min and 1 µl/min, respectively. For the pressure pump case, a multi-channel pressure pump (Elveflow OB1) was used to pump oil and water into the microchannel. Using the pressure pump, we set the oil and water pressure to 95 mbar and 55 mbar, respectively. In both cases, the Capillary number was kept the same to ensure that droplets were formed in the same regime. All the fluidic connections from the pumps to the microchip were made using flexible silicone tubing, characteristics of which are presented in Section 2.2. Pressure fluctuations caused by the unsteadiness of the flow source influencing oil and water flows are measured by pressure sensors at each inlet. For hydrodynamic damping, either 20 cm-long or 100 cm-long elastomeric tubings were used. An inverted microscope (Omano OMFL600), equipped with a camera (Optixcam OCS-5.0), was used to capture the droplet motion using a 20x objective. As shown in Fig. 2.6c, for both cases, Droplet Morphometry and Velocimetry software (DMV) was used [1] to analyze the droplet area from the recorded videos in order to obtain the coefficient of variation (CV), which is a metric used to compare droplet monodispersity. In all the experiments the data were recorded after 5 min of running the system to ensure that steady-state flow conditions are achieved. Moreover, we backed up our analysis with numerical modeling, which allows us to study the ideal fluctuation-free inlet conditions.

2.4.2 Numerical modeling

Numerical modeling of droplet-based systems is a convenient alternative for experiments, since it allows much faster investigation and analysis of several droplet generation scenarios. Level set method (LSM) is a common method for simulating two-phase flow and droplet formation [50]. Using LSM, it is possible to track time-dependent dispersed phase motion and simulate droplet generation. Change in contact angle, viscosity ratio, flow rate ratio, capillary number and interfacial tension between two immiscible fluids can be analyzed using LSM [18].

LSM is performed using the 2D Laminar Flow Two-Phase Flow, LSM interface module of COMSOL Multiphysics 5.0. Coupling continuity Eq. 2.13 and incompressible Navier–Stokes Eq. 2.14 with the level set in Eq. 2.15 allowed the tracking of time-dependent dispersed phase motion and simulation of water in oil (w/o) droplet generation.

$$\nabla.u = 0 \tag{2.13}$$

$$\rho\frac{\partial u}{\partial t} + \rho(u.\nabla)u = \nabla.[-pI + \eta(\nabla u + (\nabla u)^T)] + F_{st} \tag{2.14}$$

$$\frac{\partial \phi}{\partial t} + u.\nabla\phi = \gamma\nabla.(\epsilon\nabla\phi - \phi(1-\phi)\frac{\nabla\phi}{|\nabla\phi|}) \tag{2.15}$$

where u , ρ, t, p, η and F_{st} denote velocity (m/s), density (kg/m^3), time (s), pressure (Pa), dynamic viscosity (Pa s) and surface tension force (N/m^3), respectively. Additionally, γ and ϵ are numerical stabilization parameters, and $\phi(x,t)$ is the level set function. The fluid interface is specified by the $\phi(x,t) = 0.5$ contour of the level set function, whereas continuous and dispersed phases were modeled as $\phi(x,t) = 0$ and $\phi(x,t) = 1$, respectively. The density and dynamic viscosity are obtained using:

$$\rho = \rho_1 + (\rho_2 - \rho_1)\phi \tag{2.16}$$

$$\eta = \eta_1 + (\eta_2 - \eta_1)\phi \tag{2.17}$$

where ρ_1, ρ_2, η_1 and η_2 are densities and dynamic viscosities of fluid 1 (continuous phase) and fluid 2 (dispersed phase), respectively. Using the above equations, the formation of droplets at a Tjunction and their motion along a microchannel were simulated in 2D flow, as shown in Fig. 2.7.

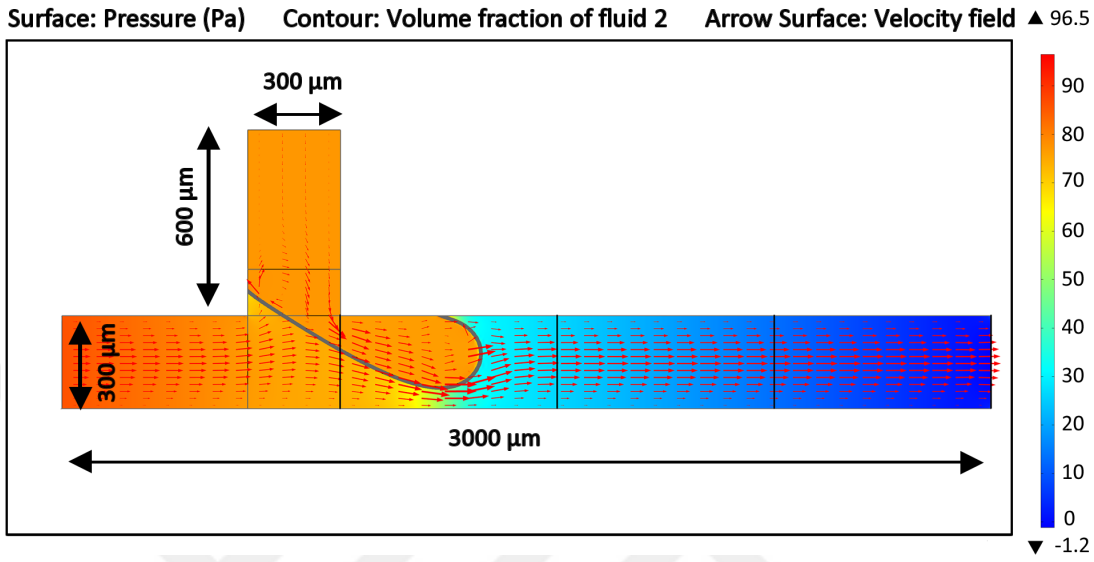

Figure 2.7: COMSOL simulation illustrating formation of the droplet.

Microdroplets were formed using two immiscible fluids, whose properties are given in Table 2.1, together with the boundary conditions. For the numerical model, no wet wall boundary conditions were used.

Table 2.1: Microfluidic device dimension.

Parameter	Fluid 1	Fluid 2
Density (kg/m^3)	1000	1000
Dynamic viscosity $(mPas)$	50	1
Flow rate for syringe pump $(\mu l/s)$	0.043	0.0086
Pressure for pressure pump (Pa)	245	78
Contact angle (rad)	$3\pi/4$	
Slip length (μm)	1	
Surface tension coefficient (N/m)	0.005	

The inlet boundary condition in simulations is determined based on the way two immiscible fluids are fed to the microfluidic device. The syringe pump is modeled as a flow rate boundary condition, whereas the pressure pump is modeled as a pressure inlet condition. Two kinds of simulations were performed in

this section: with and without inlet boundary condition fluctuation. The initial values of flow rate and pressure were tailored so that the same size of droplets was obtained as in the experiments. These values are different from the experimental values, since only a fraction of the straight main channel is simulated for computational efficiency. For the fluctuation-free simulations, the inlet pressure or flow rates values were set as constant. Then, fluctuations of pressure and flow rates were taken into account and imported as inlet parameters in the numerical modeling. The equivalent circuit of each system was formed after calculating the capacitance and resistance of the corresponding components, based on the equations given in the previous section. The calculated capacitance and resistance are given in Table 2.2.

Table 2.2: Equivalent circuit parameters.

Parameter	Tubing length (m)	Oil resistance (Pa s/m^3)	Oil capacitance (m^3/Pa)	Water resistance (Pa s/m^3)	Water capacitance (m^3/Pa)
Fluid tubing (R_t, C_t)	0.20	5.3×10^{11}	1.17×10^{-13}	1.06×10^{10}	1.17×10^{-13}
	1	26.5×10^{11}	5.84×10^{-13}	5.3×10^{10}	5.84×10^{-13}
Air tubing (R_{at}, C_{at})	1.5	3.73×10^{5}	5.1×10^{-9} (P_s = 9500 Pa)	3.73×10^{5}	8.73×10^{-9} (P_s = 5500 Pa)
Reservoir (C_a)	N/A	Negligible	1.53×10^{-9} (P_s = 9500 Pa)	Negligible	2.64×10^{-9} (P_s = 5500 Pa)
Microchannel (R_c, C_c)	N/A	78×10^{12}	1.4×10^{-15}	1.56×10^{12}	1.4×10^{-15}

The fluid tubing is the variable component in the equivalent circuit diagrams shown in Fig. 2.4. We used tubings of 20 cm and 100 cm in length for the experiments and the numerical model. Due to the resistance of the tubing, pressure drops along the tubing from the pressure sensor to the inlet of the microchannel. In addition, the compliance of tubing dampens the pressure fluctuations. Thus, in both SP and PP cases, inlet fluctuation values are less than the measured ones. The external fluctuations were measured with the pressure sensor converted to the periodic fluctuations and then were applied to the equivalent circuit simulated with LTspice software (Linear Technology). Using the equivalent circuit, we were able to obtain fluctuations for the continuous and dispersed phase solutions at different points in the circuit. The dampened fluctuations at the inlet of the

microfluidic device (node A in Fig. 2.4) were obtained for water and oil. After normalizing the periodic fluctuations and inputting them into the simulations, the effect of flow source unsteadiness was studied. All simulations were carried out using time step of 0.0005 s and 2280 mesh elements. As illustrated in Fig. 2.7, the main channel was divided into three identical domains to calculate the droplet area. After the simulation was completed, we obtained the droplet area by calculating the volume fraction in the domain which contains the droplet as a whole using post-processing options.

2.4.3 Results and discussion

Droplet monodispersity for numerical and experimental results has been analyzed by calculating the coefficient of variation (CV) of the droplet area. DMV software was used to obtain the experimental CV of the droplet area [1]. There are two ways of studying droplet size variation in 2D simulations: calculating droplet length, or calculating droplet area. We used droplet area calculation to obtain a better approximation to 3D. The comparison of droplet monodispersity, using syringe pump (SP) and pressure pump (PP), was performed for three cases: numerical results with inlet condition fluctuations (pressure or flow rate), numerical results without fluctuations and experimental results. We plotted the histograms of the droplet area that had been obtained experimentally and numerically in Figs. 2.8 and 2.9, respectively. As illustrated in Fig. 2.8, using longer tubing leads to lower CV values for the droplet area in both SP and PP cases. For the PP-driven system, approximately twofold improvement was obtained using the longer tubing. In the SP case, CV of the droplet area decreased from 4.46% to 0.388%. Order of magnitude difference between CVs of 20 cm and 100 cm tubing shows the significance of the hydrodynamic damping on droplet monodispersity.

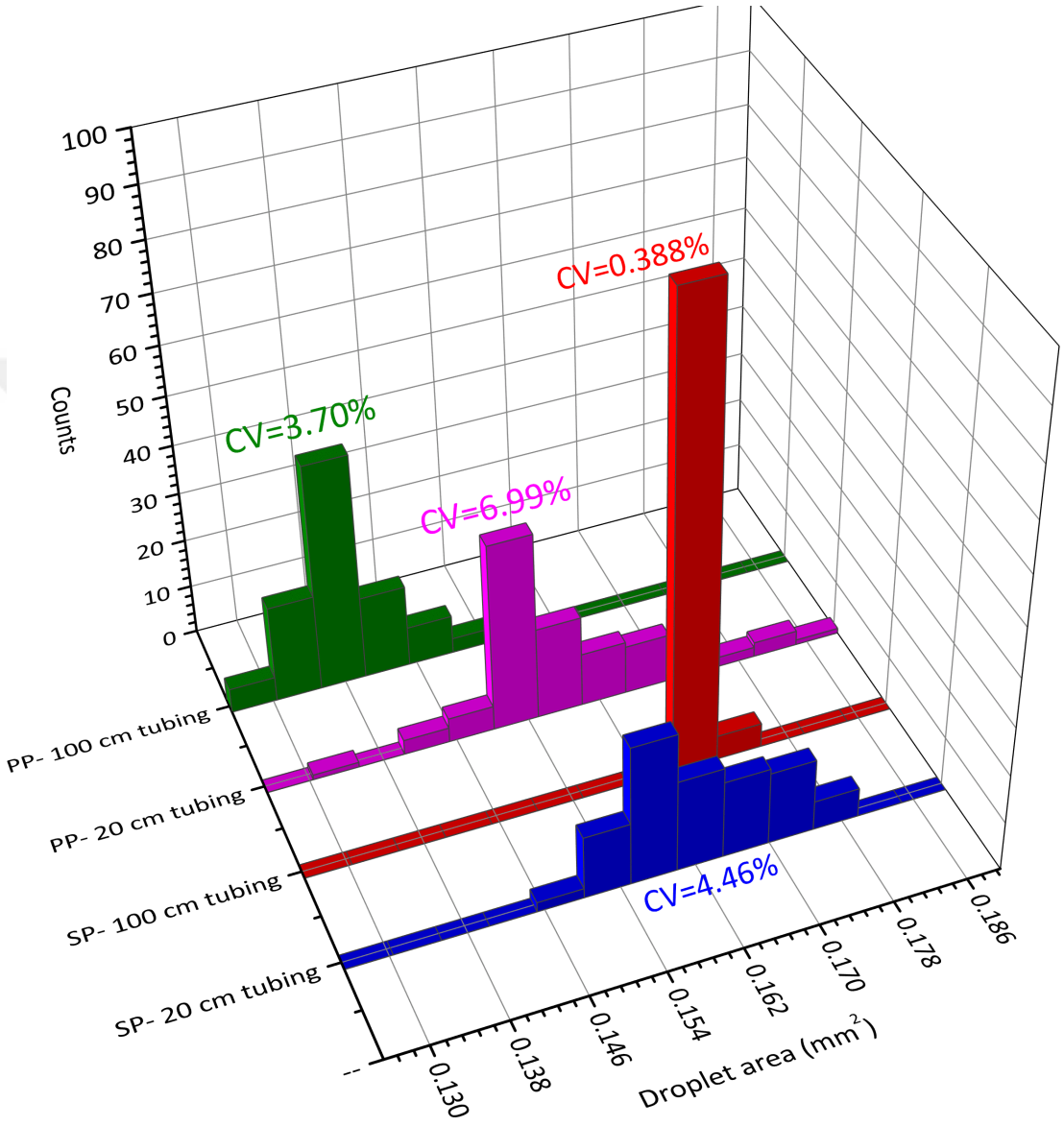

Figure 2.8: Histogram of the droplet area obtained experimentally for 100 droplets, using two different tubing lengths for syringe pump (SP) and pressure pump (PP) driven systems.

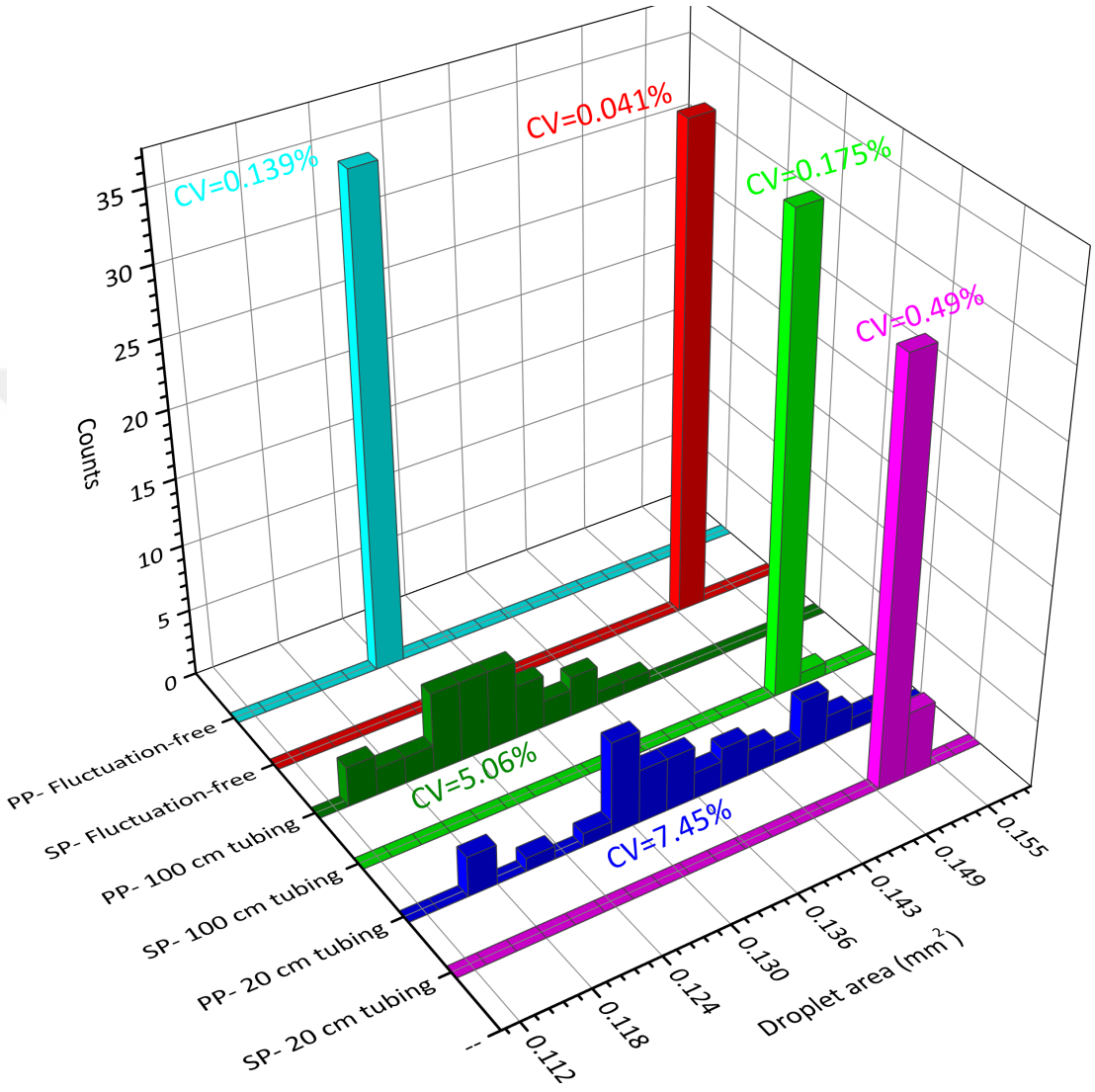

Figure 2.9: Histogram of the droplet area obtained numerically for 36 droplets in three conditions of numerical simulation for SP and PP cases.

Comparing the CV values of SP and PP shows that the effect of the fluid tubing length for SP is much higher than for PP. This is due to the fact that the fluid tubing is the only compliance, which damps the fluctuations for SP. However, in the PP case, in addition to fluid tubing, air tubing and the compressibility of the air inside the reservoir play a role in fluctuation damping. Therefore, PP driven systems inherently operate using such an enhanced compliance damping mechanism.

Fig. 2.9 summarizes the results obtained using the numerical simulations. When the flow source fluctuations were neglected, very low CV values were obtained (0.139% and 0.041%), which do not match the experimental results. On the other hand, considering the flow source fluctuations and using the methodology explained in the previous section, a strong correlation was obtained between the numerical model and the experimental results. As shown in Fig. 2.9, in the SP and PP cases, when 20-cm tubing was used, droplet area CV was 0.49% and 7.45%, respectively. Using 100 cm of the fluid tubing in the microfluidic system results in a narrower distribution of the droplet area. The CV of the droplet area using 100-cm fluid tubing for the SP and PP cases is 0.175% and 5.06%, respectively. The decrease in distribution and CV of the droplet area confirms the significance of the effect of tubing length on droplet monodispersity.

It should be noted that for the COMSOL simulations, a much shorter microfluidic channel was analyzed for computational efficiency. Therefore, we do not expect to obtain the exact same results obtained in the experiments. However, numerical simulation results provide the means to analyze the behavior of the system. In addition, the CV values given in Fig. 2.9 demonstrate the importance of including inlet fluctuations for more realistic numerical models. The comparison between fluctuation-free results for the SP and PP cases shows that syringe pump is advantageous for generating monodisperse droplets. This is because syringe pump is immune to the internal pressure fluctuations caused, due to droplet generation dynamics and the motion of the droplet inside the microchannel. Additionally, the comparison of experimental (Fig. 2.8) and numerical (Fig. 2.9) results reflects the importance of considering the flow source fluctuations. As seen, the numerical results obtained using fluctuation-free inlet conditions are much lower than the experimental results. Once inlet fluctuations were added, a satisfactory correlation was obtained. Furthermore, it is shown that by increasing the off-chip compliance with increased tubing length upstream the channel inlet, significant improvement can be achieved, especially for the syringe pumpdriven system. Fig. 2.10 shows our experimental droplet monodispersity results in more detail.

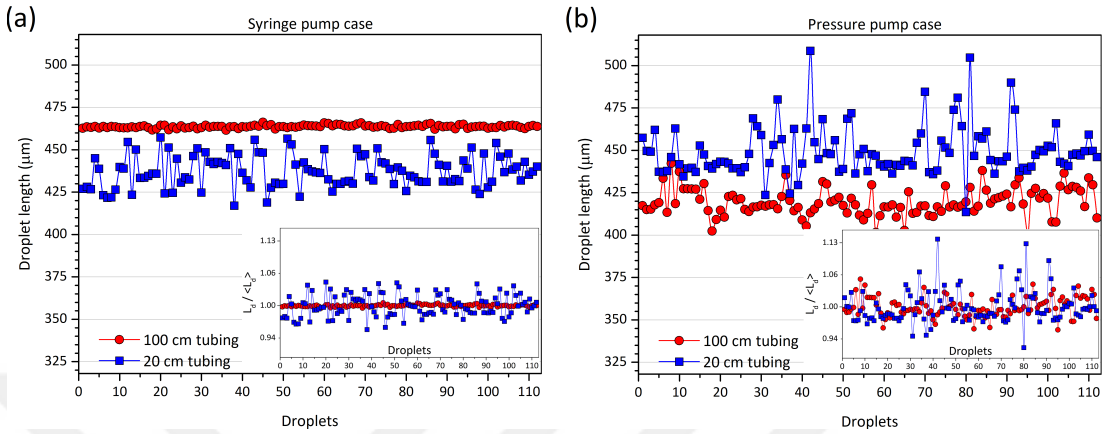

Figure 2.10: Comparison of droplet lengths obtained experimentally using 20 cm-long tubing and 100 cm-long tubing in two cases: (a) Syringe pump driven system. (b) Pressure driven system. The insets show the normalized droplet lengths, L_d.

As seen from the experimental measurements of individual droplet lengths, increasing the tubing length from 20 cm to 100 cm has a remarkable effect on droplet monodispersity. The effect of longer fluid tubing on droplet monodispersity in the syringe pump case (Fig. 2.10a) is higher than the pressure pump case (Fig. 2.10b). The insets show the difference in dimensionless form. These results challenge the monodispersity results obtained in the literature, which generally state that pressure pumps perform better than syringe pumps. Our approach shows that such pump comparisons are not conclusive, since the results not only depend on build quality, hence the brand of the pumps, but also on off-chip parts, which are often neglected and have a significant effect on the system. Thus, the microfluidic system should be designed considering both the on-chip and off-chip components and their hydrodynamic damping effects, in order to obtain higher droplet monodispersity.

2.5 Conclusion

In this chapter, we demonstrated that droplet monodispersity can be increased substantially by using off-chip compliant components in a microfluidic system. We modeled the whole system using hydrodynamic resistance and capacitance. By increasing the length of a flexible tubing which connects the flow source to the channel inlet, we showed that the flow source fluctuations can be dampened significantly. Our experimental and numerical results showed that this effect can be used for droplet generation systems that are driven by either pressure or syringe pumps. Especially for a syringe pump system, the provided method is very effective and yields order of magnitude improvement in droplet size variation. This model also explicitly shows that pressure pumps operate with such an inherent dampening mechanism which explains the better monodispersity results obtained in the literature so far.

Chapter 3

Ultra monodisperse droplet generation and theoretical limit of droplet monodispersity

Despite the wide usage of droplet-based microfluidic systems, the limit of monodispersity for droplet generation systems is still unknown. This is due to the difficulty in analytical modeling of droplet formation that is usually compensated by experimental approaches, which fall short in leading to universal conclusions. Here at this chapter, we present an analytical approach that considers all the system dynamics and internal and external factors that disturb monodispersity. We used the analogy between fluidic and electrical circuits to analyse the factors that influence droplet monodispersity. Interestingly, we were able to model the dynamics of a segmented two-phase flow system using a single-phase flow analogy, electron flow, in electrical circuits. Doing so, we reveal the sources of disturbances that lead to variation in droplet volume. Eventually, we offered a unique solution and designed guidelines to ensure ultra-monodisperse droplet generation. Our analytical conclusions were experimentally verified using a T-junction droplet generator design driven by a pressure supply. Equally importantly, we show the limiting experimental factors for reaching the theoretical maximum of monodispersity.

The content of this chapter was published in [6] as; Kalantarifard. Ali and Alizadeh-Haghighi. Elnaz and Saateh. Abtin and Elbuken. Caglar, Theoretical and experimental limits of monodisperse droplet generation, Chemical Engineering Science, vol. 229, pp. 116093, 2020.

3.1 Introduction

Droplet microfluidic systems have dramatically improved precision in many applications, such as polymerase chain reaction [51], DNA separation and compartmentalisation [52] and particle synthesis [53], in which accurate control over volume and sample concentration play a significant role. Fundamentally, the competition between interfacial tension and shear forces allows droplet formation and dictates the droplet volume. Despite the well-understood physics of droplet formation in two-phase flow systems, the long-sought-after goal of generating identical, equal-size droplets sequentially is challenging. Although the individual parameters that affect the droplet size were identified as channel dimension [14], wettability [49], viscosity [54] and flow rate or pressure ratio of the two immiscible fluids [21, 20, 22], the governing mechanism of droplet size variation is still unclear. It is shown that for the most commonly used microfluidic droplet generator designs, such as T-junction, flow-focusing, and co-flow, droplet length is correlated to the pressure [20] or flow rate [21, 46, 22] ratio of the dispersed and continuous phases. However, such correlations lack the ability to clarify the factors leading to droplet size variation. There are studies that discuss the root causes of size variation as internal and external pressure fluctuation [23, 28, 27]. While the consequences of such fluctuations are still incompletely understood, some methods have been proposed to decrease internal [33] and external fluctuations [55, 5, 56]. These approaches suffer from experimental complexity and do not lead to a comprehensive solution for the elimination of pressure and flow rate fluctuations in microdroplet generators. Hence, the theoretical and practical limits of monodispersity is not discussed yet. Here, we introduce a new approach to analyse droplet size variation that eventually leads to a thorough understanding of the root causes of droplet polydispersity. We demonstrate ultra-monodisperse

droplet generation with a coefficient of variation (CV) close to the theoretical limit of 0% CV. We use a numerical method based on the analogy between fluidic and electric circuits [57, 38] to elucidate the key parameters that affect droplet size variation. Applying high identical pressure from a single pressure supply and using a droplet-laden microfluidic channel with low hydrodynamic resistance are the key factors for ultra-monodisperse droplet generation.

3.2 Theory

The existing models that predict droplet size in microdroplet systems correlate the length of a droplet with geometrical parameters, volumetric flow rate ratio of dispersed and continuous phases, and capillary number ($Ca = \frac{\eta u}{\sigma}$, where η, u are viscosity and velocity of the continuous phase, respectively, and σ is the interfacial tension between the two immiscible fluids) [21, 46, 22]. Ideally, keeping the flow rate ratio constant would result in the generation of identical droplets, since channel geometry, fluid viscosities and interfacial tension do not change during droplet generation. The use of Hagen–Poiseuille Law is a common practice when studying microfluidic circuits as a first approximation; $\Delta P = RQ$, where ΔP, R and Q are pressure difference, hydrodynamic resistance and volumetric flow rate, respectively. For a pressure-driven two-phase flow system schematically shown in 3.1a, we can write the volumetric flow rate ratio of the two immiscible fluids as $\frac{Q_d}{Q_c} = \frac{P_{d_i} - P_{d_j}}{P_{c_i} - P_{c_j}} \frac{R_c}{R_d}$, where subscripts c and d represent continuous and dispersed phases and i and j represent channel inlet and junction, respectively. As seen from this equation, variation in the inlet and junction pressures leads to fluctuation in flow rate ratio and droplet length which, in turn, leads to droplet polydispersity. In this chapter, we demonstrate that droplet volume variation can be minimized by two fundamental approaches: flow source configuration and channel network design. Unlike single-phase flow systems, generation and movement of the droplets in the microfluidic system lead to inevitable pressure variations, which are referred to as internal fluctuations. In addition, there is pressure variation at the inlets due to pressure/flow sources imperfections, which is referred to as external fluctuations. In theory, we can keep the flow rate ratio constant

under particular conditions, that of having identical pressure for continuous and dispersed phases at the inlet ($P_{d_i} = P_{c_i}$) and the junction ($P_{d_j} = P_{c_j}$). In this case, the flow rate ratio becomes independent of any pressure fluctuations, $\frac{Q_d}{Q_c} = \frac{R_c}{R_d}$. Applying identical pressure for both phases at the inlet is a viable option, since inlet pressure is dictated by the user Fig. 3.1b. However, it is not possible to have the same pressure for continuous and dispersed phases at the junction. There is an inherent pressure difference at the junction due to the interfacial tension between the continuous and dispersed phase, which is fluctuating Laplace pressure due to the periodically changing shape of the interface during droplet formation.

To compare the effect of the external and internal pressure fluctuations, and to study the influence of varying Laplace pressure on droplet monodispersity, we rewrite the flow rate ratio equation as:

$$\begin{aligned} \frac{Q_d}{Q_c} = \frac{P_{d_i} - P_{d_j}}{P_{c_i} - P_{c_j}} \frac{R_c}{R_d} = \frac{P_{d_i} - P_{c_j} + P_{c_j} - P_{d_j}}{P_{c_i} - P_{c_j}} \frac{R_c}{R_d} = \\ \frac{P_{d_i} - P_{c_j}}{P_{c_i} - P_{c_j}} - \frac{P_{d_j} - P_{c_j}}{P_{c_i} - P_{c_j}} \frac{R_c}{R_d} = (\frac{\alpha}{\Delta P_c} - \frac{\Delta P_L}{\Delta P_c}) \frac{R_c}{R_d} \end{aligned} \tag{3.1}$$

where $\Delta P_L = P_{d_j} - P_{c_j}$ is Laplace pressure, $\Delta P_c = P_{c_i} - P_{c_j}$ is the pressure drop between the inlet and junction for the continuous phase and α is $P_c = P_{d_i} - P_{c_j}$. Note that ΔP_L, ΔP_c and α are the fluctuating terms in Equation 3.1. To investigate the effect of the fluctuating terms in this equation, we performed a numerical study based on the analogy between fluidic and electrical components. We made an electrical circuit equivalent of a T-junction droplet generator driven by a pressure supply (Fig. 3.1c).

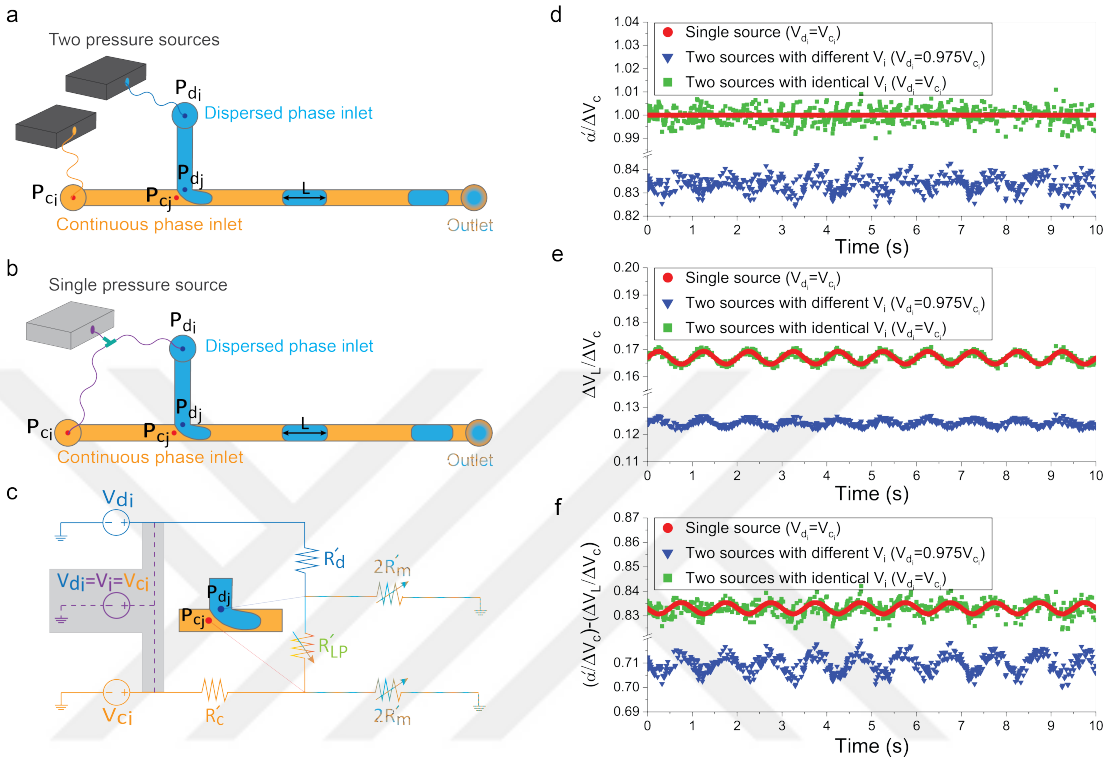

Figure 3.1: Schematic representation of fluidic and electric circuit and numerical results for the effect of fluctuating terms on droplet generation using the conventional (with two separate sources) and the proposed method (with a single source). a, Schematic illustration of the conventional, two source-driven, experimental setup. b, Schematic illustration of the proposed, single source-driven, experimental setup. c, Equivalent circuit of a T-junction droplet generator design driven by pressure supplies. Both two source- and single source (grey background)-driven architectures are shown. d, Fluctuation of $\frac{\alpha'}{\Delta V_c}$ for the conventional and proposed methods. Note that this fraction approaches unity in the proposed method. e, Fluctuation of $\frac{\Delta V_L}{\Delta V_c}$ for the conventional and proposed methods. f, Resultant fluctuations calculated by the difference of the previous two terms, representing the flow rate ratio fluctuations for the conventional and proposed methods.

3.3 Analogy and numerical results

Flow rate (Q), pressure (P) and hydrodynamic resistor (R) in the fluidic system are analogous to current (I), voltage (V) and electrical resistor ($R^{'}$) in the electrical circuit, respectively. The hydrodynamic resistance of the microchannel between droplet generator junction and outlet, which we named as main channel (R_m), fluctuates, since the pressure drop is a function of the number and the position of droplets in the main channel, especially for non-straight channel designs. Similarly, there is a variation in Laplace pressure and the corresponding hydrodynamic resistance (R_{LP}) at the junction due to the continuously varying interface geometry between the immiscible phases. We propose an equivalent circuit for the droplet generation system in which the Laplace pressure is considered in the electrical circuit analogy. The Laplace pressure drop is included at the droplet generation junction. To achieve the equivalence to the fluidic circuit, the main channel resistance was shown as identical parallel channels (for $R^{'}_{LP}$=0, main channel resistance is equivalent to $R^{'}_{m}$, prime is used to denote electrical resistances throughout the text). This approach provides new insights into the relationship between droplet size variation and the fluctuating terms in Equation 3.1. The flow rate ratio and, consequently, the droplet length is related to the current ratio ($\frac{I_d}{I_c}$) in the equivalent circuit. Therefore, the electrical equivalent of Equation 3.1 is written as:

$$\frac{I_d}{I_c} = (\frac{\alpha^{'}}{\Delta V_c} - \frac{\Delta V_L}{\Delta V_c})\frac{R^{'}_c}{R^{'}_d} \tag{3.2}$$

Using this equivalent circuit, we have studied the effect of having identical inlet pressures/voltage and external fluctuations on the variation of the fluctuating terms in Equation 3.2. Simulations were performed using a SPICE software (LTSpice, Fig. 3.2), which allows us to study the dynamic response of the system for a given droplet generation frequency.

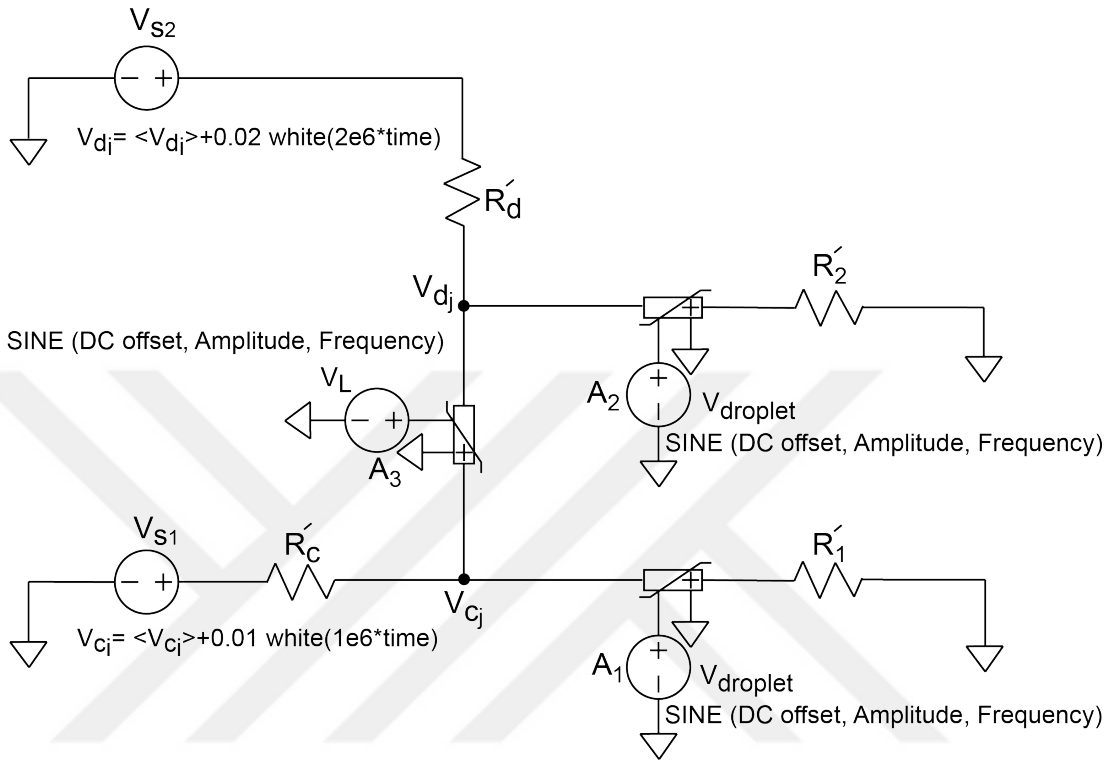

Figure 3.2: Electrical circuit equivalent of a T-junction droplet generator used for LTSpice simulation. Two voltage sources analogous to pressure pump are used to supply the desired voltage. The imperfection of the flow source (external fluctuations) is integrated into the voltage source as white noise. Varistors (voltage-dependent resistors) A_1, A_2 and A_3 are used to have periodic fluctuations in R'_m, R'_{LP}. Note that $A_1 = A_2$ and $R'_1 = R'_2 = 2R'_m$ for all simulations. s, i, j, c, d and L denote source, inlet, junction, continuous phase, dispersed phase and Laplace Pressure, respectively.

It is important to note that this approach is computationally much more efficient than the CFD-based analysis. We analysed the effect of the first term in Equation 3.2, $\frac{\alpha'}{\Delta V_c}$, second term, $\frac{\Delta V_L}{\Delta V_c}$, and their difference, $\frac{\alpha'}{\Delta V_c}$-$\frac{\Delta V_L}{\Delta V_c}$ (Fig. 3.1d-f).

The values for the components used in the equivalent circuit are calculated based on the experimental parameters such as applied pressures, the viscosity of the fluids, microchannel dimensions and the number of droplets in the main channel. As shown in Fig. 3.2, two voltage sources analogous to pressure pump

are used to supply desired voltage/pressure in the equivalent circuit. The imperfection of the flow source (external fluctuations) is integrated into the voltage source as white noise, which is set as different for each voltage source when separate sources are used. Hydrodynamic resistance of the rectangular channel containing a single phase is calculated using $R = \frac{a\mu L}{wh^3}$ where L, w, h are length, width and height of the channel, respectively. μ is the viscosity of the fluid and $a = 12[(1 - (\frac{192h}{w\pi^5}) \sum_{n=1,3,5}^{\infty} \frac{1}{n^5} \tanh(\frac{n\pi w}{2h})]^{-1}$, which is approximated as 12 for $\frac{h}{w} \ll 1$. Droplet resistance is calculated using $R_{drop}=\frac{3a\mu_c L_{drop}}{wh^3}$, where μ_c and L_{drop} are carrier fluid viscosity and droplet length, respectively [58].

The hydrodynamic resistance of the main channel is $R_m=R+nR_{drop}$, where n is the number of droplets and R is the resistance of the main channel when it is filled with the continuous phase. R_m is considered as a variable resistor since the pressure drop is a function of the number and position of the droplets in the main channel. Similarly, there is a variation in Laplace pressure and the corresponding hydrodynamic resistance (R_{LP}) at the junction due to the continuously varying interface geometry between the immiscible phases. Therefore, $R_m^{'}$ and $R_{LP}^{'}$ are varying resistors, which are modeled as voltage-controlled varistors. Using varistors (represented as A_i in Fig. 3.2), we take into account the effect of droplet generation frequency and number of droplets in the main channel. Varistors A_1, A_2 and A_3 are driven by a SINE function with a constant DC offset, amplitude and frequency, to model the time-dependent variation of $R_m^{'}$ and $R_{LP}^{'}$. Note that A_1=A_2 for all simulations. For A_1 and A_2, DC offset, Amplitude and Frequency are pressure drop of one droplet, $(\frac{\Delta P_{droplet}}{number of droplets in the main channel})$ and droplet generation frequency [59], respectively. For A_3, DC offset and Amplitude, which are respectively Laplace Pressure (ΔV_L) and $(\frac{\Delta V_L}{number of droplets in the main channel})$, are defined based on the equation and experimental studies in the literature [24] and Frequency was set according to the droplet generation frequency.

For the identical inlet pressures/voltages (V_{d_i}=V_{c_i}) shown in Fig. 3.1b, we have:

$$\frac{I_d}{I_c} = (1 - \frac{\Delta V_L}{\Delta V_c})(\frac{R_c^{'}}{R_d^{'}}) \tag{3.3}$$

which shows that fluctuations due to the first term are canceled out. In Figs. 3.1d–f, the time-dependent change of fluctuating terms in Equation 3.2 are plotted when a single source is used to drive the system (○), which is also shown as the dashed line configuration in Fig. 3.1c (grey background). For comparison, the simulations were repeated with the conventional architecture, where two separate sources with different (▽) and same values (□) were used for the inlet pressures. In practice, even if inlet source pressures are kept constant, there will be minor pressure fluctuations at the inlets due to limitations of the instruments (external fluctuations). These source imperfections are included in the simulations as random white noise. The numerical simulation results show that using a single source not only eliminates the undesired flow rate fluctuations due to the first term, but also compensates the imperfections of the source fluctuations so that an ideal response is observed, as shown in Fig. 3.1d. To further study the origin of this improvement, a comparison can be made between the results of all three simulations shown in Fig. 3.1f. The decrease in fluctuations from ▽ to □ is due to equalising the inlet pressure and addressing the polydispersity due to the first term in Equation 3.2. The further improvement from □ to ○ is due to the immunity of the single source-driven system to source imperfections. Still, absolute monodispersity, i.e. 0% CV, is not possible in a single source configuration, due to the fluctuations of the second term in Equation 3.2, as seen in Fig. 3.1e.

Increasing inlet pressure/voltage (ΔV_c) and/or decreasing the Laplace pressure (ΔV_L) would minimize the fluctuations due to this term. Hence, the system response would approach the theoretical limit of 0% monodispersity.

3.4 Experimental results

For experimental verification of these results, a PDMS/glass microfluidic chip with a T-junction droplet generator was used. Water droplets were formed inside

silicone oil (50 mPa s) using a pressure controller. For the single source configuration, a fluidic T-connector was used to split the inlet tubing into two. For the two sources configuration, the inlet pressures were set as given in Fig. 3.3a. After adjusting the input pressure(s), the system was run for 15 min for stabilization of droplet formation. The CV% measurement was performed by recording a video of droplets formed in the main channel and running an image-processing algorithm on at least 150 consecutive droplets [1]. The error bars represent the standard deviation of four repetitive experiments. The results were obtained at pressures varying from 400 to 700 mbar, for four inlet pressure configurations, one of which is the proposed single source supply system. The numerical results were carried out using the parameters matching the conditions in the experiments, and the CV% values are plotted in Fig. 3.3b. The results shown in Fig. 2 are in line with our expectation that the single-source configuration leads to the smallest CV% values at all pressures. Additionally, increasing the inlet pressure reduces the CV%, and an experimental CV% value of 0.11% was obtained. The normalised size of individual droplets for these results is also given as an inset for the single-source ($P_{d_i} = P_{c_i}$) and two-source ($P_{d_i} = 0.975P_{c_i}$) configurations. The details of the channel geometry are given in the Table. 3.1.

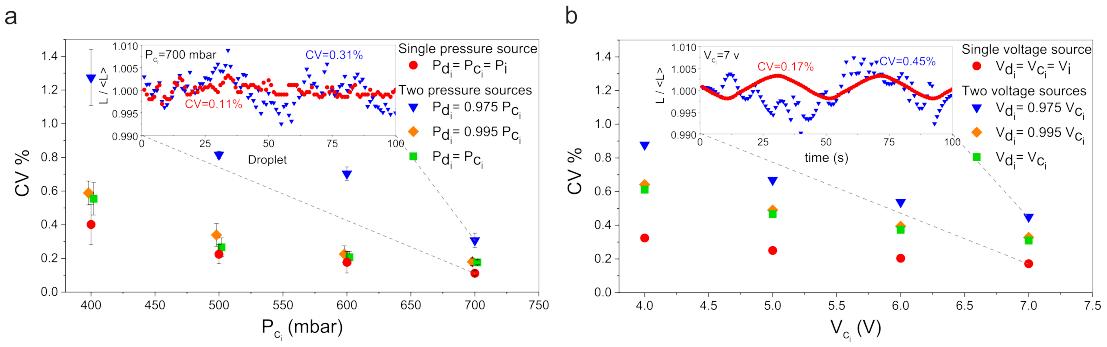

Figure 3.3: Experimental (a) and numerical (b) results of droplet monodispersity values, %coefficient of variation (CV), obtained for single-source and two-source configurations. a, For the experimental results, an image processing software, Droplet Morphometry and Velocimetry (DMV), was used to measure the size variation of droplets. 150 droplets were measured for each experiment and the mean droplet length was noted. Each experiment was carried out in four repetitions, error bars denote standard deviation. The insets show the normalized size of individual droplets for 700 mbar/7.0V inlet pressure/voltage value.

Table 3.1: Microfluidic device dimension.

	Oil channel	Water channel	Main channel
Length (cm)	1	18	18
Width (µm)	300	300	300
Thickness (µm)	80	80	80

So far, we have discussed how droplet monodispersity can be improved by flow source configuration. As seen in Fig. 3.1f, running the system by a single pressure source considerably decreases the fluctuations. However, using just a single pressure source is not sufficient to attain the theoretical limit of droplet monodispersity. Optimization of the channel network design is another way to improve droplet monodispersity. To this end, we rewrite the flow rate ratio equation by applying Kirchhoff current law to the equivalent electrical circuit shown in Fig. 3.1c. More details of this approach are shown in Fig. 3.4.

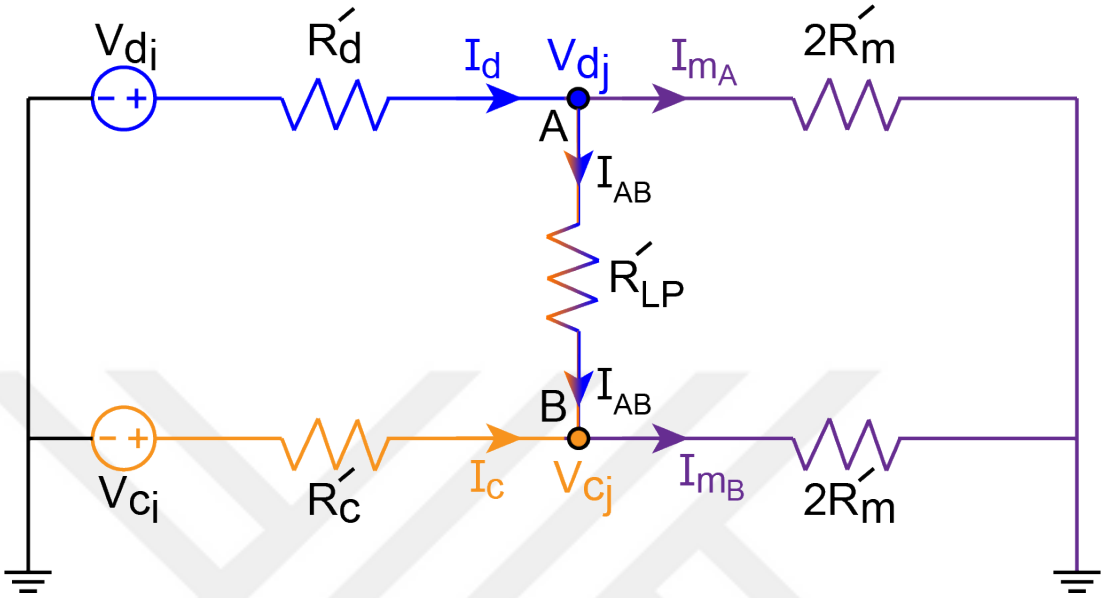

Figure 3.4: Electrical circuit equivalent of a T-junction droplet generator. KCL was written for the two nodes A and B which are identified in blue and orange, respectively.

For node A in Fig. 3.4, we have $I_d = I_{AB} + I_{m_A}$, which can be written as:

$$\frac{V_{d_i} - V_{d_j}}{R'_d} = \frac{V_{d_j} - V_{c_j}}{R'_{LP}} + \frac{V_{d_j}}{2R'_m} \tag{3.4}$$

For node B, where $I_c + I_{AB} = I_{m_B}$, we obtain

$$\frac{V_{c_i} - V_{c_j}}{R'_c} + \frac{V_{d_j} - V_{c_j}}{R'_{LP}} = \frac{V_{c_j}}{2R'_m} \tag{3.5}$$

Solving equations 3.4, 3.5 results in 3.6 that shows the relationship between current ratio, resistors and voltage sources.

$$\frac{I_d}{I_c} = \frac{2R'_m V_{d_i}(2R'_c - R'_{LP}) + R'_c R'_{LP} V_{d_i} + 4R'^2_m (V_{c_i} - V_{d_i})}{R'_d V_{c_i}(4R'_m + R'_{LP}) - 2R'_m R'_{LP} V_{c_i} - 4R'^2_m (V_{c_i} - V_{d_i})} \tag{3.6}$$

where $R_m^{'}$ represents hydrodynamic resistance of the channel (main channel) between junction and outlet of the device, and $R_{LP}^{'}$ is hydrodynamic resistance due to the Laplace pressure. When a single pressure source is used to drive both fluids ($V_{d_i} = V_{c_i} = V_i$), Equation 3.6 reduces to:

$$\frac{I_d}{I_c} = \frac{4R_m^{'}R_c^{'} - 2R_m^{'}R_{LP}^{'} + R_c^{'}R_{LP}^{'}}{4R_m^{'}R_d^{'} - 2R_m^{'}R_{LP}^{'} + R_d^{'}R_{LP}^{'}} \tag{3.7}$$

$R_m^{'}$ and $R_{LP}^{'}$ are fluctuating parameters and play a particular role in the variation of current ratio. Decreasing either $R_m^{'}$ or $R_{LP}^{'}$ to zero ($R_m^{'}\rightarrow 0$ or $R_{LP}^{'}\rightarrow 0$) causes the current ratio and, consequently, the droplet size to depend merely on resistance ratio $(R_c^{'})/(R_d^{'})$, which is constant. Additionally, regardless of the values of $R_m^{'}$ and $R_{LP}^{'}$, when $(R_c^{'})/(R_d^{'})$ ratio approaches unity, the current ratio approaches one, hence higher monodispersity values are expected. These estimations were validated both experimentally and numerically, as shown in Fig. 3.5. Firstly, the effect of decreasing R_{LP} has been studied. Although the Laplace pressure could be reduced by adding a surfactant to decrease the interfacial tension, the change is marginal due to critical micelle concentration (CMC) limit. We have added 0.5 wt% concentration SDS into the water and decreased the interfacial tension from 38 mN/m to 5 mN/m. Afterwards, the monodispersity of the droplets for both cases (with and without surfactant) was measured using the experimental procedure explained in the previous section. As shown in Fig. 3a, 20% decrease in the CV% values was obtained when Laplace pressure was reduced. Similar results were achieved numerically when the value of $R_{LP}^{'}$(Laplace pressure/voltage) was reduced accordingly.

Secondly, we studied the effect of decreasing R_m. We used microfluidic designs with five different main channel lengths with identical droplet generation portions. As our conclusions from Equation (5) imply, decreasing main channel length decreases the CV% of droplet size and improves monodispersity. For the shortest main channel of 1 cm in length, we accommodated 20 droplets in the main channel and obtained a CV of 0.24% (Fig. 3.5b). It should be noted that decreasing the channel length also decreases the number of droplets in the main channel, which

further decreases R_m.

Finally, R_c/R_d ratio was varied using a screw valve placed on the dispersed phase inlet section of the device, as shown in Fig. 3.5c. By tightening the screw, the channel height was decreased and the hydrodynamic resistance of the dispersed phase inlet channel (R_d) was increased.

Measuring the ratio of the dispersed phase and continuous phase volumes in certain section of the main channel by using image processing, and the relation between flow rate ratio and hydrodynamic resistance ratio, we obtained quantitative values of R_c/R_d ratio. The same channel design, with a main channel length of 5 cm, was used for all these experiments. The interfacial tension was 38 mN/m. The smallest experimental CV% was obtained when R_c/R_d was approximately 1 at a screw angle of $\theta° = 135°$.

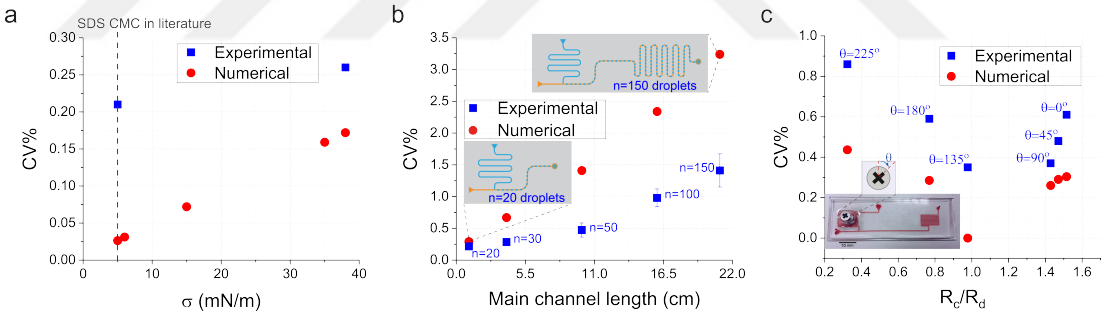

Figure 3.5: Experimental and numerical results of droplet monodispersity, CV% as a function of Laplace pressure (R_{LP}), main channel length (R_m) and (R_c/R_d) ratio. a, Interfacial tension was reduced by adding SDS to the dispersed phase. b, The main channel length was varied using five different devices, n denotes the number of droplets accommodated in the main channel for each design. Each experiment was carried out in four repetitions, error bars denote standard deviation. c The hydrodynamic resistance ratio was varied using a screw valve located over the dispersed phase inlet.

What we are proposing in this chapter is to use a single pressure source to obtain monodisperse droplets. However, the conventional approach to adjust droplet size is to change the inlet pressures. Setting the two inlet pressures to the

same value creates a limitation in the size of the droplets that can be obtained. To overcome this shortcoming and making ultra monodisperse droplets of any size, one can change the hydrodynamic resistance of the dispersed or continuous phase inlet channels. In Fig. 3.6, we show two methods to vary hydrodynamic resistance of inlet channels that allows discrete and continuous changes using plug [60] and screw valves [61], respectively.

In the plug valve technique, parallel channels equipped with a plug valve are used to supply the dispersed or continuous phase. The inlet channel hydrodynamics resistance can be varied by turning the valves on/off; discrete resistance values are obtained, which can be calculated for channels of rectangular cross sections6. We implemented this technique using three valves for the dispersed phase inlet as shown in Fig. 3.6a. The average droplet lengths (n=100) obtained for 4 valve combinations for constant shared inlet pressures are given in Fig. 3.6b.

Similarly, the hydrodynamic resistance of the inlet channels can be varied using other types of valve. To demonstrate continuous tuning of channel hydrodynamic resistance, we employed a screw valve placed over the dispersed phase inlet channel. Tightening the screw presses over the channel and decreases the channel thickness (Fig. 3.6c). Expectedly, this lowers the droplet length as shown in Fig. 3.6d. It should be noted that the screw valve enables droplet generation in a broader range with much finer control in comparison to the plug valve. The two types of valves given in Fig. 3.6 are simply to demonstrate the tunability of droplet size even when the two inlets are fed from a single pressure source. Any microfluidic valve can be used to change the hydrodynamic resistance ratio of dispersed and continuous phases.

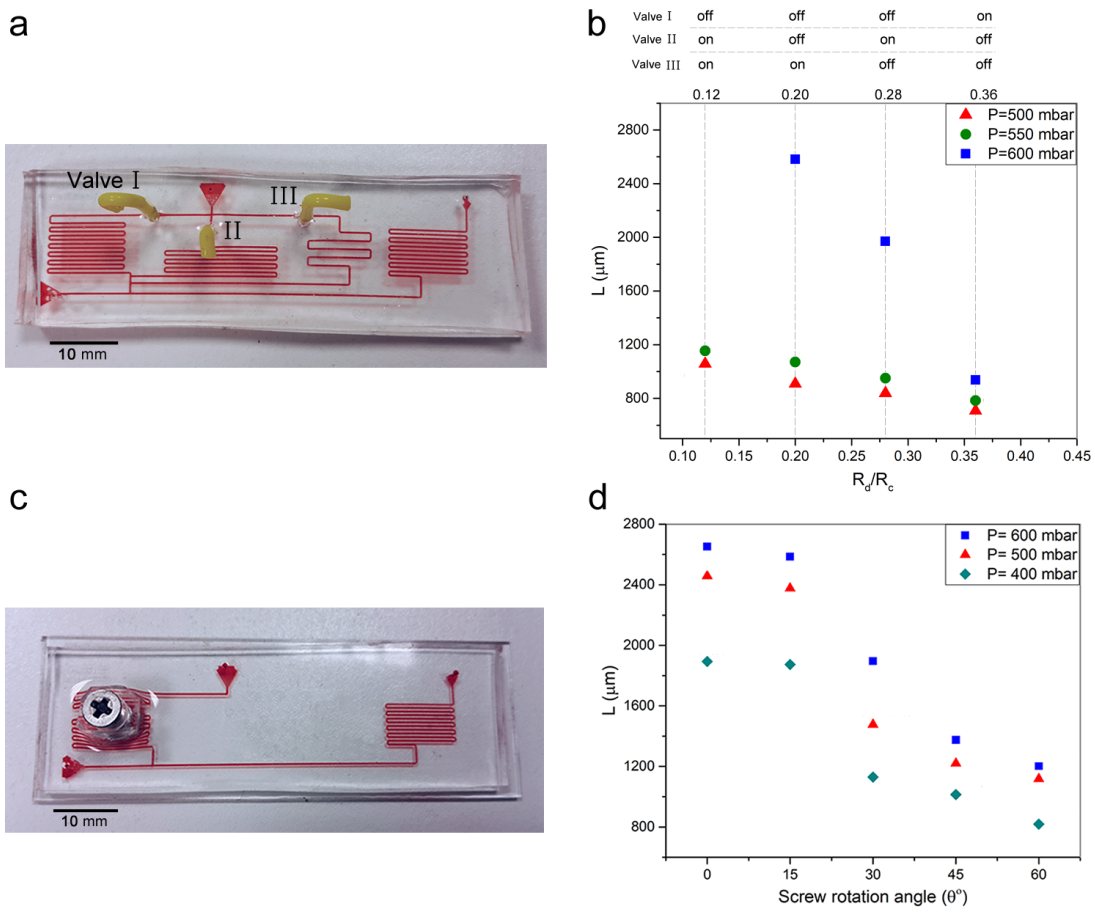

Figure 3.6: Photograph of the device and experimental results of using two different techniques to make monodisperse droplets in different sizes. a, Photograph of the microfluidic T-junction device with three parallel dispersed phase channels equipped with micro plug valves. b, Droplet lengths for different pressures and hydrodynamic resistance ratios for various micro plug valve configurations. c, Photograph of the microfluidic T-junction device equipped with screw valve. d, Droplet lengths for different pressures and rotation angles of the screw valve. The results are the average length of 100 droplets for each case.

Our experimental and numerical results given in Figs. 3.3 and 3.5 show that droplet monodispersity can be improved by optimizing several parameters, such as having a single pressure source supply that is set at high pressure, decreasing the interfacial tension, using a short main channel, and equating the resistance of the

inlet channels. It is important to note that these parameters are not independent from each other. For example, increasing inlet pressure is equivalent to decreasing the effect of the Laplace pressure, i.e. decreasing the interfacial tension. Changing R_c or R_d results in changing droplet size and droplet generation frequency which lead to changes in R_m. Hence, it is critical to determine the dominant factors that affect droplet monodispersity. To do so, we designed another microfluidic chip, which could vary the hydrodynamic resistance of each channel segment on a single device. We call this device a fluidic evaluation chip, analogous to evaluation boards in electrical circuits. Using the evaluation chip, we can quantify the effect of changing inlet pressure (P_{in}), main channel length (L_m) or resistance (R_m) and hydrodynamic resistance ratio of inlet channels (R_c/R_d), while keeping all the other system parameters the same: single pressure source configuration and the same fluidic properties. Using a single pressure source with a bifurcated tubing, the inlet pressures of the fluids were set as identical and changed simultaneously, $P_{in} = 360, 400, 440$ mbar. As shown in Figs. 3.7a and 3.7b, a screw valve was placed over the dispersed phase channel to change the channel height to vary (R_c/R_d) by setting the screw angle ($\theta^\circ = 0^\circ, 90^\circ, 180^\circ$). The serpentine main channel section was designed with multiple outlets. Only one of the outlets was used, and the others were kept closed using a microplug valve [60]. Different main channel lengths were obtained ($L_m = 13, 16.5, 20$ cm) by changing the open outlet. Hence, we were able to modify the resistance of the main channel (R_m). A photo of the device is given in Fig. 3.7b. For a real-time analysis of droplet size variation, we implemented impedimetric droplet measurement using coplanar electrodes and impedimetric droplet measurement (iDM) software [2].

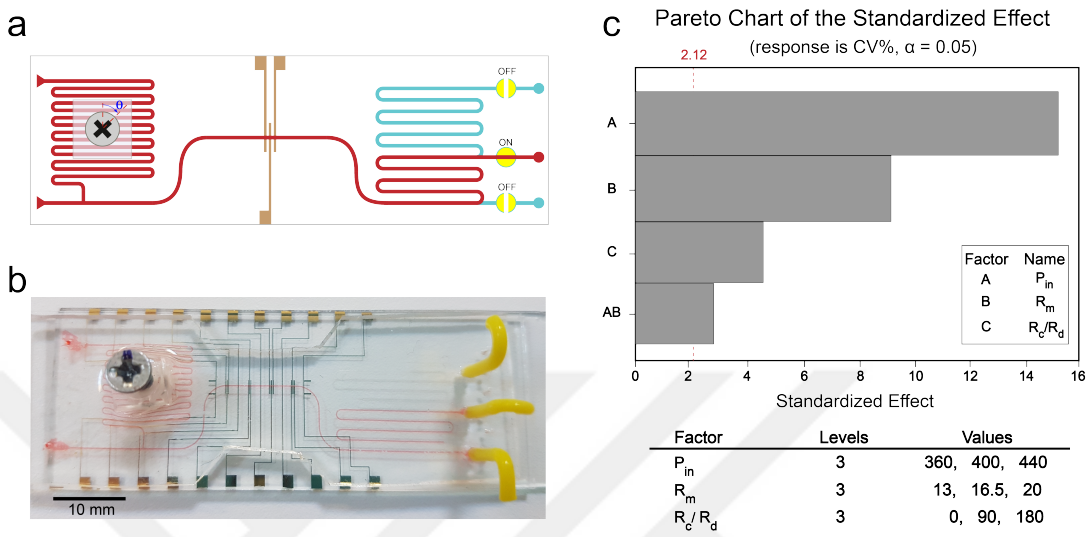

Figure 3.7: The schematic drawing (a) and the photo (b) of the monodispersity evaluation chip, (c) Pareto chart of effects. The inlets were connected to a single pressure supply (P_{in}) using a bifurcated tubing. A screw valve was used to change the inlet channel resistance ratio (R_c/R_d). The effective main channel length (R_m) was varied using plug valves. Coplanar microelectrodes were used to obtain impedimetric signals. These were analysed in real time using impedimetric droplet measurement (iDM) software to obtain real-time droplet monodispersity, CV%, for any given configuration.

Using the fluidic evaluation chip, all possible configurations were tested. The droplet length and monodispersity results of 27 experiments are given in the Table. 3.2. The results are in accordance with our previous theoretical and numerical conclusions.

Table 3.2: Experimental results of fluidic evaluation chip.

No	L_m (cm)	Pressure (mbar)	(θ°)	Mean length (µm)	CV%
1	20	360	180	400.9	1.01
2	20	360	90	426.59	1.11
3	20	360	0	442.29	1.19
4	20	400	0	455.26	1.02
5	20	400	90	431.92	1.06
6	20	400	180	402.59	0.79
7	20	440	180	418.18	0.63
8	20	440	90	448.74	0.68
9	20	440	0	462.13	0.71
10	16.5	440	0	495.82	0.67
11	16.5	440	90	479.51	0.65
12	16.5	440	180	443.55	0.54
13	16.5	400	180	425.22	0.65
14	16.5	400	90	454.67	0.70
15	16.5	400	0	468.39	0.74
16	16.5	360	0	459.41	0.92
17	16.5	360	90	435.27	0.90
18	16.5	360	180	401.62	0.89
19	13	360	180	439.16	0.87
20	13	360	90	470.31	0.88
21	13	360	0	458.22	0.94
22	13	400	0	471.09	0.75
23	13	400	90	455.06	0.71
24	13	400	180	430.42	0.63
25	13	440	180	448.81	0.52
26	13	440	90	481.55	0.55
27	13	440	0	492.84	0.57

Droplet monodispersity improves with increasing inlet pressure (P_{in}), decreasing main channel length (R_m), and equal inlet channel hydrodynamic resistances (R_c/R_d).

We employed a randomized full factorial study to compare the effects of three factors ($P_{in}, R_m, R_c/R_d$) on the monodispersity of droplets, CV%. We used a Pareto chart to report the statistical significance of the main and interaction effects (Fig. 3.7c). We conclude that $P_{in}, R_m, R_c/R_d$ and the interaction between P_{in} and R_m are significant parameters in improving droplet monodispersity. A multivariable chart for the main and interaction effects is given in the Figure 3.8 which shows the effect of each of the three parameters ($P_{in}, R_m, R_c/R_d$) on droplet monodispersity. As shown, increasing inlet pressure results in CV% improvement. Also, blue dash lines show the CV improvement with changing R_c/R_d for a constant L_m. The green dash line shows that the CV% increases with increasing main channel length. These results verify the observations obtained by previous experiments that were conducted to analyze the effect of $P_{in}, R_m, R_c/R_d$ independently.

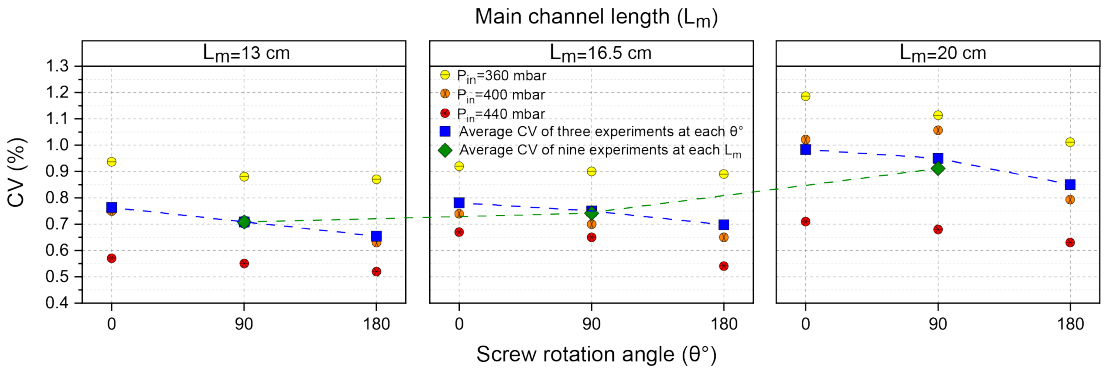

Figure 3.8: Experimental results of varying inlet pressure (P_{in}), main channel length (R_m) and inlet resistance ratio (R_c/R_d) on droplet monodispersity, CV%. The effect of changing R_c/R_d (for each L_m) on CV% is presented by blue dash lines. The green dash line shows the effect of changing L_m on CV%.

Over the past two decades, several droplet fluidic systems have been derived, a small number of which focus on the droplet formation dynamics and report

quantitative monodispersity results. Mainly, three different droplet formation geometries (T-junction, flow-focusing and coflow) and displacement (syringe) or pressure (positive or negative) pumps were used for these systems. For these systems, a summary of the droplet type, frequency and monodispersity CV% values is given in the Table. 3 and Fig. 3.9. The lowest CV% values, which are close to 1%, were all obtained by using a syringe pump. Here, we demonstrated that by using a pressure-driven system, fed from a single pressure supply and through optimization of the microfluidic channel design, it is possible to obtain much lower CV% values. When the inlet pressure was increased to 700 mbar, we obtained a 0.11% CV value. It is important to note that the CV% value of the droplet length (x directtion) is not exactly the same as CV% volume, due to the deviation of the droplet in other directions (y and z direction). However, for the plug-like droplets there is not a significant change in the droplet is y and z directions in which the droplet is confined with channel wall. To show that, we measured the CV% value of the droplet volume and it was 0.17% which confirms that for the plug-like droplet there is no big difference for CV value of length and volume. Setting the inlet pressures to the same value and equating inlet channel hydrodynamic resistances minimizes the pressure difference between the dispersed and continuous phase at the junction. Lowering the interfacial tension between the two phases serves the same purpose. Hence, the underpinning effect of our suggested design guidelines is to minimize pressure discontinuity at the droplet formation junction and to get closer to a single-phase system. When we compare the monodispersity values given in the literature, we see a victory of syringe pump-driven systems that are immune to the pressure fluctuations of the systems and are primarily affected by the variation of the inlet volumetric flow rates. However, the intrinsic internal fluctuation's effect on droplet monodispersity in syringe pump-driven systems is less than pressure-driven systems [5]. Another interesting observation is that negative pressure-driven systems performed better than positive pressure supplies [62]. Considering our analysis, these results are not surprising. A negative pressure-driven droplet generator is equivalent to setting the inlet pressures to the same value ($P_{d_i} = P_{c_i}$). Hence, the retrospective monodispersity comparison based on the literature is in accordance with the findings in this thesis. Another broadly agreed fact is that increasing capillary

number improves monodispersity [24, 63, 64, 65, 66]. The capillary number can be increased by increasing the flow rate or by decreasing the interfacial tension, both of which are equivalent to decreasing the effect of Laplace pressure. Moreover, it is important to note that increasing the flow rate implies an increase in the inlet pressure value that was shown to be the dominant parameter influencing monodispersity [23].

Table 3.3: Overview over different microfluidic droplet generators.

Flow source	Geometry	Type	Size (µm)	Frequency (Hz)	Size CV%
PP	TJ	O/W	75	0.5-2.33	2.1 [67]
SP	FF	W/O	20	-	<1 [22]
SP	TJ	W/O	-	-	1-3 [68]
SP	FF	W/O	54-62	8-40	<2 [69]
SP	TJ	O/W	50-500	-	1.35 [49]
SP	TJ	O/W	50-500	-	<2 [70]
SP	TJ	W/O	50-500	-	1.7 [49]
SP	FF	W/O	≈34	-	<2 [71]
SP	FF	O/W	35.8	13.5k	<1 [72]
SP	TJ	W/O	200-500	-	<3 [73]
SP	Coflow	O/W	10-100	-	<2 [74]
SP	TJ	O/W	90.7	6	2.2 [75]
SP	TJ	Janus	140.8	2.5	1.4 [75]
SP	Coflow	O/W	100-400	0.5	<3 [34]
SP	FF	W/O	41.5	-	0.7 [76]
NP	TJ	W/O	82-98	12	1.6 [51]
NP	TJ	W/O	100-200	2.2	2.2 [35]
SP	FF	W/O	50-230	16-110	<2 [77]
SP	TJ	W/O	75	≈378	3 [78]
NP	TJ	W/O	69-77	10	1.3 [62]
SP	TJ	O/W	20-30	-	1.7 [79]
PP	FF	W/O	300 pL	50	3.78 [55]
SP	Coflow	W/O	61	1-1000	1.87 [80]
PP	Coflow	O/W	122	-	2.5 [81]
PP	Coflow	W/O	301	-	3.2 [81]
PP	TJ	W/O	450	1.66	3.7 [5]
SP	TJ	W/O	45	21	<3 [82]
PP	TJ	W/O	400-2500	1.6	<0.2 [6]

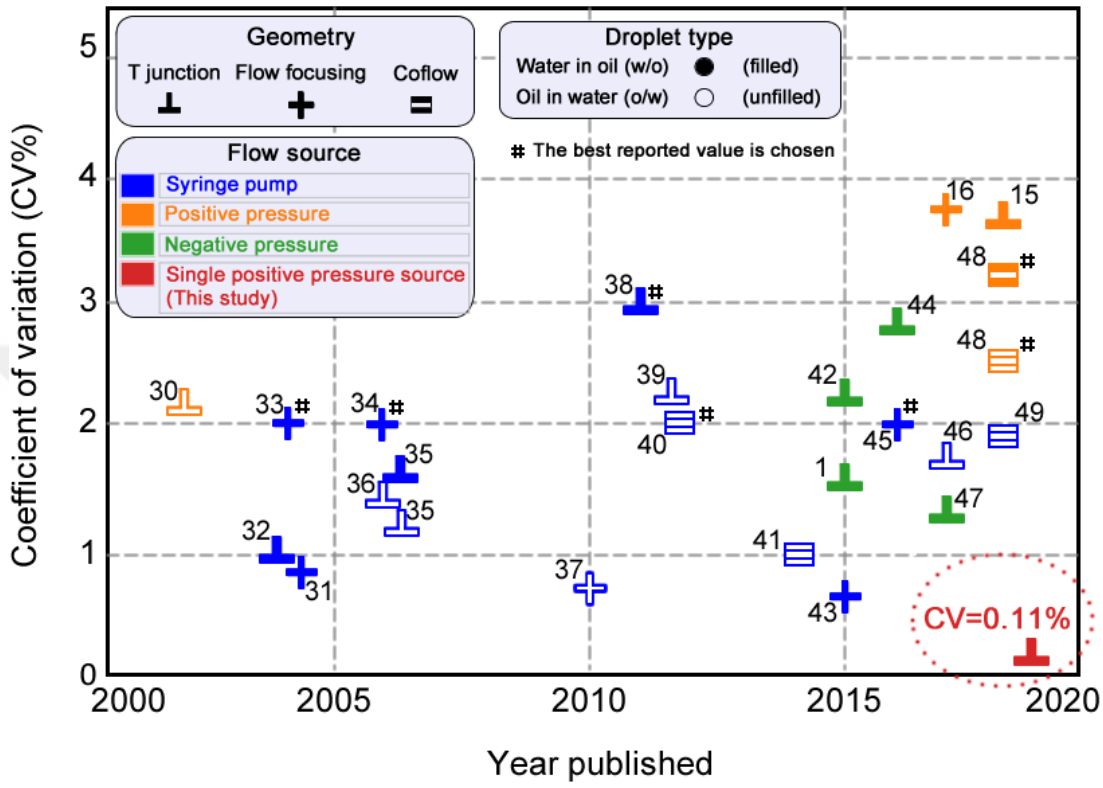

Figure 3.9: Droplet monodispersity comparison. If multiple CV values are reported in the article, the best-reported value is chosen. Some articles only reported the maximum CV% obtained.

In summary, we used the analogy between fluidic and electrical circuits to study the factors that affect droplet monodispersity. Interestingly, we were able to model the dynamics of a segmented two-phase flow system using a one-phase flow analogy, electron flow in electrical circuits. Doing so, we determined the governing factors and their effect on droplet monodispersity. Eventually, we offered a practical, yet effective solution for flow source configuration and channel network design to minimize external and internal fluctuations, respectively. We achieved a droplet monodispersity of less than 0.2% CV using a T-junction droplet generator design and a single pressure source. More importantly, we showed the limitations of reaching the theoretical asymptote of monodispersity, numerically and experimentally. The theoretical, numerical and experimental results given in this manuscript not only explain the underlying physics of droplet size variation in

microchannels, but also provide practical design guidelines to obtain high droplet monodispersity, which would lead to the highest precision in droplet microfluidic applications, such as digital ELISA [83] and droplet digital PCR [84].

Chapter 4

High throughput ultra-monodisperse droplet generation

Although microfluidic droplet systems are well developed to provide controllable size on-demand generation of droplets, due to the flow instability originate from inside or outside of the microfluidic device, reaching to extremely narrow size distribution is still challenging. In this chapter, we use the universal method that proposed in the previous chapter. Here, we show that using the proposed method for other microfluidic devices than T-junction , like flow-focusing, leads to highly monodisperse droplet generation without any need for dexterity or device fabrication complexity. I addition, we compare the performance of the syringe pump and pressure pump as a flow source for supplying fluids with the conventional and proposed method in terms of droplet monodispersity. We show that supplying an identical flow rate/pressure from a single source makes any common microfluidic droplet system such as T-junction or flow-focusing immune to the external fluctuations that come from the imperfection of the flow source. In other words, we show that the proposed design guidelines are applicable for common microfluidic devices, T-junction and flow-focusing. Using our proposed method, we could obtain ultra-monodisperse droplets in a flow-focusing device with a coefficient of

variation (CV) value of less than 0.5% for both cases, using syringe or pressure pump as a flow source.

A portion of the content of this chapter was published in [6] as; Kalantarifard. Ali and Alizadeh-Haghighi. Elnaz and Saateh. Abtin and Elbuken. Caglar, Theoretical and experimental limits of monodisperse droplet generation, Chemical Engineering Science, vol. 229, pp. 116093, 2020.

4.1 introduction

Although microfluidic droplet systems are well developed to make monodisperse droplets (1% <CV <3%), reaching to the high level of droplet monodispersity (CV <1%), called ultra-monodispersity, without any need for dexterity or device fabrication complexity is highly sought-after. Fluid instability is the main factor that compromises droplet monodispersity. The instabilities originate from the outside microfluidic device, due to the imperfection of the driving unit or inside of that owing to droplet formation and motion in the microfluidic device. Therefore, researchers have tried several strategies such as using a pulseless syringe pump, integration of compliance [5, 56, 33] or a feedback system [55], or design of a 3-D flow-focusing geometry [85] to decrease flow instabilities. Yet, these approaches suffer from fabrication and experimental complexity, long system response, limited portability and do not lead to a pervasive and cost-effective method to obtain ultra-monodisperse droplets. Since the performance of the microfluidic droplet system changes for a different design of device or flow source mechanism, using a method that applies to all common microfluidic devices and driving units is often preferred. For example, a flow-focusing device allows generating droplets in higher frequency compared to T-junction device. Therefore, researchers prefer to use a flow-focusing device when the throughput of the system is important. On the other hand, using a T-junction device helps to have better control over droplet formation which makes them beneficial for making monodisperse droplets. Also, depending on the application, typically either a syringe pump or pressure pump is used as a flow source in a microfluidic droplet system. A syringe pump

allows to drive fluids at the desired flow rate, however, it has long response time and induces more instabilities to the system compared to a pressure pump. Here, we use a universal method that enables ultra-monodisperse droplet generation without any need for skillfulness or device fabrication complexity. More importantly, the proposed method is applicable for common microfluidic devices such as T-junction and flow-focusing and flow sources like pressure and syringe pump. Also, the method is compatible with parallelization of hundreds of microfluidic channels in a single chip since all fluids would be supplied with a single flow source. In the previous chapter, we pointed out some design-recommendations that need to be accounted for when designing a T-junction microfluidic system to obtain minimum achievable monodispersity while using a pressure pump as a flow source. Here, we apply those design-rules on a flow-focusing device which has higher droplet generation frequency compared to a T-junction device. Moreover, we investigate the effect of two common flow sources, syringe and pressure pump, on the proposed method. We could generate ultra-monodisperse droplet with a CV of 0.5% using an optimized configuration regardless of a flow source type.

4.1.1 Monodisperse droplet generation using pressure pump

The droplets' length and thus their monodispersity directly depends on flow rate ratio of the dispersed phase to continuous phase. There are two kinds of flow instabilities called external (from imperfection of drive unit) and internal fluctuations (due to the droplet formation and motion in the channel) that agitate droplet formation and disturb droplet monodispersity while a pressure pump used as a flow source in the microfluidic droplet system. Thus, finding a method to minimize these fluctuations would be beneficial in generation of identically sized droplets. As explained in the previous chapter, to make the droplet-based system immune to imperfections of pressure source, so called external fluctuations, we supplied the two immiscible fluids into a flow-focusing device from a single pressure source at an identical pressure. Also, to avoid the effects of internal fluctuations that caused by generation and motion of droplets in the main channel

(the channel in which droplets form and move), effects of various parameters in design of the channel network were taken into account. According to our study on the T-junction droplet generating geometry, supplying the inlet pressures from the same source, lowering the hydrodynamic resistance of the main channel, applying equal hydrodynamic resistances for both inlet channels, and minimizing the pressure difference between the dispersed and continuous phase at the junction by lowering the interfacial tension, resulted in improved monodispersity. In this chapter, applied the proposed recommendation rules of pressure source configuration and channel network design to a flow-focusing microfluidic device to show the applicability of our proposed method to all common microfluidic devices. A flow-focusing droplet generator PDMS/glass chip (all channels are in 150 µm width and 100 µm depth) is designed to do experiments. Here, DI water and silicone oil (10 mPas) are introduced to the microfluidic device as dispersed and continuous phase respectively.

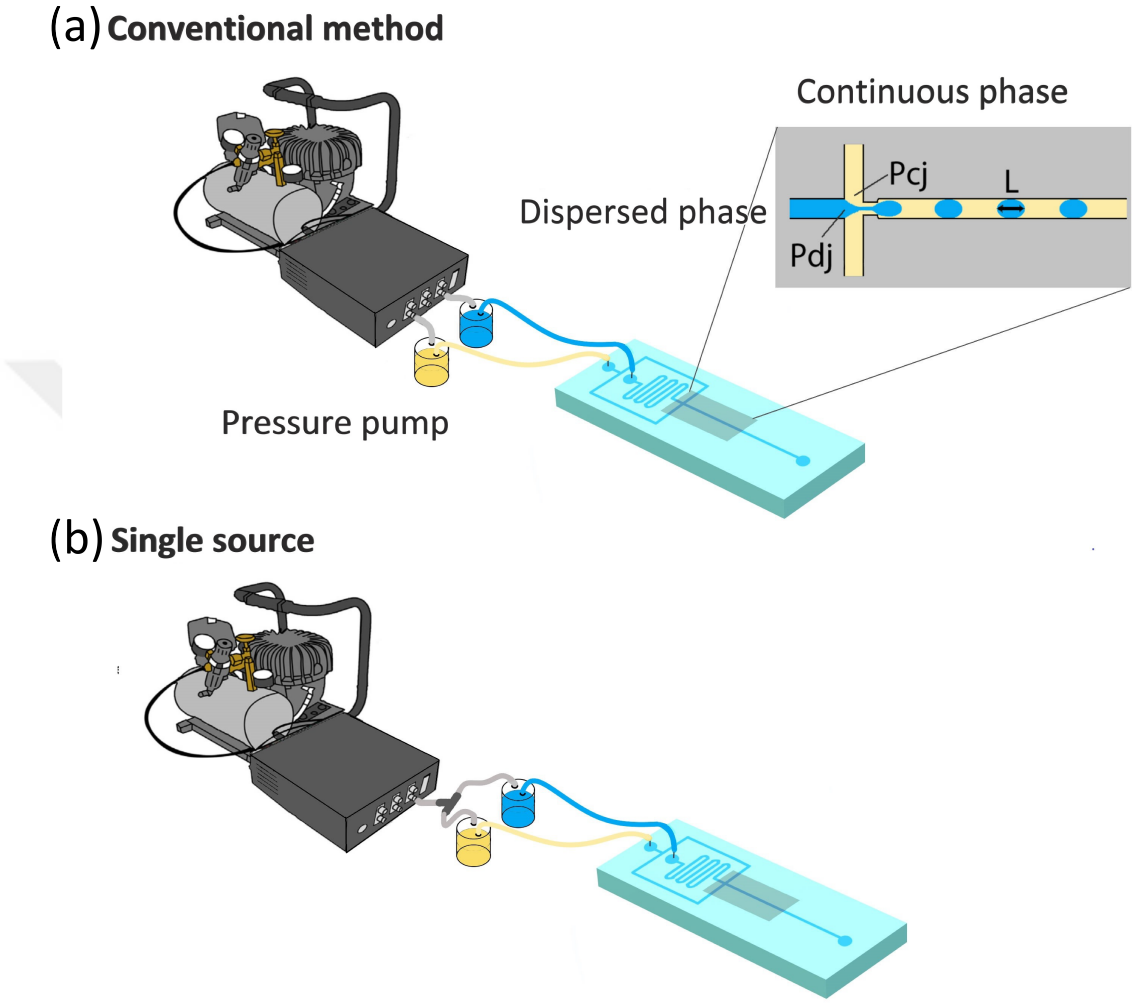

Figure 4.1: Schematic representation of (a) the conventional and (b) proposed method for supplying fluids.

As given in Fig. 4.1a, the two-source conventional configuration, two different ports of the pressure generator were utilized to drive the continuous and dispersed phases. On the other side (Fig. 4.1b) For the single source configuration a bifurcating tubing connector is used to apply the same pressure into both continuous and dispersed phases. Using the mentioned configuration, the inlet pressures for both fluids were identically set to P_{in} = 400, 450, 500, 550 mbar. To achieve a stable pattern of droplet generation, the recording process initiated 3 min after setting applied pressures. A video of the generation of droplets in the specified distance from the junction was recorded by high speed camera.

Afterwards Droplet Morphometry and Velocimetry (DMV) tool [1] which is an image-processing software was used to obtain the coefficient of variation (CV%) for at least 400 droplets. For four inlet pressure, varying from 400 to 550 mbar, the CV% results of the proposed single source (P_d=P_c) and two cases of two sources system (P_d=P_c and P_d=0.99P_c) are obtained and demonstrated in Fig. 4.2.

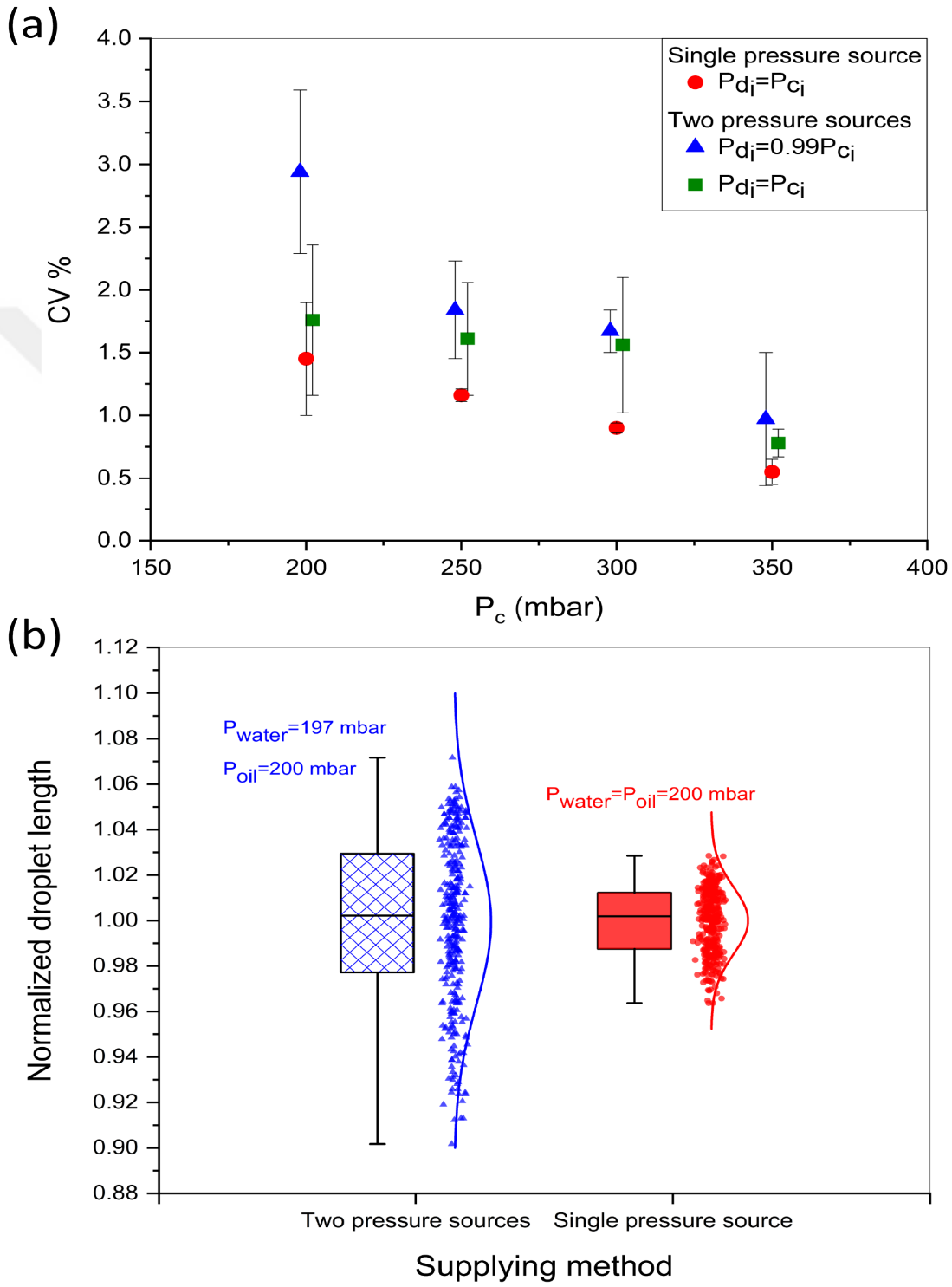

Figure 4.2: (a) Experimental results of droplet monodispersity values in different applied pressures. (b) Distribution of normalized size of individual droplets for a single and two pressure sources configuration.

As it is illustrated in Fig. 4.2 within the applied pressure range in the conventional method the CV% for the identical pressure (P_d=P_c) is lower than different pressure (P_d=0.99P_c) of the continuous and dispersed phase. This is due to the less effect of external fluctuations on flow rate ratio for identical inlet pressure case. However, application of single-source configuration results in smaller CV% values than the conventional method in every applied pressure. The higher CV values of using two pressure source are due to the asynchronous perturbations that inevitably originate from the flow source. Indeed, Using a single pressure source leads synchronous external fluctuations of continuous and dispersed phase fluids at the junction of microfluidic device. Furthermore, it can be deduced from Fig. 4.2 that smaller CV% values are obtained as the inlet pressure increase. In higher applied inlet pressures the inlet flow rates increases and consequently results in the raise of capillary number. According to the previous studies monodispersity improves by increasing capillary number [25]. Thus, as it can also be deduced from Fig. 4.2 higher monodispersity could be achieved by applying higher inlet pressures. Figure 4.2b shows the significant improvement in distribution of normalized size of 400 droplets while sypplying fluids from a single pressure source.

As we discussed before, the other way of improving droplet monodispersity is to optimize the design of channel network [6]. Hence, here also the effect of decreasing the main channel length (R_m) on droplet monodispersity has been studied as one way of network optimization. As demonstrated in Fig. 4.3 microfluidic design with flow-focusing droplet formation sections and five discrete main channel lengths have been utilized to achieve the experimental results. As it can be seen in Fig. 4.3 the serpentine main channel was punched in 5 different specified places and four micro plug valves are placed inside these cavities. This method provides 5 different main channel lengths in the same microfluidic chip and results in the precise measurement compared to the case when different chips with different main channel lengths and fabrication imperfections were used. These valves allow the fluid flows inside the main channel without any leakage problem [60]. The all valves are placed in open position and in order to obtain the desired length, the corresponding valve has been replaced with outlet tubing. Varying the open outlet Results in five different main channel lengths (L_m= 5,

7.5, 10, 12.5 and 15 cm).

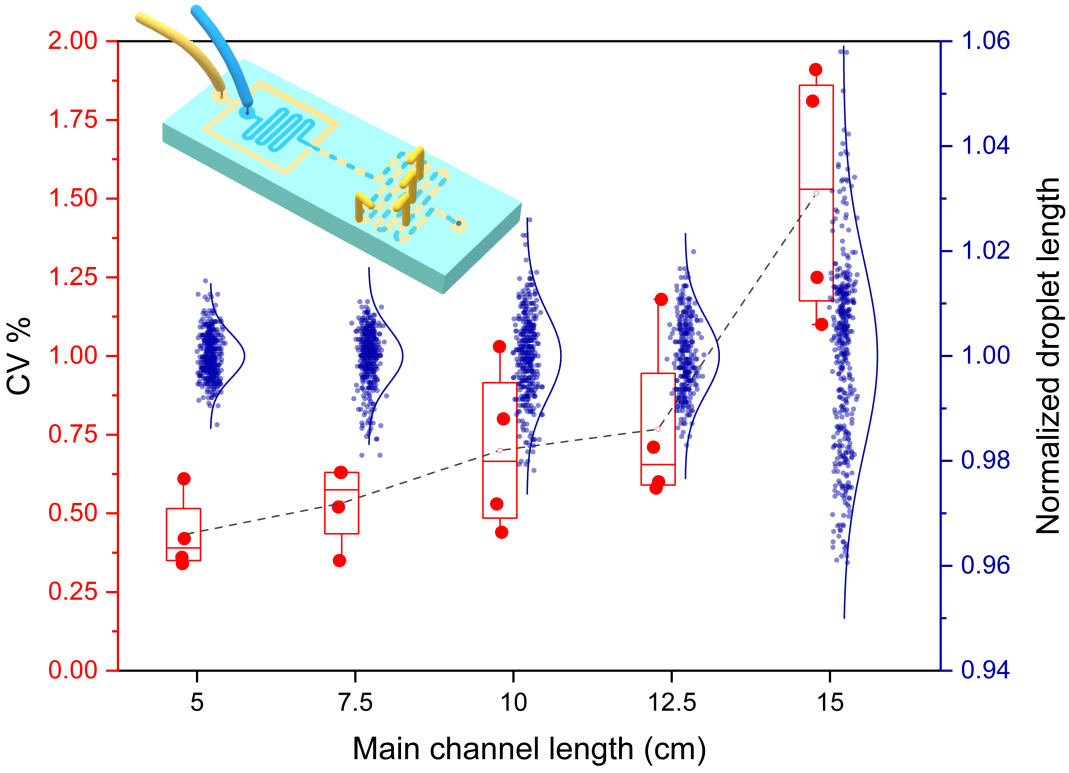

Figure 4.3: Experimental results of droplet monodispersity, CV% (left y-axix) as a function of main channel length (R_m). Distribution of normalized size of 400 individual droplets is shown in blue dots (right y-axis). The chip is equipped with micro plug valves that allows to have a main channel in five different lengths. The experiments were performed for four iterations. The red circles and boxes show CV% value at each iteration and distribution of CV% values, respectively.

As it can be deduced from Fig. 4.3 monodispersity of droplets increases and consequently the CV% of droplets size decreases as a result of decreasing main channel length. For the shortest main channel (L_m= 5 cm) in length, we accommodated 400 droplets in the main channel and obtained a CV of 0.43% (Fig. 4.4). Furthermore, the number of droplets inside the main channel decreases as the main channel shortens, which leads to further reduction of R_m. As a result, it can be deduced from Fig. 4.4 that monodispersity would improve by keeping the main channel length short enough to minimize the effect of internal pressure

fluctuations. More importantly, based on the distribution of CV% values at each main channel length which is shown in red boxes in the fig. 4.3, experiment with longer main channel is more prone to uncertainties.

Another way of optimizing the channel network design to enhance monodispersity is approaching the hydrodynamic resistance of the dispersed phase channel to continuous phase channel (R_c/R_d) to unity. As demonstrated in Fig. 4.4, the identical flow-focusing droplet generating design with a main channel length of 15 cm was applied in these experiments. The R_c/R_d was changed by screwing down or up of a screw valve mounted on the serpentine section of the dispersed phase channel.

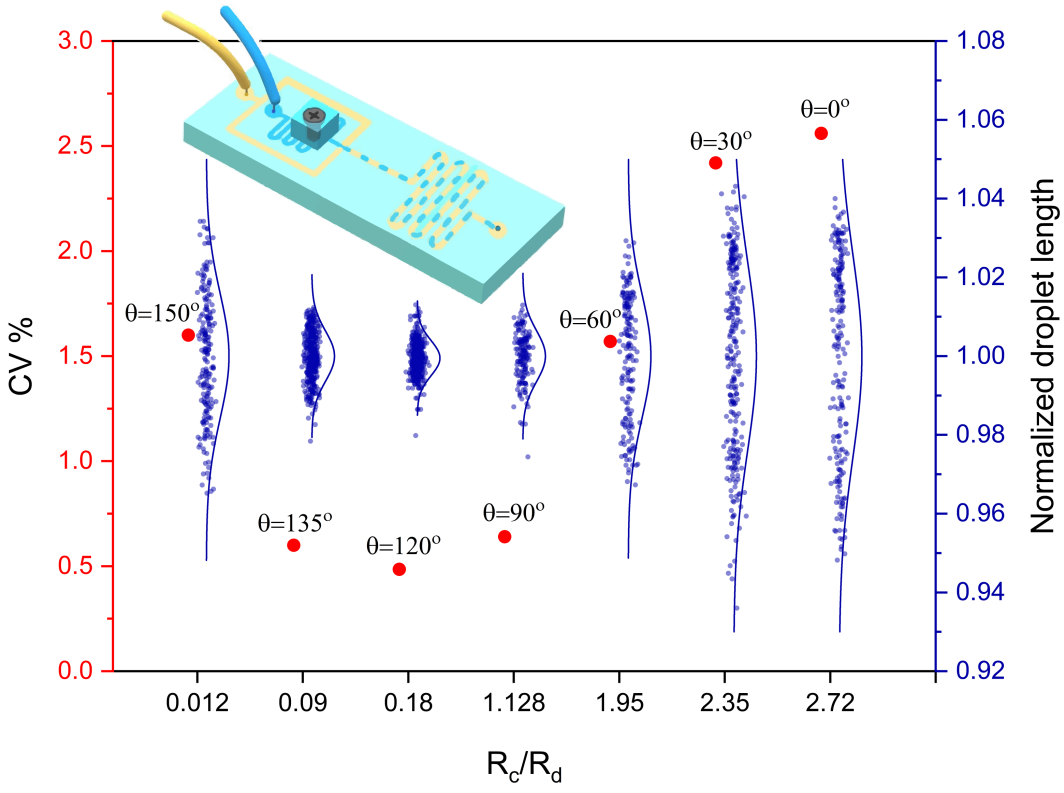

Figure 4.4: Experimental results of droplet monodispersity, CV% as a function of hydrodynamic resistance ratio (R_c/R_d) for the microfluidic device equipped with the screw valve to adjust the R_c/R_d.

Tightening the screw resulted in decreasing channel height and consequently

increasing hydrodynamic resistance (R_d) of the dispersed phase channel. Afterwards, using image processing, quantitative values of R_c/R_d were obtained by measuring the volume ratio of the dispersed phase to the continuous phase in the main channel. Note that, the interfacial tension between water and oil is considered 38 mN/m for all experiments. The screw angles of ($\theta^\circ = 0^\circ, 30^\circ, 60^\circ, 90^\circ, 120^\circ, 135^\circ, 150^\circ$) were set to vary ($R_c/R_d$) by changing the height of the dispersed phase channel. As it can be seen in Fig. 4.4 tightening the screw to the angle of θ°=120 which approximately corresponded to R_c/R_d= 1, resulted in the smallest experimental CV%. The experimental results given in Figs. 4.2,4.3-4 indicate that methods, such as applying high pressure single source supply, a design with short main channel length, and same inlet channel resistances can result in enhanced droplet monodispersity. It is important to know that all obtained results for flow-focusing device is totally in good agreement with the result of a T-junction device (discussed in chapter 3).

4.1.2 Monodisperse droplet generation using syringe pump

Syringe pump is a common flow source used in microfluidic droplet systems to supply fluids in a desired flow rate. On the other hand, for the pressure pump driven systems, high monodispersity was achieved when a single source was used to drive both fluids and R_c/R_d=1. Indeed, these conditions are equivalent to the equal flow rate of dispersed and continuous phase (Q_c=Q_d). Here, the effect of using a single syringe pump to drive both continuous and dispersed phases is studied and compared to the conventional method when two syringe pumps are used to drive fluids. Both single source and conventional method of supplying fluid are demonstrated in Fig. 4.5.

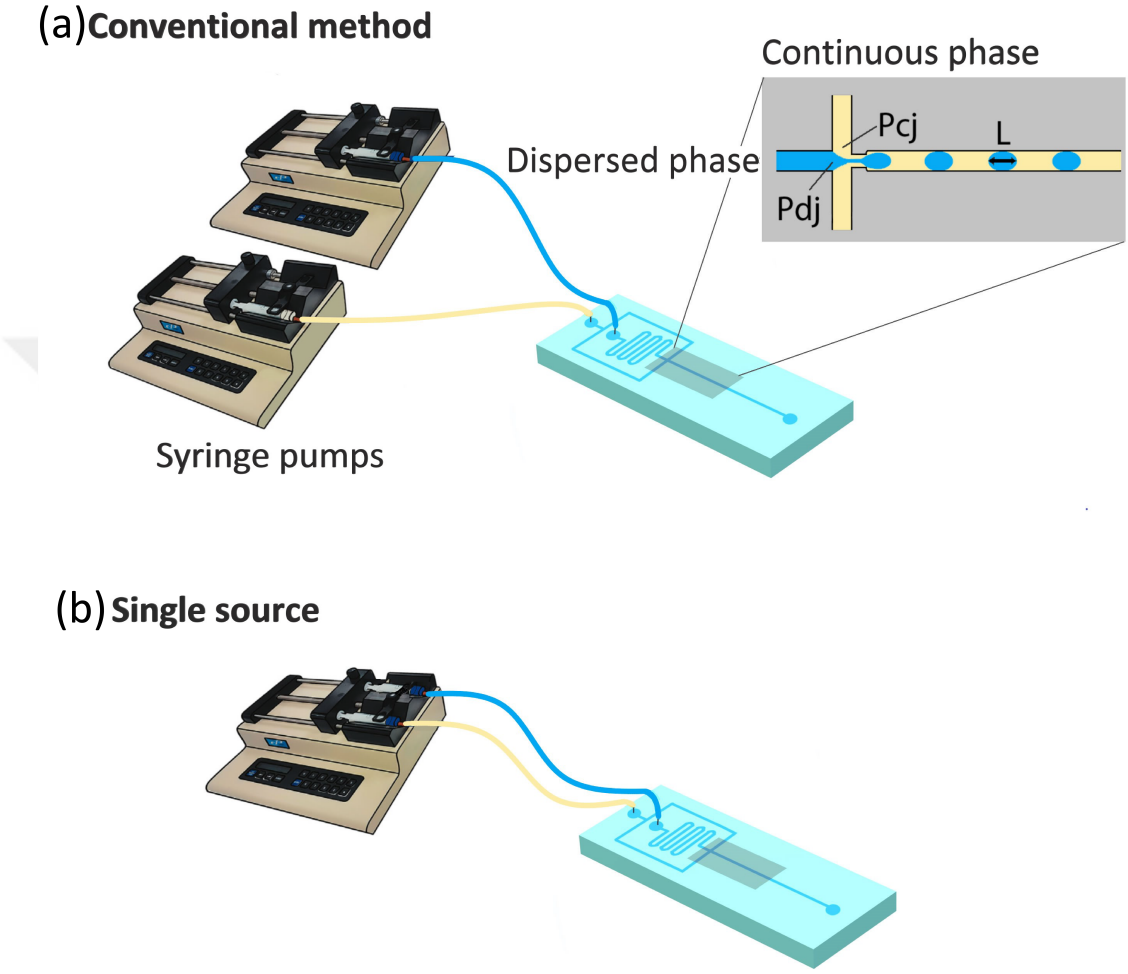

Figure 4.5: Schematic representation of (a) the conventional and (b) proposed method for supplying fluids.

For the single source configuration, the two syringes with the same volume of 5 ml were placed in the same syringe pump and identical flow rates of $Q_c = Q_d$=1, 1.5, 2, 2.5 µl/min were applied. In the conventional method, two different syringe pumps are used to drive the fluids for two cases of inlet flow rates $Q_c = Q_d$ and $Q_c = 0.99Q_d$. The effect of increasing flow rate on monodispersity and the difference between application of single source and two sources are studied. The system ran for 10 min after adjusting the input flow rates to obtain the stable droplet formation. The coefficient of variation (CV%) for different cases are obtained by analyzing recorded video with a high speed camera and postprocessing

using the DMV software for at least 400 consecutive droplets. The CV% results for three cases (single source $Q_c = Q_d$, two sources $Q_c = Q_d$ and two sources $Q_c = 0.99Q_d$) are demonstrated for four inlet flow rates configurations in Fig. 4.6.

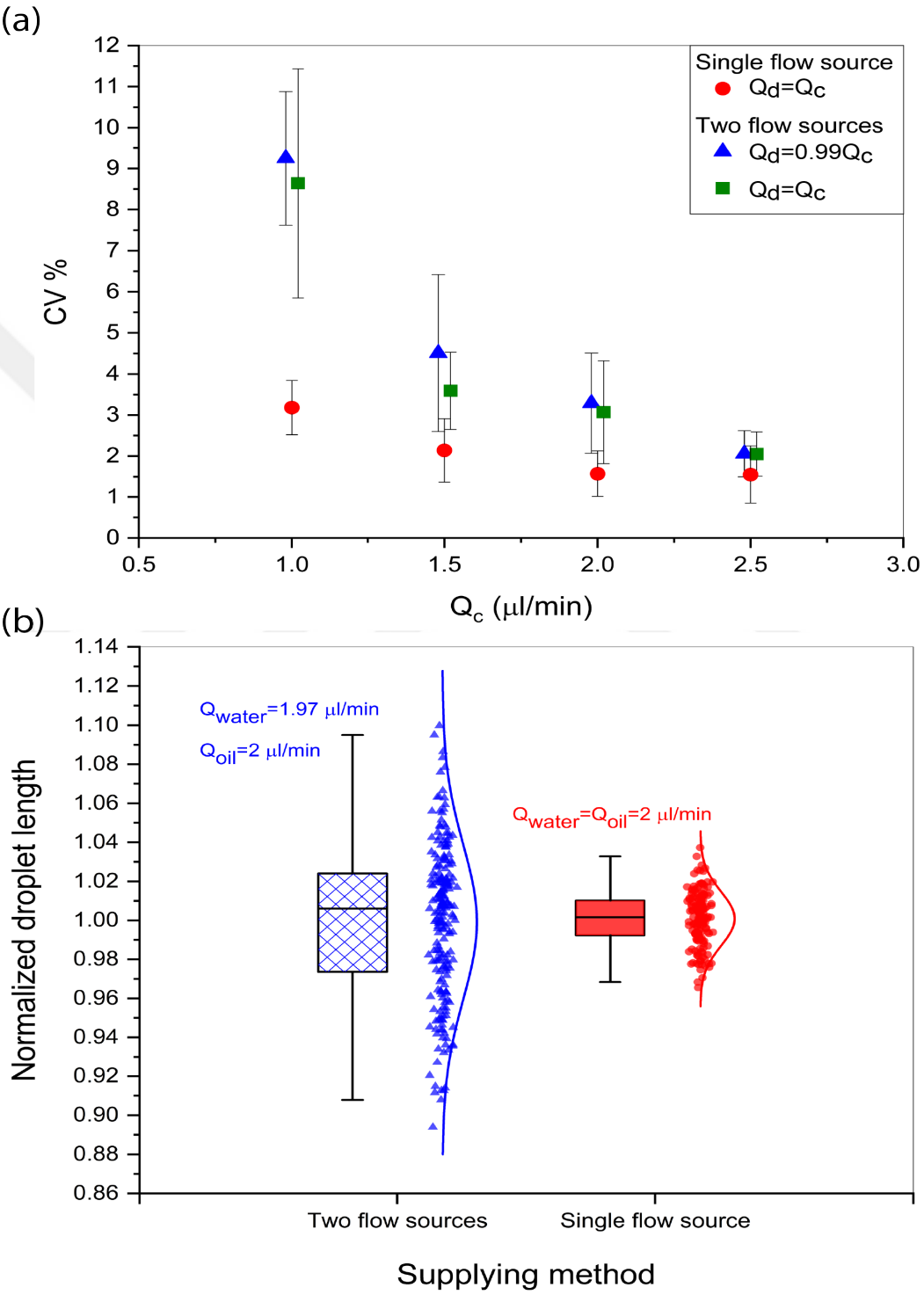

Figure 4.6: (a) Experimental results of droplet monodispersity values in different applied flow rates. (b) Distribution of normalized size of individual droplets for single and two flow sources configuration.

As it can be deduced from Fig. 4.6 like the pressure pump case using single source results in droplet monodispersity improvement by diminishing the effect of external fluctuations of the flow rate caused by the syringe pump. On the other hand, increment of the flow rate and consequently the capillary number resulted in the smaller CV% values which is completely in line with obtained results when using a pressure pump as flow source. Another way to improve droplet monodispersity in the droplet generating with syringe pump driven system is reducing external fluctuations. In order to damp these hydrodynamic fluctuations (discussed in chapter 2), we applied elastomeric off-chip tubing which leads to steady flow rates. Here, the elastomeric off-chip tubing in five different lengths 10, 40, 70, 100, 130 is applied on the single source configuration to obtain the best possible droplet monodispersity. The effect of application of different flexible tubing lengths on droplet monodispersity for the applied 1 µl/min are demonstrated in terms of CV% and normalized droplet length in Fig 4.7.

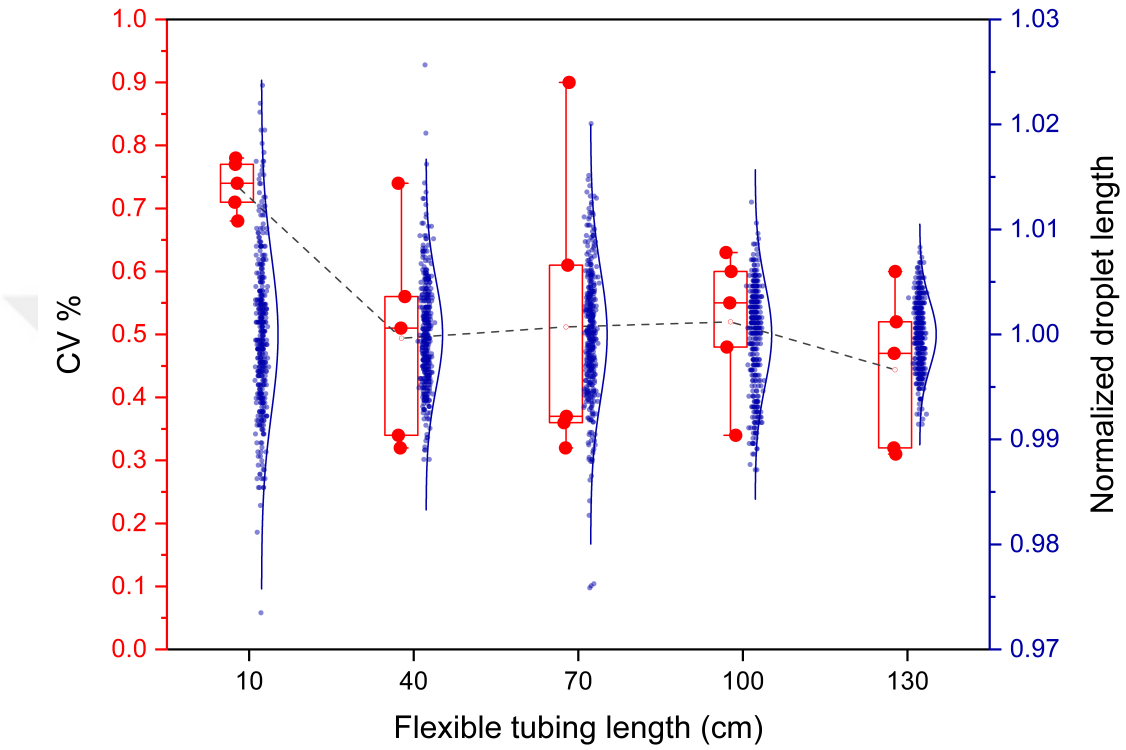

Figure 4.7: CV% and normalized droplet length results of different elastomeric off-chip tubing lengths for the applied 1 µl/min.

As it can be seen in Fig. 4.7 as the length of the flexible tubing rises the monodispersity improves but the improvement is not so considerable since the CV% results for the case with single flow source are already very low and the further reduction is not significant. Note that although the shorter flexible tubing leads to higher CV%, it is less prone to experimental uncertainties (as shown as red boxes in fig. 4.7).

In summary, here we used all recommendation rules that we proposed before to achieve ultra-monodispersity for a flow-focusing device. Doing so, we achieved a droplet monodispersity of 0.5% CV using a flow-focusing droplet generator design and a single pressure source. The verification of previous chapter results shows that our proposed method for droplet monodispersity is a universal method that

can be applied to common microfluidic device such as T-junction or flow-focusing device. More importantly, we compared the performance of common flow sources (pressure and displacement driven pump) in terms of droplet monodispersity while using the offered guidelines. Doing so, we confirmed that our proposed method is valid for the both common drive unit, regardless of their quality.

Chapter 5

Particle synthesis and reaction kinetics using monodisperse droplets

Extremely low volume monodisperse microdroplets are used for chemical, biochemical and biological applications. By using microdroplets researchers can carry out particle synthesis [86], reaction kinetic studies [53], DNA analysis, protein crystallization [87] and various other biochemical applications more precisely [88]. Emulsion is a simplest and high throughput way of droplet generation which is putting together immiscible liquids such as water and oil inside a container without any control of generated droplet size. However, microfluidic techniques provide a simple and reliable route to produce highly controllable droplets inside microfluidic devices. Therefore, droplet-based microfluidic systems allow to have reaction of different materials with different concentrations inside certain and individual volumes. Microfluidic devices with several inlets help to study reactions of different materials for different parameters such as reaction time and speed. Using a flow source like pressure pump we can supply liquids in different pressure into the microfluidic device to have different size of droplets that lead to synthesize various microparticles in different appearance like raspberry or donuts shape. Also, based on the synthesis method reactions can occur inside or at the surface of

droplets that led to have different morphology of synthesized particles. Although particle synthesis in microfludic systems has been done for more than a decade, making monodisperse particles leading to perfect well-ordered pack of particles is still challenging. Indeed, any deviation in droplet size represented as an imperfection in a synthesized particles pattern. At this chapter, we show that the level of droplet monodispersity differentiate the quality of the synthesized particles pattern. Applying our proposed methods to a droplet-based microfluidic system including T-junction or flow-focusing microfluidic device and a pressure pump, we have synthesized mesoporous silica particle, polyethylene glycol (PEG) and supra-molecular capsules in a well-ordered packed pattern. Also, using monodisperse droplets, the reaction kinetics of poly dopamine and hydrogen peroxide has been investigated.

5.1 Silica particle synthesis

At this section we report a simple method to synthesize monodisperse silica particles. Unlike emulsion method, using droplet based microfluidic system allows to have control over individual droplets and consequently, synthesize microparticle in different sizes. A microfluidic T-junction device was used to generate uniform size of aqueous droplets containing catalyst ammonia and cationic surfactant cetyltrimethylammonium bromide (CTAB) which were moving within a carrier fluid consisting heptane and tetraethyl orthosilicate (TEOS) as silica precursor. This method is based on the interfacial polymerization method in which hydrolysis and condensation of the reagents take place at the surface of droplets. In other words, each droplet turns to one particle during reactions. Using a pressure pump as a flow source, we dictate different pressures and consequently can control reaction time of the reagents inside individual droplets. Making monodisperse droplets helps to produce silica particles in a well-ordered hexagonal lattice which can be used in High-performance liquid chromatography (HPLC) columns.

we performed a simple one-step approach to synthesize monodisperse silica microparticles using a T-jucntion microfluidic device. At this approach which

is based on the stober process (sol-gel approach), polymerization takes place at the surface of the monodisperse water-in-oil droplets [86]. A T-junction device with two perpendicular inlet channels with 300 µm width and 80 µm height was used for droplet formation. Supplying aqueous phase (Vwater/Vethanol=1:1) containing catalyst ammonia and cationic surfactant cetyltrimethylammonium bromide (CTAB) from one inlet and heptane and tetraethyl orthosilicate (TEOS) as a silica precursor from the other inlet of the device, we synthesized silica particles (Fig. 1). Ethanol was used as a solvent to enhance mixing of TEOS and water which are initially immiscible. Note that, hydrolysis and condensation of the reagents occur at the surface of the droplets. Then, produced particles transfer to the outside the chip and put in between two glasses to have a better observation of their pattern and uniformity. Making monodisperse droplets and consequently monodisperse silica particle result in produced particles keep their lattice type without any imperfection.

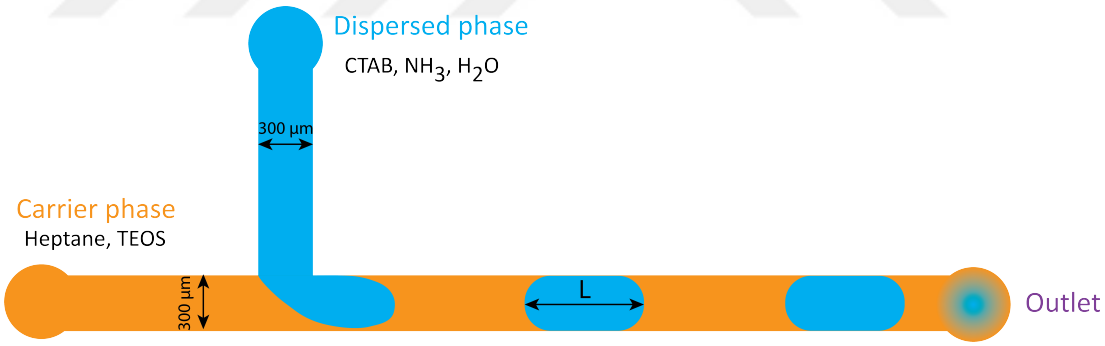

Figure 5.1: Schematic representation of droplet generation inside T-junction microfluidic device.

There are several parameters such as pressure/flow rate fluctuations, dimension of the channel and interfacial tension between two fluids that affect droplet size. Since the droplet size is critical in reaction time, researchers try to have control over the particle size. In addition, since the sol-gel process takes place at the surface of the droplets, we can consider each individual droplet as one particle. In other words, we have one particle per droplet at this approach. we could make uniform silica particles in different sizes by changing pressure of the either dispersed or carrier phase. In addition, any size variation of the droplet may

change the morphology of the final particles. Therefore, we attempt to make highly monodisperse droplets to end up with highly monodisperse silica particles. As shown in figure 5.1, the droplets generated with introducing fluids into the channels. Depending on the flow source that we use, the pressure or flow rate might have some fluctuations that disturb droplet size uniformity. We used a pressure pump as a single flow source to supply liquids based on our results in previous chapters. Also, as we showed in the previous chapters at higher inlet pressure we can generate droplets with better monodispersity. As shown in figure 5.2, silica particle with less coefficient of variation (CV) in size make a well-ordered hexagonal lattice pattern which is highly demanded in HPLC columns. Compare to common emulsion approach, this method is more reliable and simpler and more importantly highly controllable way for particle synthesis.

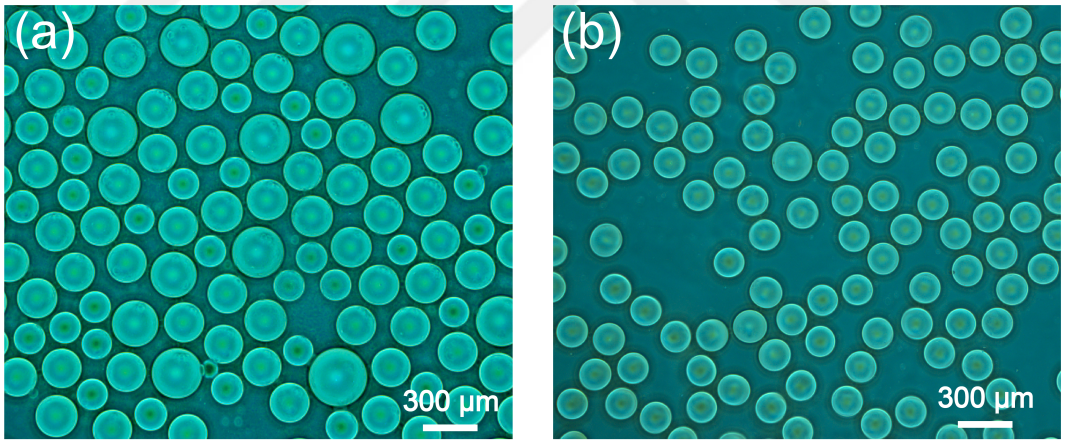

Figure 5.2: Silica Microparticles were synthesized by Interfacial Polymerization. (a) Polydisperse silica particle (CV=4%). (b) Monodisperse silica particle (CV=2.2%).

5.2 PEG particle synthesis

Applying our proposed methods led to monodisperse droplet generation which can be used in different applications. Synthesis of monodisperse particles are one of these applications which is studied in this section. Using the improved

droplet generation design, we produced polyethylene glycol (PEG) particles. For the synthesis of these particles, a mixture of Polyethylene glycol (PEG) diacrylate (42.2% wt) and the photo-initiator (2-Hydroxy-4′-(2-hydroxyethoxy)-2- methyl-propiophenone) (3.7% wt) was prepared and this aqueous solution is used as the dispersed phase. On the other hand, mineral oil together with span 80 (5% wt) as the oil-soluble surfactant is applied as the continuous phase. These solutions were inserted in the optimized droplet generating flow-focusing microchip to generate monodisperse aqueous droplets inside the oil phase. In order to prevent merging of close droplets an additional flow of mineral oil is applied before the outlet as spacer. Pressures of the aqueous phase, continuous phase and additional spacer flow, were all set to the same value of 30 mbar. Generated droplets were transferred into a Petri dish, in which UV photo-polymerization was performed using a LED UV gun (Thor Labs, CS2010). In order to cure droplets, UV exposure (365 nm) for 1 s at 27 w/cm^2 power was applied. Consequently, spherical PEG particles with an average diameter of 65 µm were synthesized.

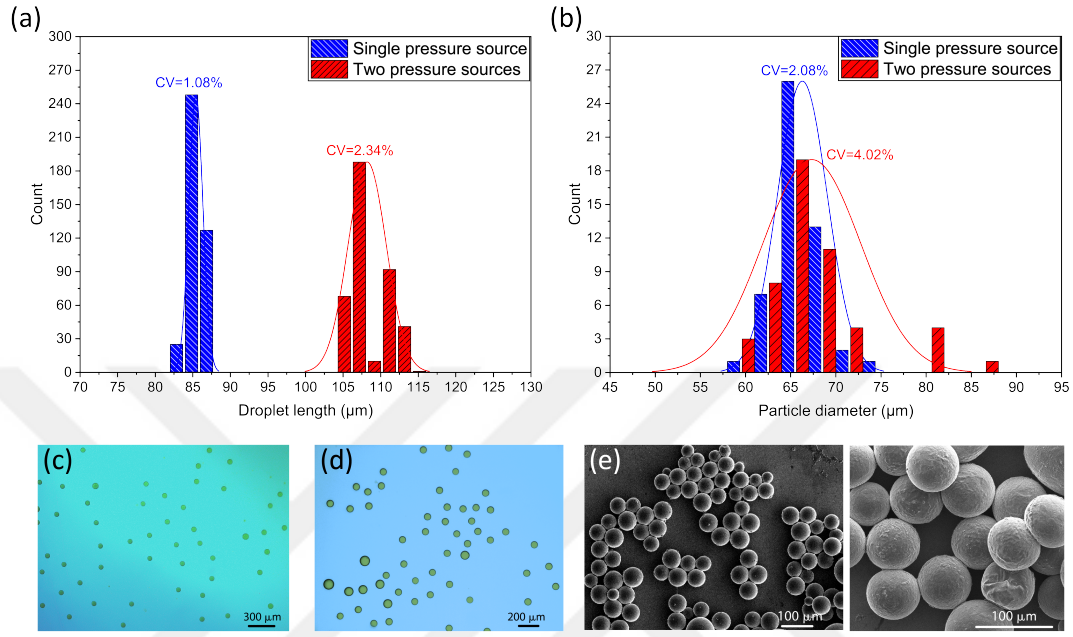

Figure 5.3: (a) histogram of droplet length results measured by DMV for single pressure source and conventional method with two pressure sources for the applied pressure of 30mbar. (b) histogram of polyethylene glycol (PEG) particle diameters synthesized using microfluidic system with single pressure source and two pressure sources for the applied pressure of 30 mbar measured by optical image processing. (c) optical image of monodisperse droplets produced applying single pressure source. (d) optical microscopy image of polydisperse droplets produced applying two pressure sources. e) Electron microscopy images of PEG particles.

Scanning electron microscopy (SEM) image were taken to confirm the spherical shape of the synthesized particles. Applying an optical microscope, the diameter of the particles was determined and the images are demonstrated in Fig. 5.3. The CV value for the diameter measurement of 50 PEG particles was obtained by optical microscopy image analysis as 2.08%. Using DMV analyses the CV of the size of droplets which results these particles was achieved as 1.08%. The histograms for the droplet and particle size distribution are given in Fig. 5.3(a) and (b) respectively. Diameter shrinkage of 23.5% is observed during photopolymerization.

5.3 Supramolecular polymer capsule synthesis

Droplet based systems make it possible to have interfacial assembly of polymers in capsule shape. Depending on the material concentration and reaction rate the final morphology of the capsules will be different. Here, using the proposed guidelines of ultra monodisperse droplet generation, we could make highly monodisperse capsules. As shown in figure 11, we used a pressure source as a single flow source to supply Azide, cucurbit[6](CB[6]) and DI water as a dispersed phase and Hexadecane, Chloroform and Alkyne in $CHCL_3$ as a continuous phase to a flow-focusing microfluidic device. Using the efficiency of cucurbit[6]uril host–guest supramolecular chemistry, we could make network shape of supramolecular polymer. Microcapsules formed after evaporation of the chloroform from droplet, resulting in a wrinkled shape structure. Diameter shrinkage of 40% is observed during wrinkled shape formation.

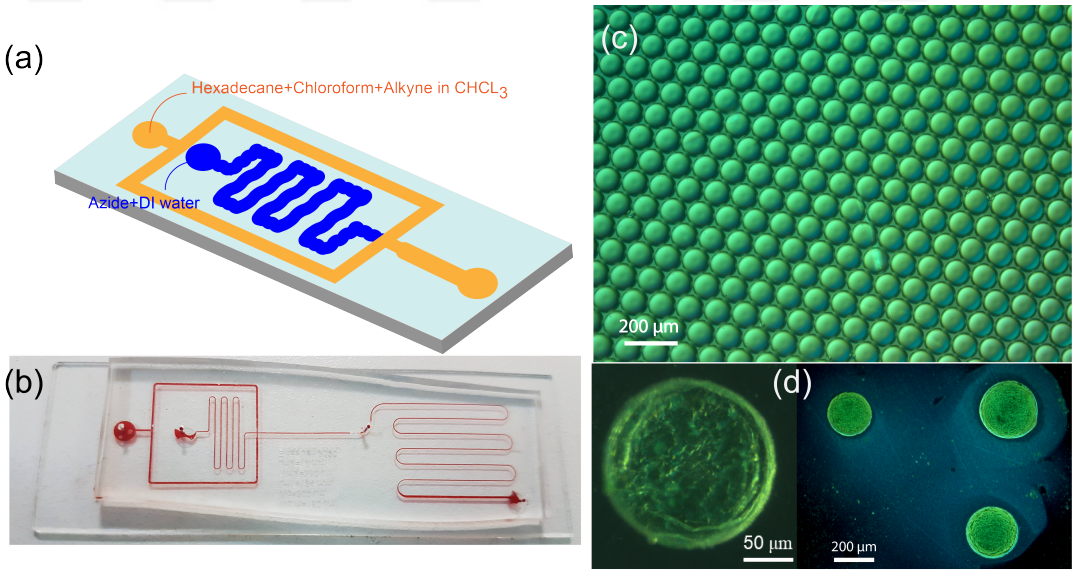

Figure 5.4: The schematic representation (a) and the photograph (b) of the microfluidic flow-focusing device used for supramolecular capsule generation. (c) The ultra-monodisperse microdroplets stored in a petri dish. (d) Optical microscopy image of wrinkled shape supramolecular capsules.

The dispersed phase was prepared by dissolving Azide and CB[6] in water,

while the carrier phase consists of a 1:5 v/v mixture of chloroform in hexadecane, into which Alkyne in $CHCL_3$ was dissolved. We added 3 wt% of the surfactant Span 80 to the continuous phase to prevent microdroplets from merging. Based on our proposed method, the continuous phase (oil) and dispersed phase (aqueous) were pumped into the device at identical pressure of 60 mbar. Then, microdroplets were collected in the pteri dish or on the surface of glass slide for optical image. As shown in the fig. 5.4(c), ultr-monodisperse droplets allows to have well-ordered hexagonal packing of capsules were produced.

5.4 Reaction kinetics

At this section, we use the ultra-monodisperse droplet generation system for reaction kinetics measurement. Specifically, we have studied the autopolymerization of spontaneously oxidized dopamine (DA) to polydopamine and fluorescence enhancement of (PDA) by H_2O_2. DA is a potential biomarker for several neurological diseases such as schizophrenia, Huntington's and Parkinson's diseases. PDA is known for its nontoxicity and biodegradability. Aggregation induced quenching (AIQ) of PDA is inhibited by addition of H_2O_2 yielding fluorescence enhancement. This phenomenon is still unexplored and can be an important H2O2 probe once the reaction is fully understood. In this section, we used an ultra monodisperse droplet system to understand the reaction kinetics involved in PDA polymerization and AIQ inhibition of PDA.

Microfluidics offer advantages for studying reaction kinetics, such as high spatio-temporal resolution, using very low sample volumes and high sensitivity. Using droplet-based microfluidic systems, reaction kinetics have been investigated [1,2]. Droplet monodispersity plays a significant role in such reaction kinetic measurements since any variation in droplet size reflects itself as concentration variation. Therefore, precision reaction kinetic studies require a highly monodisperse droplet system.

Reaction of dopamine and hydrogen peroxide has been very recently discovered, but the kinetics is still unknown [5, 6]. The photoluminescence emission spectra of the polydopamine (PDA) show that the concentration of the reagent and substrate (hydrogen peroxide and dopamine) plays a significant role on reaction kinetics. Using our enhanced monodisperse droplet system, we investigate the reaction kinetics of the increased fluorescent emission of PDA. Figure 5.5, shows the illustrative schematic of our microfluidic system.

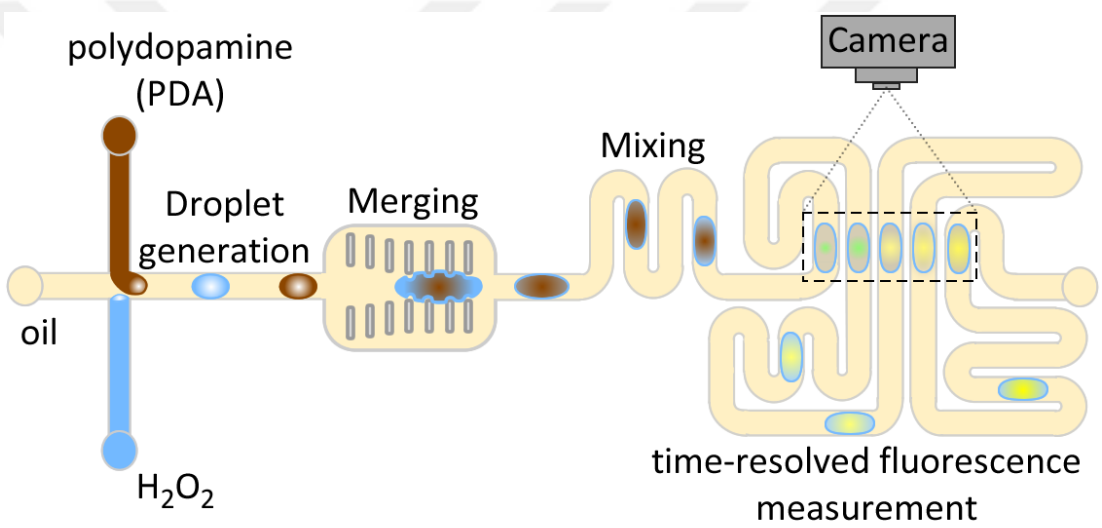

Figure 5.5: Schematic of ultra-monodisperse droplet system used for reaction kinetics investigation. Merging of H_2O_2 and polydopamine droplets were studied.

Monodisperse droplets of two fluids to be mixed are formed individually and mixed so that the concentration of the final droplet is precisely regulated. After droplet merging, five long channel segments with the same length is used to characterize the reaction in the time scale (Fig. 5.6).

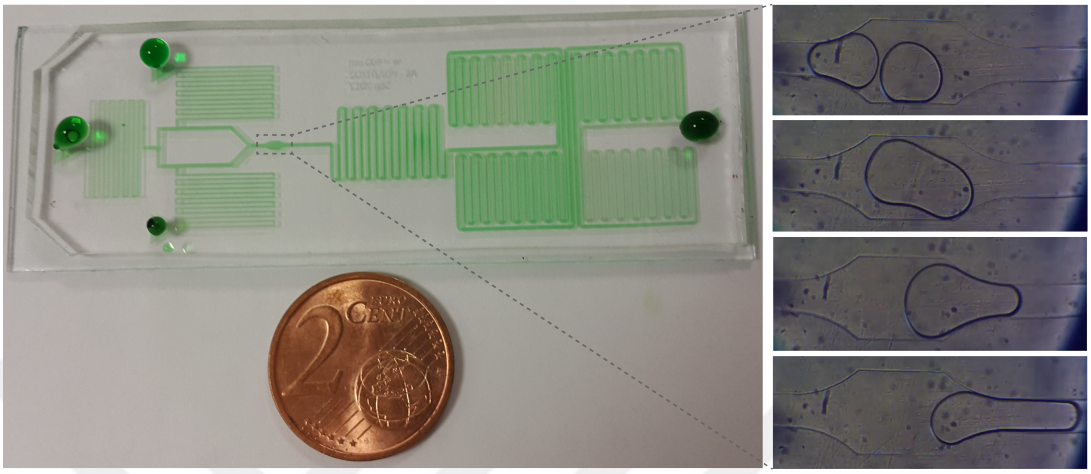

Figure 5.6: Fabricated microfluidic device containing two T-junction droplet generation module, a passive droplet merging unit and long channel segments for temporal study of the reaction.

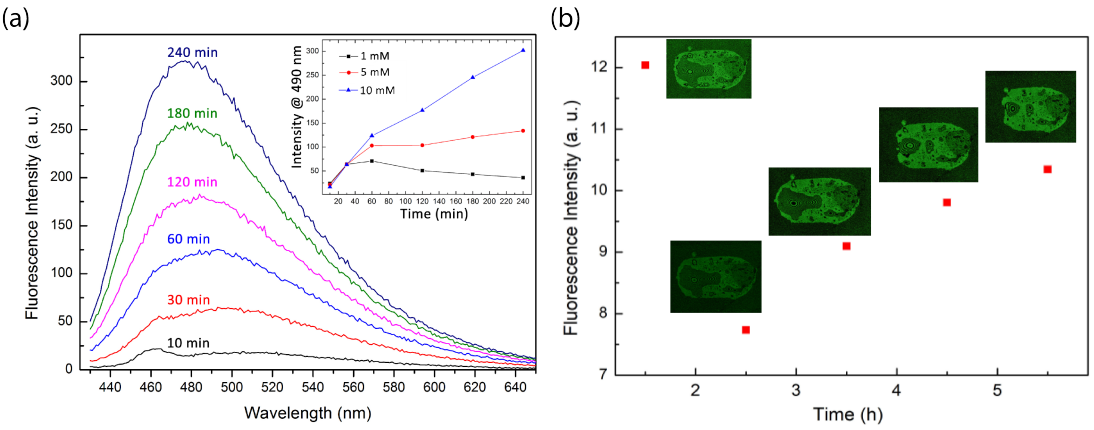

Figure 5.7: (a) Bulk spectrometer fluorescence intensity at 490 nm in the presence of 1 mM, 5 mM and 10 mM H_2O_2 . (b) Time-dependent fluorescence spectra of PDA inside droplets for 50 mM H_2O_2.

First monodisperse droplets of two fluids were formed and monodispersity, thus concentration precision, was ensured. Then, the change of the fluorescence intensity of PDA due to the change of reaction time is studied. Time-dependent fluorescence spectra of PDA in the presence of 50 mM H_2O_2 was investigated

with the droplet system (Fig. 5.7b) and verified with spectrometer results (Fig. 5.7a)

After all, the ultra monodisperse droplet-based system provides a sensitive and automated platform to study particle synthesis and reaction kinetics in high precision. Using an automated microfluidic device results reaction kinetics for varying reagent concentrations can be studied to investigate response curves and limit of detection for potential assays.

Chapter 6

Summary and Future Directions

6.1 Summary

Droplet fluidics already has a history of 20 years. Droplet monodispersity is one of the most basic requirements of such systems, which aims for identical volume droplet generation. Although the physics of droplet formation and the individual factors that affect droplet size are identified previously, the governing mechanism of droplet size variation remains elusive thus far.

We have addressed this very fundamental question and developed a very practical method and design guidelines to obtain the most monodisperse droplets reported so far. In this thesis, we present new approaches to tackle the fundamental question of monodisperse droplet generation. We use the analogy between electrical and fluidic circuits to model the droplet generation dynamics. Although this similarity has been commonly used for single-phase flow systems, it was not applicable to droplet systems, mainly due to the fact that electrical systems only govern flow of a single phase, i.e. electrons. We were able to introduce circuit elements to model the discrete phase so that the droplets in two-phase flow microfluidic systems can be represented in electrical terms. This approach provided us a deeper insight into the dynamics involved in droplet size variation and led

to some surprising results. We also coupled this numerical method with an analytical approach. Consequently, we have shown the factors that sacrifice droplet monodispersity. We have verified our numerical and analytical results with extensive experiments. Furthermore, we provide very basic and practical design guidelines to improve droplet monodispersity which are grouped in two categories: (i) flow source configuration and (ii) channel network design. Applying these design rules, we were able to obtain the world-record monodispersity values reported in the literature so far. More importantly, we explained the practical limit of achieving absolute monodispersity, 0% coefficient of variation.

Additionally, it was shown that our proposed method is valid for common microfluidic devices such as T-junction and flow-focusing devices. Also, we compared the performance of the syringe pump and pressure pump as a flow source for supplying fluids using the conventional and proposed method in terms of droplet monodispersity.

Finally, the generated monodisperse droplets allowed to investigate reaction kinetics of poly dopamine and hydrogen peroxide in a droplet-based microfluidic system with a good control on the reagents concentration and reaction time. Moreover, we could synthesize silica and polyethylene glycol (PEG) particles and supramolecular polymer capsules in a well-ordered hexagonal lattice pattern thank to high level of droplet monodispersity that we achieved.

6.2 Future Directions

Today, droplet-based systems are expanding, e.g. digital PCR, the monodispersity is becoming ever more important, since it affects assay quantification results directly. Additionally, droplet based biochemical analysis techniques are now becoming standard tools in research laboratories. Lately, 10xGenomics has shown a variety of droplet-based advanced precise analysis products. Although it has been more than ten years that the first droplet digital polymerase chain reaction (DPCR) was commercialized for quantifying target nucleic acids in a sample, the

minimum volume uncertainty of such commercial instruments reported so far is 0.8% [89]. However, the need for monodisperse droplet generation (low volume uncertainty) is very critical for such high precision instruments.

For some applications of droplet microfluidics, high variation in droplet volume may be acceptable. However, for certain applications, such as polymerase chain reactions (PCR) or enzyme-linked immunosorbent assay (ELISA), any variation in droplet volume reflects itself directly as imprecision in the final result, which is equivalent to the uncertainties in detection of single entities (nucleic acid, proteins, or cells).

We envision that the methods we propose in this thesis will be utilized for all the upcoming droplet fluidic systems with digital assay in which each isolated droplet considered as a container of a discrete number of biological entities (0, 1, 2, 3, . . .). At these systems, achieving to ultra-monodispersity bring a new level of precision and sensitivity in quantifying nucleic acids, measuring proteins and their enzymatic activity, and probing single-cell genotype and phenotype. Also, synthesizing particle with high level of monodispersity enables making well-ordered pack of particles in a desired size which can dramatically increase precision of measurements in High Performance Liquid Chromatography (HPLC) or can be used as template in photonic crystals.

Bibliography

[1] A. S. Basu, "Droplet morphometry and velocimetry (DMV): A video processing software for time-resolved, label-free tracking of droplet parameters," *Lab on a Chip*, vol. 13, no. 10, pp. 1892–1901, 2013.

[2] A. Saateh, A. Kalantarifard, O. T. Celik, M. Asghari, M. Serhatlioglu, and C. Elbuken, "Real-time impedimetric droplet measurement (iDM)," *Lab on a Chip*, vol. 19, no. 22, pp. 3815–3824, 2019.

[3] Z. Isiksacan, M. T. Guler, A. Kalantarifard, M. Asghari, and C. Elbuken, "Lab-on-a-chip platforms for disease detection and diagnosis," in *Biosensors and Nanotechnology: Applications in Health Care Diagnostics*, pp. 155–181, 2018.

[4] A. Kalantarifard, A. Saateh, and C. Elbuken, "Label-free sensing in microdroplet-based microfluidic systems," 2018.

[5] A. Kalantarifard, E. Alizadeh Haghighi, and C. Elbuken, "Damping hydrodynamic fluctuations in microfluidic systems," *Chemical Engineering Science*, vol. 178, pp. 238–247, mar 2018.

[6] A. Kalantarifard, E. Alizadeh-Haghighi, A. Saateh, and C. Elbuken, "Theoretical and experimental limits of monodisperse droplet generation," *Chemical Engineering Science*, vol. 229, p. 116093, jan 2021.

[7] C. K. Law and W. A. Sirignano, "Unsteady droplet combustion with droplet heating-II: Conduction limit," *Combustion and Flame*, vol. 28, no. C, pp. 175–186, 1977.

[8] M. Suzuki and K. Asano, "A mathematical model of droplet charging in ink-jet printers," *Journal of Physics D: Applied Physics*, vol. 12, no. 4, pp. 529–537, 1979.

[9] A. Bhardwaj and S. Hartland, "Dynamics of Emulsification and Demulsification of Water in Crude Oil Emulsions," *Industrial and Engineering Chemistry Research*, vol. 33, no. 5, pp. 1271–1279, 1994.

[10] M. E. Fraser, W. K. Lu, A. E. Hamielec, and R. Murarka, "Surface tension measurements on pure liquid iron and nickel by an oscillating drop technique," Tech. Rep. 3, 1971.

[11] B. Madivala, S. Vandebril, J. Fransaer, and J. Vermant, "Exploiting particle shape in solid stabilized emulsions," *Soft Matter*, vol. 5, no. 8, pp. 1717–1727, 2009.

[12] R. G. Harrison, A. L. Washburn, A. T. Pickett, and D. M. Call, "Assembly of CdSe nanoparticles into microspheres by a liquid droplet emulsion process," *Journal of Materials Chemistry*, vol. 18, no. 31, pp. 3718–3722, 2008.

[13] T. S. Kaminski and P. Garstecki, "Controlled droplet microfluidic systems for multistep chemical and biological assays," *Chemical Society Reviews*, vol. 46, no. 20, pp. 6210–6226, 2017.

[14] T. Thorsen, R. W. Roberts, F. H. Arnold, and S. R. Quake, "Dynamic pattern formation in a vesicle-generating microfluidic device," *Physical Review Letters*, vol. 86, no. 18, pp. 4163–4166, 2001.

[15] J. H. Xu, S. W. Li, J. Tan, Y. J. Wang, and G. S. Luo, "Controllable preparation of monodisperse O/W and W/O emulsions in the same microfluidic device," *Langmuir*, vol. 22, no. 19, pp. 7943–7946, 2006.

[16] A. M. Gañán-Calvo and J. M. Gordillo, "Perfectly monodisperse microbubbling by capillary flow focusing," *Physical Review Letters*, vol. 87, no. 27 I, pp. 2745011–2745014, 2001.

[17] M. De menech, P. Garstecki, F. Jousse, and H. A. Stone, "Transition from squeezing to dripping in a microfluidic T-shaped junction," *Journal of Fluid Mechanics*, vol. 595, pp. 141–161, 2008.

[18] S. Bashir, J. M. Rees, and W. B. Zimmerman, "Simulations of microfluidic droplet formation using the two-phase level set method," *Chemical Engineering Science*, vol. 66, no. 20, pp. 4733–4741, 2011.

[19] A. B. Theberge, F. Courtois, Y. Schaerli, M. Fischlechner, C. Abell, F. Hollfelder, and W. T. Huck, "Microdroplets in microfluidics: An evolving platform for discoveries in chemistry and biology," *Angewandte Chemie - International Edition*, vol. 49, no. 34, pp. 5846–5868, 2010.

[20] T. Ward, M. Faivre, M. Abkarian, and H. A. Stone, "Microfluidic flow focusing: Drop size and scaling in pressure versus flow-rate-driven pumping," *Electrophoresis*, vol. 26, no. 19, pp. 3716–3724, 2005.

[21] P. Garstecki, M. J. Fuerstman, H. A. Stone, and G. M. Whitesides, "Formation of droplets and bubbles in a microfluidic T-junction - Scaling and mechanism of break-up," *Lab on a Chip*, vol. 6, no. 3, pp. 437–446, 2006.

[22] J. H. Xu, S. W. Li, J. Tan, and G. S. Luo, "Correlations of droplet formation in T-junction microfluidic devices: From squeezing to dripping," *Microfluidics and Nanofluidics*, vol. 5, no. 6, pp. 711–717, 2008.

[23] T. Glawdel and C. L. Ren, "Global network design for robust operation of microfluidic droplet generators with pressure-driven flow," *Microfluidics and Nanofluidics*, vol. 13, no. 3, pp. 469–480, 2012.

[24] A. R. Abate, P. Mary, V. Van Steijn, and D. A. Weitz, "Experimental validation of plugging during drop formation in a T-junction," *Lab on a Chip*, vol. 12, pp. 1516–1521, apr 2012.

[25] P. A. Romero and A. R. Abate, "Flow focusing geometry generates droplets through a plug and squeeze mechanism," *Lab on a Chip*, vol. 12, no. 24, pp. 5130–5132, 2012.

[26] N. R. Beer, K. A. Rose, and I. M. Kennedy, "Observed velocity fluctuations in monodisperse droplet generators," *Lab on a Chip*, vol. 9, no. 6, pp. 838–840, 2009.

[27] V. van Steijn, M. T. Kreutzer, and C. R. Kleijn, "Velocity fluctuations of segmented flow in microchannels," *Chemical Engineering Journal*, vol. 135, no. SUPPL. 1, pp. S159–S165, 2008.

[28] P. M. Korczyk, O. Cybulski, S. Makulska, and P. Garstecki, "Effects of unsteadiness of the rates of flow on the dynamics of formation of droplets in microfluidic systems," *Lab on a Chip*, vol. 11, no. 1, pp. 173–175, 2011.

[29] Z. Li, S. Y. Mak, A. Sauret, and H. C. Shum, "Syringe-pump-induced fluctuation in all-aqueous microfluidic system implications for flow rate accuracy," *Lab on a Chip*, vol. 14, no. 4, pp. 744–749, 2014.

[30] J. Ruzicka, G. D. Marshall, and G. D. Christian, "Variable Flow Rates and a Sinusoidal Flow Pump for Flow Injection Analysis," *Analytical Chemistry*, vol. 62, no. 17, pp. 1861–1866, 1990.

[31] W. Zeng, I. Jacobi, S. Li, and H. A. Stone, "Variation in polydispersity in pump- and pressure-driven micro-droplet generators," *Journal of Micromechanics and Microengineering*, vol. 25, no. 11, 2015.

[32] W. Zeng, I. Jacobi, D. J. Beck, S. Li, and H. A. Stone, "Characterization of syringe-pump-driven induced pressure fluctuations in elastic microchannels," *Lab on a Chip*, vol. 15, no. 4, pp. 1110–1115, 2015.

[33] Y. Pang, H. Kim, Z. Liu, and H. A. Stone, "A soft microchannel decreases polydispersity of droplet generation," *Lab on a Chip*, vol. 14, no. 20, pp. 4029–4034, 2014.

[34] S. J. Hwang, S. K. Moon, S. E. Kim, J. H. Kim, and S. W. Choi, "Production of uniform emulsion droplets using a simple fluidic device with a peristaltic pump," *Macromolecular Research*, vol. 22, no. 5, pp. 557–561, 2014.

[35] C. Li, J. Xu, and B. Ma, "A self-powered microfluidic monodispersed droplet generator with capability of multi-sample introduction," *Microfluidics and Nanofluidics*, vol. 18, no. 5-6, pp. 1067–1073, 2015.

[36] D. R. Link, S. L. Anna, D. A. Weitz, and H. A. Stone, "Geometrically Mediated Breakup of Drops in Microfluidic Devices," *Physical Review Letters*, vol. 92, no. 5, p. 4, 2004.

[37] J. H. Xu, S. W. Li, J. Tan, Y. J. Wang, and G. S. Luo, "Controllable preparation of monodisperse O/W and W/O emulsions in the same microfluidic device," *Langmuir*, vol. 22, pp. 7943–7946, sep 2006.

[38] K. W. Oh, K. Lee, B. Ahn, and E. P. Furlani, "Design of pressure-driven microfluidic networks using electric circuit analogy," *Lab on a Chip*, vol. 12, no. 3, pp. 515–545, 2012.

[39] H. Bruus, "Theoretical microfluidics," 2008.

[40] S. R. Schmid, B. J. Hamrock, and B. O. Jacobson, *Fundamentals of Machine Elements, Third Edition: SI Version*. CRC Press, 2014.

[41] M. Aurelio, C. Ayala, and M. S. M. Engineering, *Hydrodynamic Resistance and Sorting of Deformable Particles in Microfluidic Circuits PhD in Mechanical Engineering Hydrodynamic Resistance and Sorting of Deformable Particles in Microfluidic Circuits*. PhD thesis, 2013.

[42] T. Glawdel, C. Elbuken, and C. L. Ren, "Droplet formation in microfluidic T-junction generators operating in the transitional regime. I. Experimental observations," *Physical Review E - Statistical, Nonlinear, and Soft Matter Physics*, vol. 85, no. 1, pp. 1–12, 2012.

[43] T. Glawdel, C. Elbuken, and C. L. Ren, "Droplet formation in microfluidic T-junction generators operating in the transitional regime. I. Experimental observations," *Physical Review E - Statistical, Nonlinear, and Soft Matter Physics*, vol. 85, no. 1, pp. 1–9, 2012.

[44] C. Y. Lee, Y. H. Lin, and G. B. Lee, "A droplet-based microfluidic system capable of droplet formation and manipulation," *Microfluidics and Nanofluidics*, vol. 6, no. 5, pp. 599–610, 2009.

[45] A. Raj, R. Halder, P. Sajeesh, and A. K. Sen, "Droplet generation in a microchannel with a controllable deformable wall," *Microfluidics and Nanofluidics*, vol. 20, no. 7, pp. 1–16, 2016.

[46] V. Van Steijn, C. R. Kleijn, and M. T. Kreutzer, "Predictive model for the size of bubbles and droplets created in microfluidic T-junctions," *Lab on a Chip*, vol. 10, no. 19, pp. 2513–2518, 2010.

[47] X. Wang, A. Riaud, K. Wang, and G. Luo, "Pressure drop-based determination of dynamic interfacial tension of droplet generation process in T-junction microchannel," *Microfluidics and Nanofluidics*, vol. 18, no. 3, pp. 503–512, 2015.

[48] J. H. Xu, S. W. Li, J. Tán, Y. J. Wang, and G. S. Luo, "Preparation of highly monodisperse droplet in a T-junction microfluidic device," *AIChE Journal*, vol. 52, no. 9, pp. 3005–3010, 2006.

[49] J. H. Xu, G. S. Luo, S. W. Li, and G. G. Chen, "Shear force induced monodisperse droplet formation in a microfluidic device by controlling wetting properties," *Lab on a Chip*, vol. 6, no. 1, pp. 131–136, 2006.

[50] D. A. Boy, F. Gibou, and S. Pennathur, "Simulation tools for lab on a chip research: Advantages, challenges, and thoughts for the future," *Lab on a Chip*, vol. 8, no. 9, pp. 1424–1431, 2008.

[51] H. Tanaka, S. Yamamoto, A. Nakamura, Y. Nakashoji, N. Okura, N. Nakamoto, K. Tsukagoshi, and M. Hashimoto, "Hands-off preparation of monodisperse emulsion droplets using a poly(dimethylsiloxane) microfluidic chip for droplet digital PCR," *Analytical Chemistry*, vol. 87, no. 8, pp. 4134–4143, 2015.

[52] J. Y. Kim, S. W. Cho, D. K. Kang, J. B. Edel, S. I. Chang, A. J. Demello, and D. O'Hare, "Lab-chip HPLC with integrated droplet-based microfluidics for

separation and high frequency compartmentalisation," *Chemical Communications*, vol. 48, no. 73, pp. 9144–9146, 2012.

[53] A. J. DeMello, "Control and detection of chemical reactions in microfluidic systems," *Nature*, vol. 442, no. 7101, pp. 394–402, 2006.

[54] M. Nekouei and S. A. Vanapalli, "Volume-of-fluid simulations in microfluidic T-junction devices: Influence of viscosity ratio on droplet size," *Physics of Fluids*, vol. 29, no. 3, 2017.

[55] D. F. Crawford, C. A. Smith, and G. Whyte, "Image-based closed-loop feedback for highly mono-dispersed microdroplet production," *Scientific Reports*, vol. 7, no. 1, pp. 1–9, 2017.

[56] Y. J. Kang and S. Yang, "Fluidic low pass filter for hydrodynamic flow stabilization in microfluidic environments," *Lab on a Chip*, vol. 12, no. 10, pp. 1881–1889, 2012.

[57] B. Mosadegh, C. H. Kuo, Y. C. Tung, Y. S. Torisawa, T. Bersano-Begey, H. Tavana, and S. Takayama, "Integrated elastomeric components for autonomous regulation of sequential and oscillatory flow switching in microfluidic devices," *Nature Physics*, vol. 6, no. 6, pp. 433–437, 2010.

[58] A. Grimmer, X. Chen, M. Hamidović, W. Haselmayr, C. L. Ren, and R. Wille, "Simulation before fabrication: a case study on the utilization of simulators for the design of droplet microfluidic networks," *RSC Advances*, vol. 8, no. 60, pp. 34733–34742, 2018.

[59] S. A. Vanapalli, A. G. Banpurkar, D. Van Den Ende, M. H. Duits, and F. Mugele, "Hydrodynamic resistance of single confined moving drops in rectangular microchannels," *Lab on a Chip*, vol. 9, no. 7, pp. 982–990, 2009.

[60] M. T. Guler, P. Beyazkilic, and C. Elbuken, "A versatile plug microvalve for microfluidic applications," *Sensors and Actuators, A: Physical*, vol. 265, pp. 224–230, 2017.

[61] S. Elizabeth Hulme, S. S. Shevkoplyas, and G. M. Whitesides, "Incorporation of prefabricated screw, pneumatic, and solenoid valves into microfluidic devices," *Lab on a Chip*, vol. 9, no. 1, pp. 79–86, 2009.

[62] Y. Murata, Y. Nakashoji, M. Kondo, Y. Tanaka, and M. Hashimoto, "Rapid automatic creation of monodisperse emulsion droplets by microfluidic device with degassed PDMS slab as a detachable suction actuator," *Electrophoresis*, vol. 39, no. 3, pp. 504–511, 2018.

[63] J. Sivasamy, T. N. Wong, N. T. Nguyen, and L. T. H. Kao, "An investigation on the mechanism of droplet formation in a microfluidic T-junction," *Microfluidics and Nanofluidics*, vol. 11, no. 1, pp. 1–10, 2011.

[64] M. Zagnoni, J. Anderson, and J. M. Cooper, "Hysteresis in multiphase microfluidics at a T-junction," *Langmuir*, vol. 26, no. 12, pp. 9416–9422, 2010.

[65] Y. Yan, D. Guo, and S. Z. Wen, "Numerical simulation of junction point pressure during droplet formation in a microfluidic T-junction," *Chemical Engineering Science*, vol. 84, pp. 591–601, 2012.

[66] X. B. Li, F. C. Li, J. C. Yang, H. Kinoshita, M. Oishi, and M. Oshima, "Study on the mechanism of droplet formation in T-junction microchannel," *Chemical Engineering Science*, vol. 69, pp. 340–351, feb 2012.

[67] S. Sugiura, M. Nakajima, and M. Seki, "Preparation of monodispersed emulsion with large droplets using microchannel emulsification," *JAOCS, Journal of the American Oil Chemists' Society*, vol. 79, no. 5, pp. 515–519, 2002.

[68] D. R. Link, S. L. Anna, D. A. Weitz, and H. A. Stone, "Geometrically Mediated Breakup of Drops in Microfluidic Devices," *Physical Review Letters*, vol. 92, no. 5, p. 4, 2004.

[69] A. I. Lee, Y.-c. Tan, J. S. Fisher, A. P. Lee, and V. Cristini, "Design of microfluidic channel geometries for the control of droplet volume, chemical concentration, and sorting," *Lab on a Chip*, vol. 4, no. 4, p. 292, 2004.

[70] J. H. Xu, G. S. Luo, S. W. Li, and G. G. Chen, "Shear force induced monodisperse droplet formation in a microfluidic device by controlling wetting properties," *Lab on a Chip*, vol. 6, no. 1, pp. 131–136, 2006.

[71] S. L. Anna and H. C. Mayer, "Microscale tipstreaming in a microfluidic flow focusing device," *Physics of Fluids*, vol. 18, no. 12, 2006.

[72] W. A. C. Bauer, M. Fischlechner, C. Abell, and W. T. Huck, "Hydrophilic PDMS microchannels for high-throughput formation of oil-in-water microdroplets and water-in-oil-in-water double emulsions," *Lab on a Chip*, vol. 10, no. 14, pp. 1814–1819, 2010.

[73] K. Wang, Y. C. Lu, J. H. Xu, J. Tan, and G. S. Luo, "Generation of micromonodispersed droplets and bubbles in the capillary embedded T-junction microfluidic devices," *AIChE Journal*, vol. 57, pp. 299–306, feb 2011.

[74] J. H. Xu, P. F. Dong, H. Zhao, C. P. Tostado, and G. S. Luo, "The Dynamic Effects of Surfactants on Droplet Formation in Coaxial Microfluidic Devices," *Langmuir*, vol. 28, pp. 9250–9258, jun 2012.

[75] T. Nisisako, T. Ando, and T. Hatsuzawa, "High-volume production of single and compound emulsions in a microfluidic parallelization arrangement coupled with coaxial annular world-to-chip interfaces," *Lab on a Chip*, vol. 12, no. 18, pp. 3426–3435, 2012.

[76] X. Wang, A. Riaud, K. Wang, and G. Luo, "Pressure drop-based determination of dynamic interfacial tension of droplet generation process in T-junction microchannel," *Microfluidics and Nanofluidics*, vol. 18, pp. 503–512, mar 2015.

[77] S. Gulati, K. Vijayakumar, W. W. Good, W. L. Tamayo, A. R. Patel, and X. Niu, "Microdroplet formation in rounded flow-focusing junctions," *Microfluidics and Nanofluidics*, vol. 20, no. 1, pp. 1–9, 2016.

[78] E. Amstad, M. Chemama, M. Eggersdorfer, L. R. Arriaga, M. P. Brenner, and D. A. Weitz, "Robust scalable high throughput production of monodisperse drops," *Lab on a Chip*, vol. 16, no. 21, pp. 4163–4172, 2016.

[79] W. Treesuwan, M. A. Neves, K. Uemura, M. Nakajima, and I. Kobayashi, "Preparation characteristics of monodisperse oil-in-water emulsions by microchannel emulsification using different essential oils," *LWT - Food Science and Technology*, vol. 84, pp. 617–625, 2017.

[80] L. Mei, M. Jin, S. Xie, Z. Yan, X. Wang, G. Zhou, A. Van Den Berg, and L. Shui, "A simple capillary-based open microfluidic device for size on-demand high-throughput droplet/bubble/microcapsule generation," *Lab on a Chip*, vol. 18, no. 18, pp. 2806–2815, 2018.

[81] Z. Zhou, T. Kong, H. Mkaouar, K. N. Salama, and J. M. Zhang, "A hybrid modular microfluidic device for emulsion generation," *Sensors and Actuators, A: Physical*, vol. 280, pp. 422–428, 2018.

[82] C. H. Y. Chung, B. Cui, R. Song, X. Liu, X. Xu, and S. Yao, "Scalable production of monodisperse functional microspheres by multilayer parallelization of high aspect ratio microfluidic channels," *Micromachines*, vol. 10, no. 9, 2019.

[83] D. M. Rissin, C. W. Kan, T. G. Campbell, S. C. Howes, D. R. Fournier, L. Song, T. Piech, P. P. Patel, L. Chang, A. J. Rivnak, E. P. Ferrell, J. D. Randall, G. K. Provuncher, D. R. Walt, and D. C. Duffy, "Single-molecule enzyme-linked immunosorbent assay detects serum proteins at subfemtomolar concentrations," *Nature Biotechnology*, vol. 28, no. 6, pp. 595–599, 2010.

[84] K. R. Emslie, J. L. McLaughlin, K. Griffiths, M. Forbes-Smith, L. B. Pinheiro, and D. G. Burke, "Droplet volume variability and impact on digital pcr copy number concentration measurements," *Analytical Chemistry*, vol. 91, pp. 4124–4131, mar 2019.

[85] W. C. Jeong, J. M. Lim, J. H. Choi, J. H. Kim, Y. J. Lee, S. H. Kim, G. Lee, J. D. Kim, G. R. Yi, and S. M. Yang, "Controlled generation of submicron emulsion droplets via highly stable tip-streaming mode in microfluidic devices," *Lab on a Chip*, vol. 12, no. 8, pp. 1446–1453, 2012.

[86] D. Li, Z. Guan, W. Zhang, X. Zhou, W. Y. Zhang, Z. Zhuang, X. Wang, and C. J. Yang, "Synthesis of uniform-size hollow silica microspheres through interfacial polymerization in monodisperse water-in-oil droplets," *ACS Applied Materials and Interfaces*, vol. 2, no. 10, pp. 2711–2714, 2010.

[87] Y. Zhu and Q. Fang, "Analytical detection techniques for droplet microfluidics-A review," *Analytica Chimica Acta*, vol. 787, pp. 24–35, 2013.

[88] F. He, M. J. Zhang, W. Wang, Q. W. Cai, Y. Y. Su, Z. Liu, Y. Faraj, X. J. Ju, R. Xie, and L. Y. Chu, "Designable Polymeric Microparticles from Droplet Microfluidics for Controlled Drug Release," *Advanced Materials Technologies*, vol. 1800687, pp. 1–23, 2019.

[89] A. S. Basu, "Digital Assays Part I: Partitioning Statistics and Digital PCR," 2017.

Appendix A

Publication List

All license agreements between Ali Kalantarifard and the License Suppliers are made by means of Copyright Clearance Center.

1. A Kalantarifard, E Alizadeh-Haghighi, A Saateh, C Elbuken, Theoretical and experimental limits of monodisperse droplet generation, Chemical Engineering Science, vol. 229, p. 116093, 2020.

2. A Saateh, A Kalantarifard, OT Celik, M Asghari, M Serhatlioglu, C Elbuken, Real-time impedimetric droplet measurement (iDM), Lab on a Chip, vol. 19, no. 22, pp. 3815-3824, 2019.

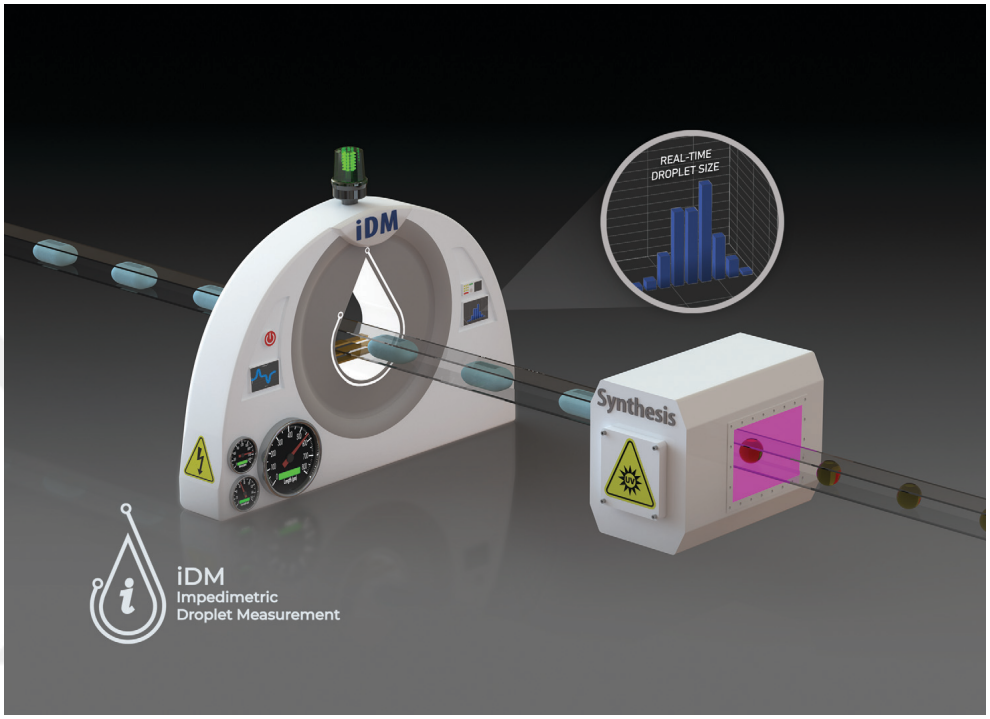

Featuring research from the Microfluidics Laboratory of Dr. Elbuken's, National Nanotechnology Research Center (UNAM), Bilkent University, Ankara, Turkey.

Real-time impedimetric droplet measurement (iDM)

Detecting morphological parameters of microdroplets and providing in situ statistical analysis for applications requiring real-time droplet size measurement, such as particle synthesis.

As featured in:

See Caglar Elbuken *et al.*, *Lab Chip*, 2019, **19**, 3815.

ROYAL SOCIETY OF CHEMISTRY | Celebrating IYPT 2019

rsc.li/loc

Registered charity number: 207890

Figure A.1: Lab on a Chip cover [2].

3. A Kalantarifard, A Saateh, C Elbuken, Label-Free Sensing in Microdroplet-Based Microfluidic Systems, Chemosensors, vol. 6, no. 2, p. 23, 2018.

4. A Kalantarifard, EA Haghighi, C Elbuken, Damping hydrodynamic fluctuations in microfluidic systems, Chemical Engineering Science, vol. 178, pp. 238-247, 2018.

5. Z Isiksacan, MT Guler, A Kalantarifard, M Asghari, C Elbuken, Lab-on-a-Chip Platforms for Disease Detection and Diagnosis, Biosensors and Nanotechnology: Applications in Health Care Diagnostics, pp. 155-181, 2018.

6. Ali Kalantarifard, Elnaz Alizadeh-Haghighi, Caglar Elbuken, A novel design of microfluidic droplet systems for ultra-monodisperse droplet generation (*submitted*).